RHODES UNIVERSITY

Where leaders learn

Electrospun fiber based colorimetric probes for Aspartate Aminotransferase and 17β-estradiol

A thesis submitted to Rhodes University in fulfillment of the requirements for the degree of

Doctor of Philosophy (Science)

By

Bellah Oreeditse Pule

Supervisor: Professor Nelson Torto

Dedication

To Tiiso Pule, love you...

Acknowledgments

Prof Nelson Torto: whoever coined the following was spot on as these are the words you used that inspired and shaped me;

"There is never just one thing that leads to success for anyone. It's always a combination of passion, dedication, hard work and being in the right place at the right time"

Thanks Prof...

Martha Pule: To say you are my pillar of strength will be an understatement... Thanks mom for giving me room to dream and the freedom to grow...

Sissy Valerie Seemule: You are the best sister ever, thanks for playing a major role in making me the person I am today...

Tuduetso Mims Pule: Thanks for holding the fort; you are so incredible...

Boitumelo Mudabuka, Alicia Singh, Linda Kunene and Roxy Openshaw: You guys rock in your own unique way. Thanks for making things feel better.

F-12 colleagues: You were such am amazing group. Thank you all...

Chemistry Department, Rhodes University: Thank you for all the assistance and support.

Sandisa Imbewu: For funding the research. Thank you.

To the rest of my family and friends: Thank you for giving me the strength to soldier on...

Abstract

Fabrication, characterization and application of electrospun polymer composite based colorimetric probes are presented in this thesis. The first part of the thesis involved the development of a protocol for *in situ* reduction of gold trication (Au^{3+}) into metallic gold atoms with sodium borohydride. The prepared PS-Au NPs showed an SPR band at 542 nm. Furthermore the absorbance of the colloidal Au NPs in polystyrene exhibited a good linear correlation (r^2 = 0.9934) to E_2 concentration in the range 5 to 50 ppb. The lowest naked eye detection limit was found to be 0.5 ppb and could further be easily monitored by UV-vis spectrophotometer. Upon interaction with E_2 Au NPs aggregated to give nanoparticle clusters, confirmed through TEM analysis. Different concentrations of Au NPs were found to have a significant effect on the conductivity of the PS-Au NPs solution. At low concentrations of Au NPs (0.002, 0.015 and 0.025% w/v) PS-Au NPs solution could be electrospun without clogging. The FE-SEM images showed a non-beaded morphology of PS-Au NPs composite fibers. Upon interaction of the colorimetric probe strips with various E_2 concentrations it was observed that with increasing E_2 concentrations (50 ng/mℓ to 1000 µg/mℓ) the colour of the probe changed gradually from white to shades of pink and eventually to shades of blue at higher E_2 concentrations. The visible cut-off concentration was 100 ng/mℓ. The second component of the thesis focussed on the development of diazonium dye-nylon 6 colorimetric probe for aspartate aminotransferase. At optimal pH 7.4 the enzyme was stable, highly active and catalyzed a reaction that was susceptible to detailed kinetic analysis by continuous optical methods. The K_M values for L-aspartate, α- ketoglutarate and oxaloacetate were 2.60, 0.59 and 0.066 mM, respectively. On the basis of these K_M values the solid-state colorimetric probe was developed. A colour change occurred when an electrospun dye-N 6 probes were exposed to visibly detectable concentrations of oxaloacetate, an AST-catalyzed reaction product. While monitoring AST activity at 530 nm, a linear relation was obtained between oxaloacetate concentrations ranging from 0.4 – 7.4 µg/mℓ. Naked eye detection limit of 2.4 µg/mℓ oxalaoacetate equivalence of 10 times the normal AST activity was attained. The colorimetric probe was in addition, tested against co-substrates aspartate, ketoglutarate and a variety of other compounds such as alanine, pryruvate, as well as glutamic, malaic and succinic acids known to interfere with AST activity. Each compound elicited a distinct and unambiguous colour change upon interaction with the colorimetric probe. Further X-ray powder diffraction (XRD), duNouy ring tensiometer, Brunauer–Emmett–Teller (BET) and energy dispersive X-ray spectroscopy (EDS/EDX) characterization confirmed composition and stability of the colorimetric probes. Colorimetric probes developed in this thesis are relatively cost effective, simple and "rugged" for measurement of analytes with visual detection without sample pretreatment in matrices, such as plasma and dairy effluents. The probes warrant further investigation as they have shown potential and offer a promising solid-state platform for both clinical diagnostics and environmental monitoring.

Table of Contents

List of abbreviations

A	Absorbance
AAS	Atomic absorption spectrometry
AES	Auger electron spectroscopy
AFM	Atomic force microscopy
ALP	Alkaline phosphatase
ALT	Alanine aminotransferase
AST	Aspartate aminotransferase
ATR-IR	Attenuated total reflection infrared spectroscopy
Au NPs	Gold nanoparticles
BAu	Albumin decorated gold
BET	Brunauer–Emmett–Teller
BJH	Barret, Joyner and Halenda
BPA	Bisphenol-A
C	Carbon
Cl	Chlorine
CoASH	Coenzyme
Cu	Copper

DSC	Differential scanning calorimetry
DDAB	Didodecyldimethylammonium bromide
DILI	Drug-induced liver injury
DMF	N, N-dimethylformamide
DNA	Deoxyribonucleic acid
DNP	Dynamic nuclear polarization
DTNB	5,5′-dithiobis(2-nitrobenzoic acid)
E_1	Estrone
E_2	17β-estradiol
E_3	Estriol
EDCs	Endocrine disrupting chemicals
EDX	Energy dispersive X-ray analysis
EE_2	17α-ethynylestradiol
ERα	Estrogen Receptor alpha
ERβ	Estrogen Receptor beta
F	Fluorine
ESCA	Electron spectroscopy for chemical analysis
FE-SEM	Field Emission Scanning Electron Microscope
GC	Gas chromatography

GGT	Gamma-glutamyl transferase
HAc	Glacial acetic acid
$HAuCl_4.3H_2O$	Gold (III) chloride trihydrate
HIV	Human immunodeficiency virus
HNAr	Aliphatic amine
I_0	Incident light
I	Transmitted light
ICP-MS	Inductively coupled plasma mass spectroscopy
IR	Infrared spectroscopy
Km	Substrate concentration that yield a half-maximal velocity
kV	Kilovolts
IUPAC	Union of Pure and Applied Chemistry
L	Sample path length in centimeters
LOD	Lowest detection limit
MALDI-TOF	Matrix-assisted laser desorption/ionization time-of-flight mass spectrometry
MDH	Malate dehydrogenase
MeOH	Methanol
mM	Millimolar
mM cm^{-1}	Millimolar per centimeter

M_W	Molecular weight
mN/m	Millinewton per meter
N	Nitrogen
N6	Nylon 6
Na	Sodium
$NaBH_4$	Sodium borohydride
NADH	Nicotinamide adenine dinucleotide
NAD^+	Aldehyde dehydrogenase
NC	Nitrocellulose
NFN	Nanofiber nets
NH_2	Amine group
NH_2R	Primary amine
ng/mℓ	Nano-grams per milliliter
nM	Nanomolar
nm	Nanometer
NMR	Nuclear magnetic resonance
4-NP	4-nonylphenols
4-*t*-OP	4-*t*-octylphenol
O	Oxygen
OH	Hydroxide

P	Phosphorus
PA	Polyamide
PCBs	Polychlorinated biphenyls
PEEM	Photoelectron emission microscopy
PES	Polyethersulfone
ppb	Parts per billion
PS	Polystyrene
PT	Plasma prothrombin time
PTFE	Polytetrafluoroethylene
PVA	Polyvinyl alcohol
PVP	Poly (vinyl pyrolidone)
R^2	Correlation coefficient
S	Sulfur
SAXS	Small-angle X-ray scattering
SDH	Sorbitol dehydrogenase
SEM	Scanning electron microscope
SIMS	Secondary ion mass spectrometry
SPR	Surface Plasmon resonance
SSNMR	Solid-state nuclear magnetic resonance
Std Dev	Standard Deviation

STXM	Scanning transmission X-ray microscopy
TEM	Transmission electron microscopy
THF	Tetrahydrofuran
UV-Vis	Ultraviolet-visible spectroscopy
U/L	Units per liter
Vmax	Maximum velocity
WAXS	Wide-angle X-ray scattering
Wh/m^2	Watt-hours per square meter
XPS	X-ray photon spectroscopy
XRD	X-ray diffraction
Zn	Zinc
Å	Angstrom
ε	Molar extinction coefficient
µg/mℓ	Micro-grams per milliliter
µS/cm	Microsiemens per centimeter
π - π*	Pi to Pi* electronic transition
% w/v	Percentage weight per volume
% wt	Percentage weight
% wt/wt	Percentage weight by weight
λ	Wavelength

List of Figures

List of Tables

Chapter 1

Introduction

1.1 Analytical process

There is a well-recognized trend towards simplification ("easy to implement or do"), automation ("electro-mechanically self-operation") and miniaturization ("small scale"; "make to a very small scale") of the analytical process (Ríos et al., 2006). The interface between these three characteristics is identified as an attractive area for various developments, defining the ever evolving field of analytical chemistry. Fundamentally, an analytical process comprises three major steps as outlined in Fig. 1.1. Over the years, each component has been faced with various challenges associated with analyte and matrix complexities which have driven researchers to continuously think of ways to improve the analytical process (Chigome and Torto, 2011).

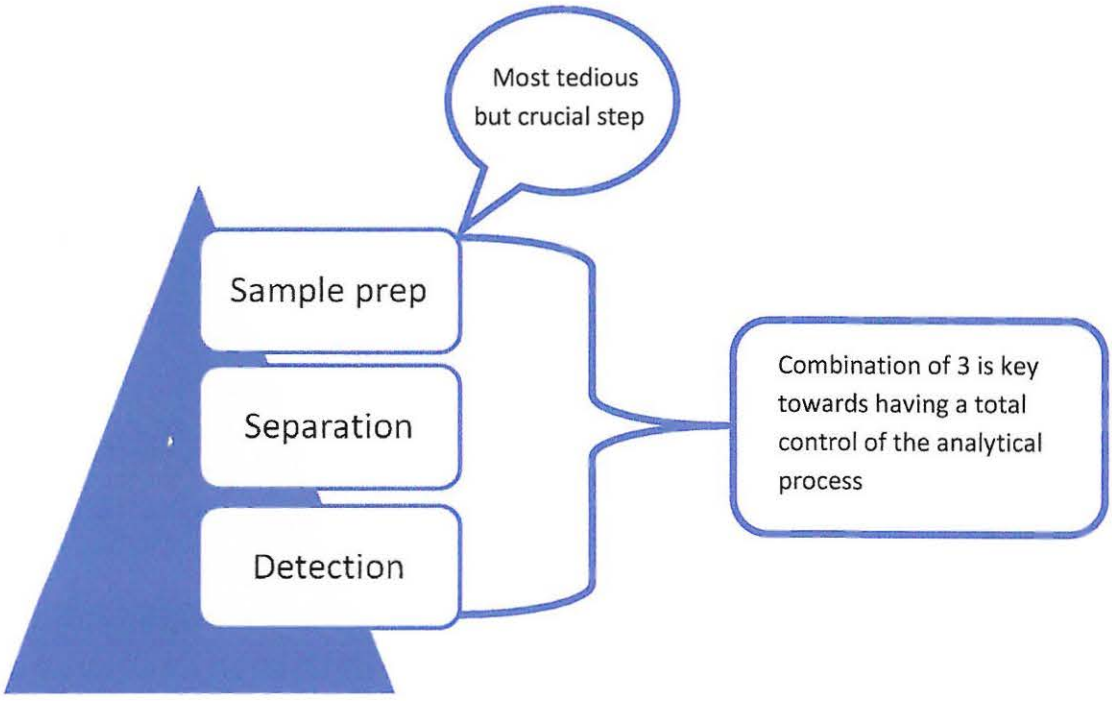

Figure 1.1: Analytical process; sample preparation, separation and detection

It is also worth mentioning that an analytical chain comprises a number of other crucial steps that need to be considered in order to be successful. A more complete chain includes the following steps: sampling strategy/methodology; sample transport/storage; separation/detection; data evaluation/statistical treatment and reporting data. The data should be reported in such a way that the work done may be scrutinized and reproduced if need be. In addition, research efforts have since been channeled towards improving analyte selectivity that also facilitates sensitive detection and most importantly reduced time for the whole analytical process.

Several good traditional techniques that include chemiluminescence, spectrophotometry, fluorescence, atomic absorption spectrometry (AAS), mass spectrometry, electrochemical techniques and inductively coupled plasma mass spectroscopy (ICP-MS) have been employed for detection in environmental and clinical diagnostics. These traditional methods however, constitute expensive and sophisticated instrumentation, coupled to handling complicated sample preparation processes and also require skilled personnel. The methods are not only time consuming but also involve the use of relatively large sample volume (ml – L) and are not suitable for on-site analysis or point of care detection. Advancements in analytical methods have therefore been focused towards developing rapid, facile and inexpensive but also practical and well repeatable protocols to detect analytes in real environmental samples as well as for diagnosis in the clinical sector.

Monitoring of the presence and quantity of the contaminants in the environment is prudent as many of the compounds are toxic, hence pose a threat to both human health and ecosystems. Often, the first step in monitoring is to measure discharges at the points of release for air- and waterborne toxic releases. Subsequent steps involve understanding the movement and transport of key contaminants within the given environmental media; their transfer from one medium to another; and changes in their physical, chemical, and biological characteristics. In all practical cases, there is often a trade-off between the monitoring costs (in terms of instruments and manpower, number of samples, and sensitivity of analytical methods) associated with the contaminants and the degree of information that can be collected regarding the distribution, transport and fate of the contaminants in different environmental media (Gupta, 2011).

Similarly, several superior but complex techniques such as those already mentioned (chemiluminescence, spectrophotometry and fluorescence) have been employed for detecting the biomarker enzymes particularly aspartate aminotransferase (AST) activity from biological fluids (Huang et al., 2006). Such an analyte is very important especially as it is a good indicator for liver toxicity associated with alcoholism or high dose of drug intake associated with HIV/AIDS. Elevated levels of these enzymes in serum have been used to detect if the heart or liver is damaged.

In the midst of all the developments and progress achieved to date, non-invasive analytical devices have evoked interest. Among these, colorimetric based non invasive analytical devices are especially appealing because of their potential to enable naked-eye detection. With the intent to reduce the use of complex and expensive instrumentation and also based on the principle of colorimetric analysis we ventured into developing cheaper colorimetric probes. The use of colorimetric assay, whereby the presence of the analyte causes a visual change in colour, is particularly an attractive way for diagnostic tests of a range of compounds in clinical and environmental applications, given their quick and easy to use properties.

Several labels, such as nanoparticles, quantum dots and dyes have been employed as colour signaling reagents in colorimetric assays. Gold nanoparticles (Au NPs) and azo dyes are of interest for this thesis. In simple terms, the principle of colorimetric analysis for gold nanoparticles is that Au NPs present different colours, from red, to purple or blue, based on interparticle reactions during aggregation, or dispersion of Au NPs aggregates. While for dye based colorimetric detection a chemical group (as an azo group) absorbs light at a specific frequency and imparts colour to the system. The dye employed is inexpensive and known to be selective towards the product of AST. Furthermore the chromophore produced from the interaction of the dye and the analyte gives a colour visible to the naked eye. We also took advantage of benefits from noble metal nanoparticles properties. Gold nanoparticles were explored mainly because of their brilliant colours due to the surface plasmon resonance absorption.

However, most studies have utilized solution-phase colorimetric systems, which have necessarily limited the wider application of the probes. This is because for practical reasons, many colorimetric devices require solid-state materials that are stable, reusable and amenable to large-scale fabrication (Gill and Ballesteros, 2003). To address these challenges a facile technique, electrospinning, was employed to fabricate fibers as a platform for the colorimetric probe. The important advantages of electrospinning technique include the production of very thin fibers to the order of few nanometers with large surface area to volume ratio, their porous structure, ease of functionalization for various purposes, superior mechanical properties and ease of process as suggested by many experts in this field. The possibility of large scale productions combined with the simplicity of the process makes this technique very attractive for many different applications. We, furthermore, envisaged that the fibers will be able to retain the colour signaling reagent (Au NPs or dye) within the porous network while allowing the analyte access to interact with the reagent. It is, therefore, the significance of this thesis to highlight some of the interesting developments that demonstrate the application opportunities of electrospun nanofibers.

The objective of the studies in this thesis was to develop colour signaling group incorporated electrospun fiber protocols that are simple, rugged and should achieve in-situ sample preparation for qualitative as well as semiquantitative eyeball detection of enzyme-markers for liver toxicity, AST and an endocrine disrupting chemical, 17β-estradiol.

1.2 Colorimetric probes

Colorimetric assays result in a coloured reaction product or chromogen that absorbs light in the visible range at a characteristic wavelength. The optical density of the reaction product is typically proportional to the amount of analyte being measured (www.nature.com). Figure 1.2 shows a typical example of a colorimetric assay.

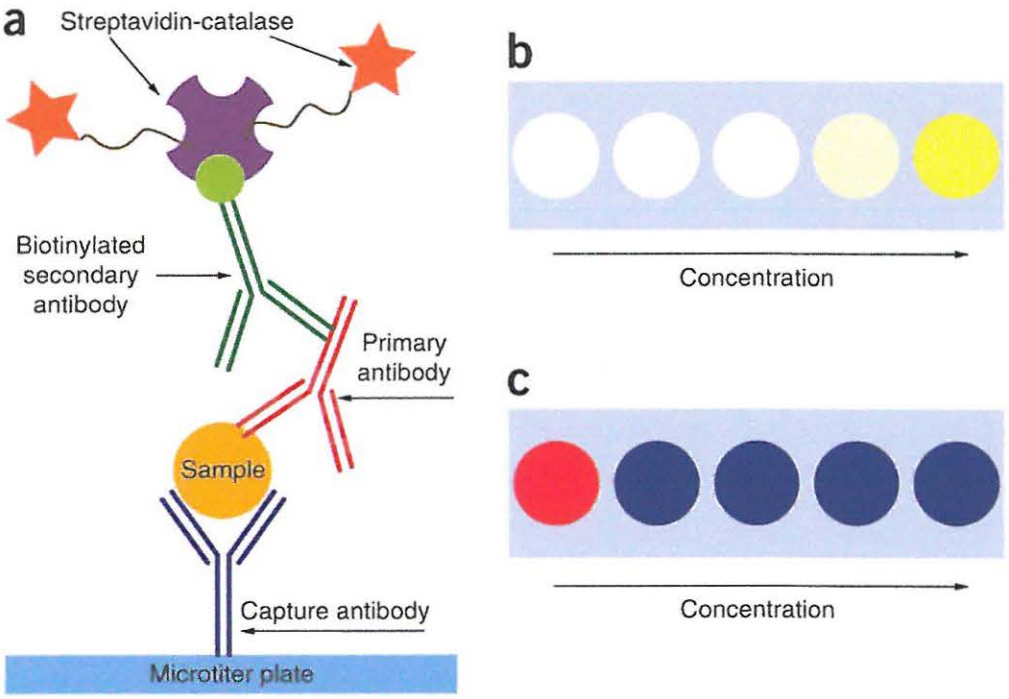

Figure 1.2: (a) Model sandwich immunoassay in which the enzyme label is linked to the immunocomplex by biotin-streptavidin interactions; (b) Visual detection with the conventional colorimetric ELISA; (c) Visual detection using the plasmonic ELISA (www.nature.com/nnano/journal/v7/n12/full/nnano.2012.186.html)

Colorimetric and other absorbance assays are based on the molar extinction coefficient, an experimental measure of absorbing power of the substance under investigation. The molar extinction coefficient, also referred to as the absorptivity coefficient maybe determined mathematically through the Beer-Lambert law.

Beer-Lambert law, most commonly known as Beer's law, is used in analytical techniques that deal with quantitative measurements of the spectral distribution of radiant energy (i.e., light) in understanding the interaction of light with the properties of matter e.g. solid, liquid, or even human tissue (Maikala, 2010). Beer's law states that the optical absorbance of a chromophore in a transparent solvent varies linearly with both the sample cell path length and the chromophore concentration.

Absorbance is measured in a spectrophotometer by passing a collimated beam of light at wavelength λ (380–800 nm which gives a visible sensation to the human eye) through a plane parallel slab of material that is normal to the beam (see Fig. 1.3). For liquids, the sample is held in an optically flat, transparent container called a cuvette. Absorbance (A) is calculated from the ratio of light energy passing through the sample (I_0) to the energy that is incident on the sample (I) see Eqn. 1.1:

$$A = -\log\frac{I}{I_0} \qquad \ldots (1.1)$$

Beer's law follows (Eqn. 1.2):

$$A = \varepsilon CL \qquad \ldots (1.2)$$

ε = molar absorptivity or extinction coefficient of the chromophore (the optical density of a 1-cm thick sample of a 1 M solution). E is a property of the material and the solvent.

L = sample path length in centimeters

C = concentration of the compound in the sample, in molarity (mol L^{-1})

Light is usually attenuated not only by the chromophore but also by reflections from the interface between air and the sample, the sample and the cuvette and absorbance by the solvent. These factors can be quantified separately, but are often removed by defining I_0 as the light passing through a sample "blank" or "baseline" or reference sample, for example, a cuvette filled with solvent but zero concentration of the chromophore is used as the blank (http://www.oceanoptics.com/technical/beerslaw.asp).

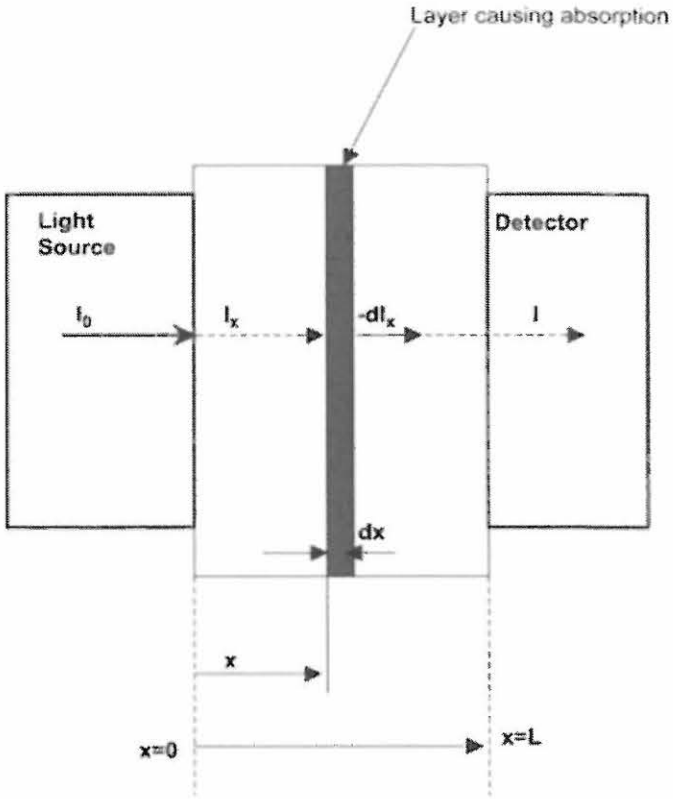

Figure 1.3: Lambert–Beer Law using in vitro cuvette model. Io = incident light energy of a definite monochromatic wavelength; I = transmitted light through a layer of medium; x = pathlength or thickness of the layer; a = wavelength-dependent absorption or extinction coefficient. Ix = monochromatic light passing through an infinitesimal slab of thickness 'dx' in a medium per second, at a distance 'x' from the entrance of the absorbing path; –dIx = amount of light energy passing through the slab; L = pathlength of light through the cuvette, ignoring the thickness of the cuvette walls (Adapted from Maikala, 2010)

Dyes and noble metal nanoparticles are ideal colour reporting groups for colorimetric probes because they have high extinction coefficients in the visible region (Liu and Lu, 2007, Sun et al., 2012, Kim et al., 2013).

Over years several dye and noble metal nanoparticles based colorimetric probes have been developed for routine analysis particularly in clinical and environmental fields amongst many other applications.

1.2.1 Gold Nanoparticles

Gold, similar to silver nanoparticles have attracted much interest in various fields because of their unique properties, including large optical field enhancements resulting in the strong scattering and absorption of light (Jain et al., 2006). The optical and photothermal properties of the noble metal nanoparticles can be tuned depending on the shape, size, and dielectric constants of both the metal and the surrounding material (Coronado et al., 2011). The enhancement takes place on the surface of the nanoparticles and is referred to as surface plasmon resonance (SPR) (see Fig. 1.4 for a summary illustration of the SPR phenomenon). The plasmon resonance can either radiate light (Mie scattering), a process that finds great utility in optical and imaging fields, or be rapidly converted to heat (absorption); the latter mechanism of dissipation has opened up applications in several new areas.

In brief, when visible light shines on metal nanoparticles, the light of a resonant wavelength is absorbed by the nanoparticles and induces surface electron oscillation. Small Au NPs (e.g., 13 nm in diameter) absorb green light, which corresponds to a strong absorption band (surface plasmon band) at~520 nm in the visible light spectrum; therefore solutions of Au NPs appear red in colour.

For small Au NPs, surface electrons are oscillated by the incoming light in a dipole mode. As the size of the Au NP increases, light can no longer polarize the nanoparticles homogeneously, and higher order modes at lower energy dominate. This causes a red-shift and broadening of the surface plasmon band (Zhao et al., 2008).

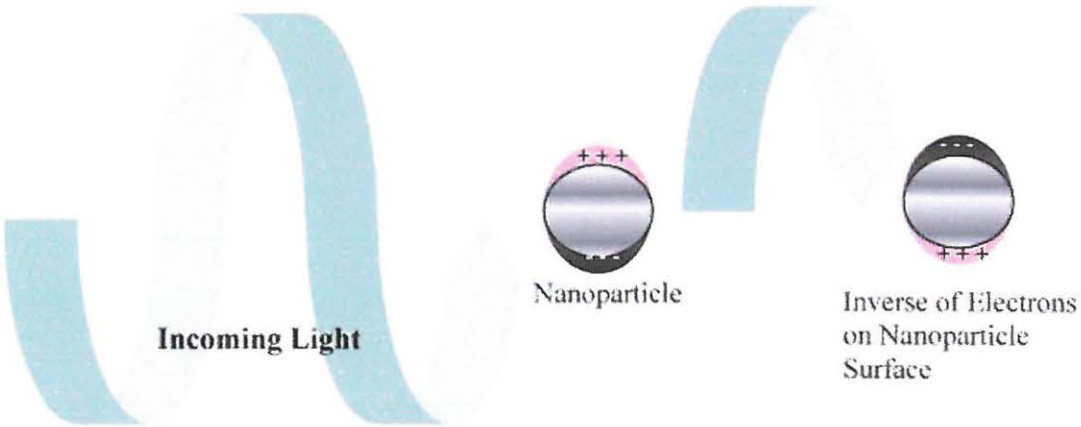

Figure 1.4: Origin of surface plasmon resonance due to coherent interaction of the electrons in the conduction band with light (Eustis and El-Sayed, 2006)

When Au NPs aggregate, their surface plasmons combine (interparticle plasmon coupling), and the aggregate could be considered as a single large particle in simplified terms. Interparticle plasmon coupling is rather complex and dependent on many factors, such as aggregate morphology and nanoparticle density. Due to the unique surface plasmon resonance noble metal nanoparticles distinguish themselves from other nanoplatforms such as semiconductor quantum dots, magnetic and polymeric nanoparticle. Figure 1.5 shows examples of specific optical, fluorescence and magnetic properties for gold nanoparticles quantum dots and magnetic nanoparticles respectively.

Gold nanoparticles (Au NPs) have been brought to the forefront of various researches over the years because of their high chemical stability, facile synthesis and ease of surface modification, strongly enhanced and tunable optical properties as well as excellent biocompatibility feasible for clinical settings and environmental screening (Huang and El-Sayed, 2010, Wang et al., 2010).

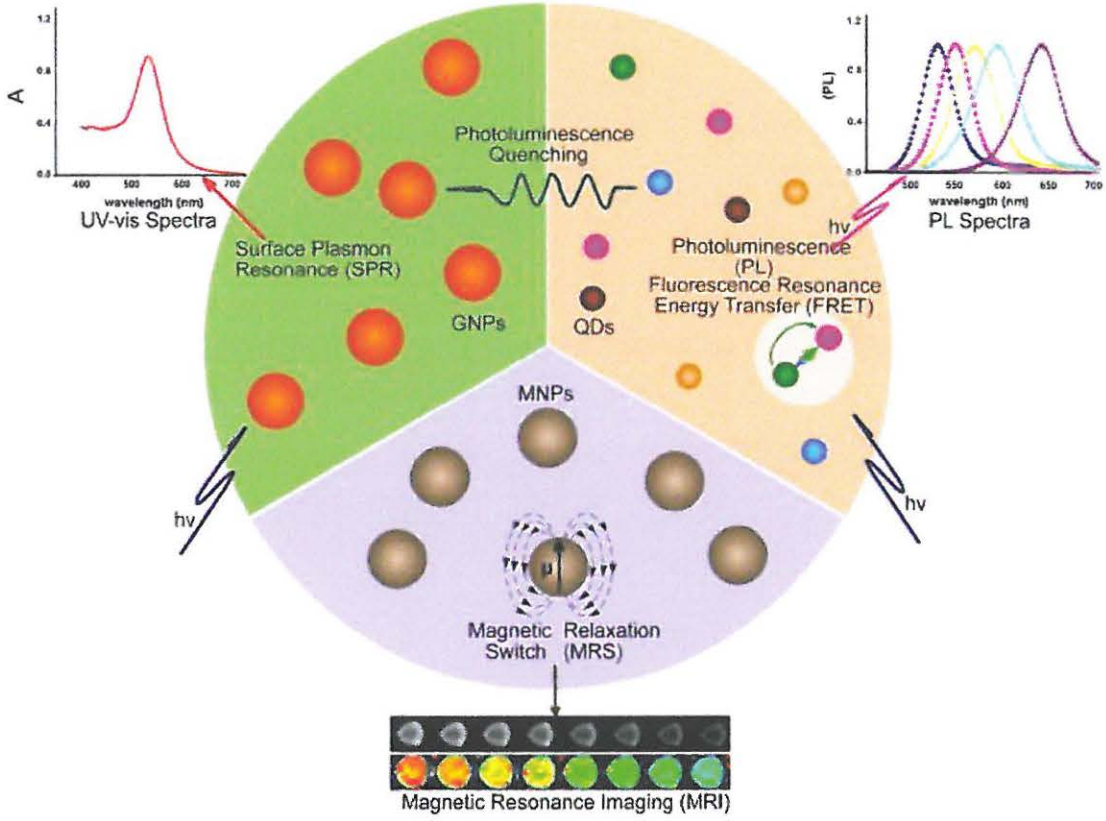

Figure 1.5: A schematic of different optical properties resulting from the interaction of light with gold NPs (Au NPs/GNPs), quantum dots (QDs), and magnetic NPs (MNPs) (Adapted from Wang et al., 2010)

The methods for synthesizing these gold nanoparticles are diverse and have tremendously evolved with time.

1.2.1.1 Synthesis of gold nanoparticles

In the first step, the redox reaction of gold ions (Au III) with reducing agent leads to the gold nuclei formation, with further growth results in Au NPs formation as shown in Fig. 1.6. Subsequently, obtained nanoparticles agglomerate to a larger scale, due to the presence of Van der Waals forces (Luty-Blocho et al., 2011). The procedure maybe a single step whereby Au (III) salt is reduced to Au (0) to form an activated species, or it could proceed via Au (I) intermediate followed by reduction to Au (0) (Guo et al., 2010, Gao et al., 2012). Based on the synthetic protocol Au NPs can be manufactured into a variety of shapes including Au nanospheres (Cunningham and Lamela, 2010) triangular nanoparticles (Smitha and Gopchandran, 2013, Reyes-Gasga et al., 2008) nanorods (Huang et al., 2009) nanoshells (Ashayer et al., 2008), nanooctahedrons (Kim et al., 2009), nanocubes (Kalishwaralal et al., 2009), nanoclusters (Zhang et al., 2013) and nanostars (Kooij et al., 2012).

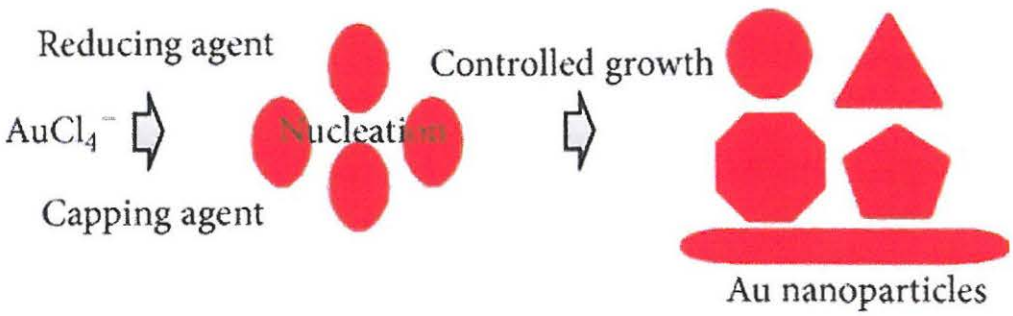

Figure 1.6: A typical Synthetic route of growth of gold nanoparticles (Chandra et al., 2013)

Addition of stabilizer is usually done at a precise time before coagulation of the nanoparticles takes place.

Methods to prepare nanoscale Au rely on photochemical and chemical reductions, electrochemical methods and radiolytic methods (Medina-Ramírez et al., 2009). Figure 1.7 shows a summary of the various methods for Au NPs preparation based on a literature compilation regarding commonly applied synthetic methods for nanoparticles. One of the major disadvantages of the mentioned reduction methods is that the Au NPs aggregate due to the van der Waals force interactions between Au atoms (Sousa and Teixeira, 2013). The van der Waals forces in the particle–particle pair interaction can be described in Eqn. 1.3.

$$\omega(r) = -\frac{A}{\pi^2 \rho_1 \rho_2 r^6} \qquad \ldots (1.3)$$

ρ_1 and ρ_2 = the number of atoms per unit volume in two interacting bodies
A = Hamaker constant
r = particle center-to-center distance

The van der Waals forces between two identical particles are generally attractive while the electrostatic forces, due to the overlapping of electrical layers of the two like particles are repulsive. The combination of the two interactions typically generates an energy barrier. The height of the energy barrier determines whether nanoparticles will be stable or undergo coagulation (Zhou et al., 2009).

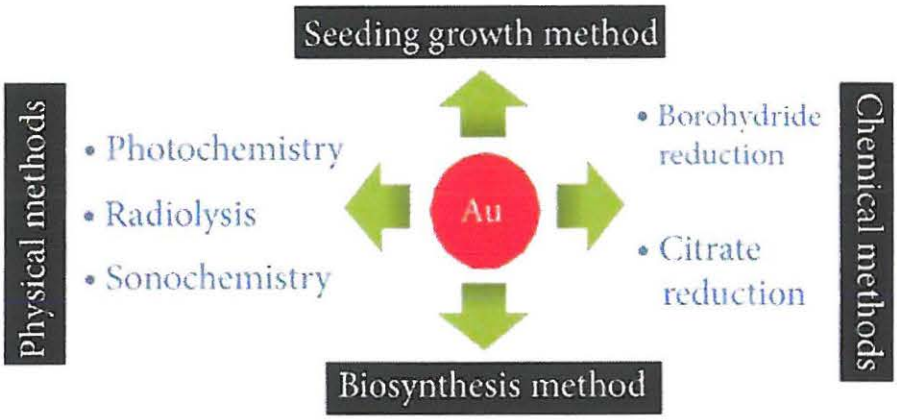

Figure 1.7: Various methods for Au NPs preparation based on a literature compilation regarding commonly applied synthetic methods for nanoparticles (Chandra et al., 2013)

A wide range of reducing agents have been utilized for reduction of trivalent gold to zero valent gold for preparation of uncapped and capped nanoparticles. Application of nanoparticles is a determining factor when choosing reducing and capping agents. For instance, nanoparticles may be used *in vivo* where cytotoxicity of nanoparticles is a major factor or *in vitro* where biocompatibility and environmental impact should be considered (Colvin, 2003, Shukla et al., 2005). Among a variety of stabilizers and protective capping agents for gold nanoparticles, citrate is commonly used, it stabilizes the gold nanoparticles through mutual electrostatic repulsion between neighboring gold nanoparticles (Patungwasa and Hodak, 2008). Some of the advantages of using citrates and other reducing agents such as ascorbic and aspartic acid are that the nanoparticles are non-toxic; the reaction rate is usually rapid and associated with high reproducibility (Li et al., 2011). However, the citrate, ascorbic or aspartic reduced systems are characterized by minimal stability of the nanoparticle with changes in pH, temperature or ionic strength. In addition, citrates have low redox potential hence reactions are carried out under relatively more severe conditions (e.g. at high temperature).

Borohydride reduction is another popularly used method for gold nanoparticles production (Selvakannan et al., 2004). Unlike citrates borohydrides have high redox potential which allows the reaction with borohydride to proceed at ambient temperature. The borohydride (BH_4^-) ions may play the role of a stabilizer *in situ*. However, the borohydride anions are not efficient stabilizers due to secondary interactions with the environment (Singha et al., 2014). For instance, borohydride anions adsorbed on nanoparticles may be consumed by water, driving the nanoparticles to aggregate (Seo et al., 2009).

Other reducing agents that are less frequently used than sodium borohydride include hydrazine hydrate (Zargar and Hatamie, 2013), aldehydes (Scampicchio et al., 2009), lower acid amides, formamide and N, N-dimethylformamide (Pastoriza-Santos and Liz-Marzán, 2000) and hydroxylamine (Jiali et al., 2007). In most cases, stabilizers are usually introduced into the starting reaction medium as additional components.

Gold nanoparticles capped with alkanethiol (Moon et al., 2010), alkylamine molecules (Liu et al., 2013), phospholipids (He and Urban, 2005), didodecyldimethylammonium bromide (DDAB) (Li et al., 2008) biomolecule including peptides, proteins, carbohydrates, antibodies and oligonucleotides (Dykman and Khlebtsov, 2012) or embedded in polymers, e.g. poly(vinyl pyrolidone) (PVP) (Corbierre et al., 2001, Khanna et al., 2005, Merican et al., 2007, Tsunoyama et al., 2009) have also been reported.

Gold nanoparticles may be stabilized through electrostatic and steric modes. For electrostatic stabilization, in order to maintain electroneutrality, an equal number of counter-ions with the opposite charge will surround the nanoparticles and give rise to overall charge-neutral double layers (Zhou et al., 2009). While in charged electrostatic stabilization, it is the mutual repulsion of the induced double layers surrounding particles that provides stability. Steric stabilization, on the other hand, is achieved by the coordination of sterically bulky organic molecules that act as protective shields on the metallic surface. Figure 1.8 shows a typical electrostatic and steric contribution towards nanoparticles stability.

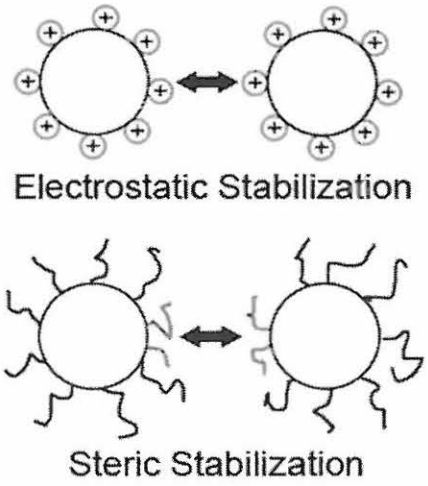

Figure 1.8: Electrostatic stabilization as shown by two like charged particles repelling each other and the steric stabilization shown by polymer chains opposing being pushed together causing repulsion (http://File:Electro-Steric_Stabilization.jpg)

Size and chemical nature of the molecules determine the degree of stabilization. An effective stabilization is brought about if the length of the stabilizer is significantly longer or the molecule is bulky and larger than the characteristic size of the nanoparticles, a sphere can be formed encapsulating the nanoparticle and provides stabilization. Because of high molecular weights polymers are often employed as stabilizers for nanoparticles (http://www.matsceng.ohio-state.edu/ and http://materialrulz.weebly.com/).

The main classes of protective groups described in the literature include polymers and block copolymers (Takahashi et al., 2008); P, N, and S donors (e.g., phosphanes, amines, thioethers); solvents such as THF, THF/MeOH, and propylene carbonate; long-chain alcohols; surfactants; and organometallics (Zhou et al., 2009).

1.2.1.1.1 Polymers as nanoparticle stabilizers

When two polymer-covered surfaces approach each other, they experience a force once the outer most segments begin to overlap (Bergstrand, 2003). The interaction leads to a repulsive osmotic force due to the unfavorable entropy associated with compressing the polymer chains between the surfaces in a good solvent. Polymers protect nanoparticles against coagulation and lead to steric stabilization of a colloid. In a poor solvent, however, coagulation can occur as the polymer layer collapses and van der Waals forces dominate (Cote et al., 2008). The forces induced depend on the coverage of polymer on the surface of the nanoparticle and on whether the polymer is simply adsorbed from solution or grafted onto the surfaces as well as on the nature of the solvent (Kochkodan et al., 2013). Polymers play important roles in many industrial processes, for example, in paints, emulsions, cosmetics, pharmaceuticals, soils and lubricants. A combination of polymers and nanoparticles has other benefits besides stabilization of nanoparticles. Polymer nanocomposites exhibit unprecedented performance, improved properties compared to the polymers and nanoparticles as individuals, design flexibility, lower life-cycle costs and uniquely large applicability of nanocomposites in various industrial fields (Hersam and Weiss, 2011).

The coupling of polymer and nanoparticles is promising since the nanoparticles with their unique properties due to quantum size effect provide additional qualities such as process ability, solubility, mechanical and thermal stability on the overall polymeric composite (Takahashi et al., 2008). Furthermore, uniform dispersion of nanoparticles produces ultra-large interfacial area per volume between the nanoelement and host polymer. This immense internal interfacial area and the nanoscopic dimensions of nanoelements, fundamentally distinguish polymer/nanocomposites from traditional composites and filled plastics (Chrissafis and Bikiaris, 2011). Figure 1.9 shows the various types of nanomaterials.

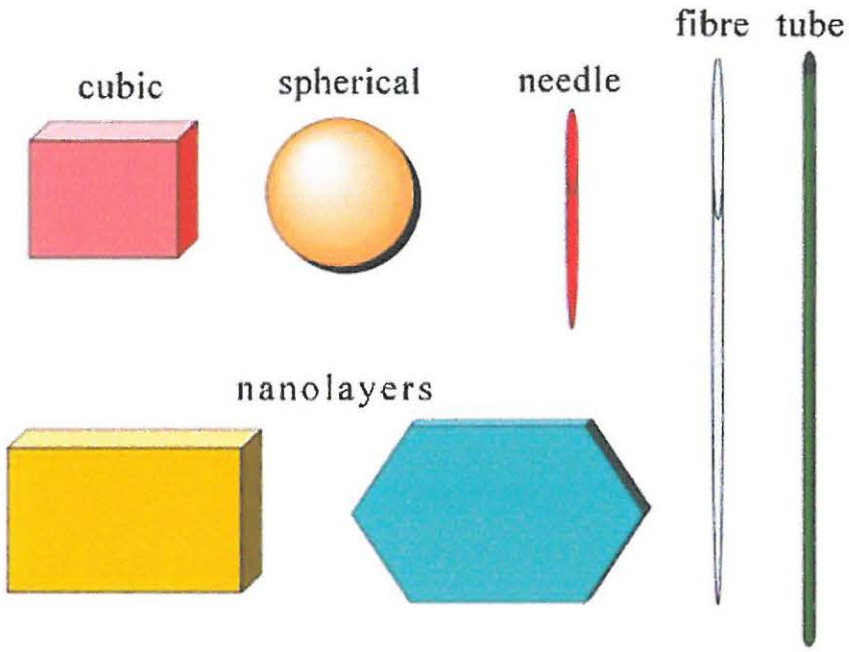

Figure 1.9: Various types of nanoscale materials classified into three categories depending on the dimensions of the dispersed particles: 1) Nanoparticles; spherical nanoparticles, nanogranules and nanocrystals; 2) Nanotubes; 3) Nanolayers (Chrissafis and Bikiaris, 2011)

A wide variety of other additives such as plasticizers, anti-plasticizers, processing aids, lubricants and heat stabilizers, highly functional organic molecules including dyes for textiles or film images and pharmaceuticals in drug delivery systems have been incorporated in polymers (Slark and Hadgett, 1999).

1.2.2 Dyes

Dyes absorb electromagnetic energy in the visible range (~350-700 nm) hence they are coloured. They are made up of chromophores and auxochromes. Chromophores are delocalized electron systems with conjugated double bonds where as auxochromes are electron-withdrawing or electron donating substituents (Erkurt et al., 2007). The chromophore imparts the colour to the dye molecule while auxochrome intensifies the colour of the chromophore by altering the overall energy of the electron system. Typical chromophores comprise C=C, C=N, C=O, N=N, $-NO_2$ and quinoid rings. The auxochromes include $-NH_3$, -COOH, $-SO_3H$ and –OH (Kim and Sun, 2000). Figure 1.10 shows an example of a dye with chromophores and auxochromes.

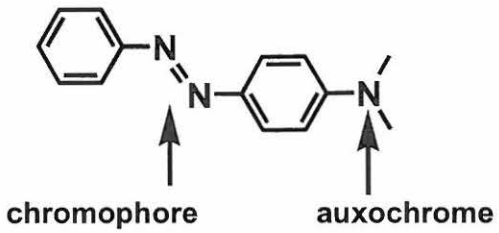

Figure 1.10: Azo dye showing chromophore and auxochrome

Dyes like nanoparticles have strong extinction coefficients in the visible wavelength range. The *molar extinction coefficient* (ε) indicates the strength of a dye at low concentrations and is usually evaluated employing the Beer-Lambert Law (Eqn. 1). As an example, azo dyes have very high extinction coefficients and give bright intensive colours at lower concentrations (Inglot et al., 2009). Due to these optical properties dyes can serve as a platform for visual detections based on colour change. They may be employed for colorimetric determination of analytes either independently or integrated with ligands or biomaterials which exhibit unique recognition, catalytic and inhibition properties. On the other hand, dye based colorimetric assays may be coupled with spectroscopic instruments for quantitative and qualitative measures. However, similar to the growing demand for simple, rapid and flexible online analyses, the development of colorimetric receptors that allow naked-eye detection without the use of any spectroscopic instrument is equally a field of great interest (Sun et al., 2012).

1.2.2.1 Classification of dyes

Dyes may be classified on the basis of chemical structure (colour index names) or chromophore, for example azo (monoazo, disazo, triazo, tetrakisazo, polyazo), anthraquinone, phthalocyanine, triarylmethane, diarylmethane, indigoid, azine, oxazine, thiazine, xanthene, nitro, nitroso, methine, thiazole, indamine, indophenol, lactone, aminoketone, hydroxyketone stilbene and sulphur dyes (Erkurt et al., 2007). They may also be categorized based on their application field (food dyes, textile dyes and spectral sensitizers) (Holčapek et al., 2007). Amongst the plethora of dyes azo and anthraquinone types have been frequently employed for visual detection.

1.2.2.1.1 Azo dyes

Azo dyes are by far the most studied class, accounting for a substantial number of commercial dyes. The azo group is usually attached to two moieties of which at least one, but more frequently both are aromatic groups (benzene or naphthalene rings) (Bindu et al., 2000). The attached groups exist in the *trans* form (see Fig. 1.11) in which the bond angle is approximately 120° and the nitrogen atoms are sp^2 hybridized (Hunger (Ed), 2003). The R group is often an electron-accepting substituent and 'R is electron-donating (e.g. hydroxyl and amino groups in monoazo dyes).

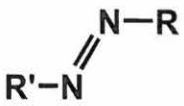

Figure 1.11: The general structure of azo dyes

If composed of one or more heterocyclic groups, the dyes are known as heterocyclic azo dyes. Azo dyes derived from heterocyclic systems exhibit modified dying and optical properties (Zamanloo et al., 2012). Direct influence of hetero-atoms on the molecular orbitals, low aromaticity and hyperpolarizibility along with dependence of energy levels to substituent groups are the most important characteristics of heterocyclic compounds to access the diversity of optical absorption properties.

Azo dyes are versatile and have been widely employed in various fields. For example, in the dyeing of textile fiber, colouring of different materials (e.g. plastics), bio-medical studies, advanced applications in organic synthesis and as thermally stable, solvatochromic probes which have found applications in electro-optical devices and sensors (Raposo et al., 2009). Typical examples of azo dyes include Methyl Orange, Acid Orange, Orange II, Methyl Red, Reactive Red, Reactive Orange, Reactive Black, Congo Red, Solvent Red, Direct Blue, Basic Yellow, Basic Blue, Disperse Orange, Disperse Red, Amido Black, Remazol Brilliant Orange and Amaranth (Rauf et al., 2010). Table 1.1 shows the representative examples of dyes and their respective type. The azo bonds and their associated chromophores and auxochromes including the presence of azo/hydrazone tautomerism have a strong influence on the photo-physical and photo-chemical (e.g. colour) of azo dyes (Saçmacı et al., 2012).

Table 1.1: Representative examples of various types of azo dyes (Rauf et al., 2010)

Class	Representative dye	Structure
Monoazo	Orange II	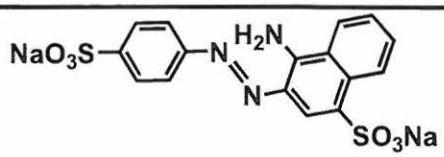
Diazo	Congo Red	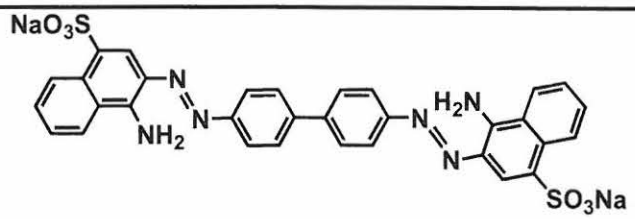
Triazo	Direct Blue 71	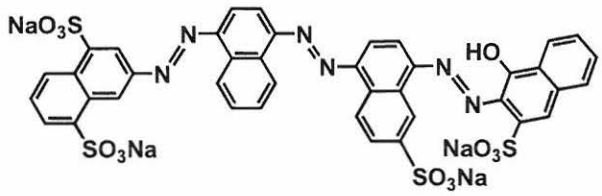

1.2.2.1.2 Anthraquinones

In contrast to azo dyes, which have no natural counterparts, all important natural red dyes are anthraquinones. However, the importance of anthraquinone dyes has declined due to their low cost-effectiveness (Hunger (Ed), 2003). Anthraquinone dyes are based on 9, 10-anthraquinone (Fig. 1.12), which is essentially colourless. Introducing strongly electron-donating groups (amino or hydroxyl) into one or more of the four positions (1, 4, 5 and 8) has led to the production of commercially useful dyes. For optimal opical properties of anthroquinones primary, secondary amino groups and hydroxyl groups are employed. These groups (OH<NH_2<NHR<HNAr) are known to induce a maximum degree of π orbital overlap, enhanced by intramolecular hydrogen-bonding, with minimum steric hindrance. An appropriate selection of donor groups and substitution patterns gives rise to a wide variety of colours.

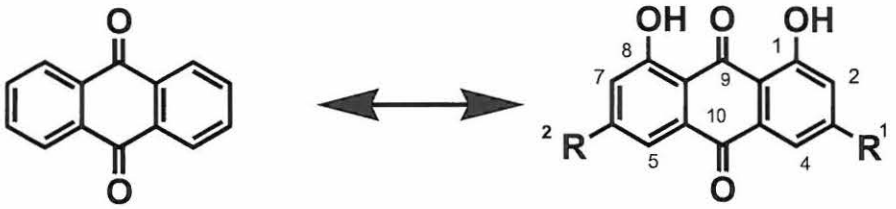

Figure 1.12: Anthraquinone structure (Agarwal et al., 2000)

1.2.2.1.3 Biomimetic dyes

Azo dyes and anthraquinone monochlorotriazine dyes are among the most commonly used dyes in enzyme studies (Labrou and Clonis, 1995). The main challenge with these synthetic dyes is their relative lack of selectivity compared to biological ligands (Mazitsos et al., 2002). With the aim to alter binding specificity of synthetic dyes, strategies have been developed towards creating dye-ligands of superior affinity for target protein such as enzymes (Burton et al., 1988). Thus the 'biomimetic' dye concept. Biomimetic dyes mimic the structure or binding mode of natural biological ligands.

Biomimetic interactions include protein molecular modeling with ligand docking for target enzymes, such as the ketocarboxyl-group recognizing l-malate dehydrogenase or glutathione-group targeting formaldehyde dehydrogenase. Figure 1.13 shows an example of a biomimetic dye-ligand that is widely used in immunodiagnostics and molecular biology.

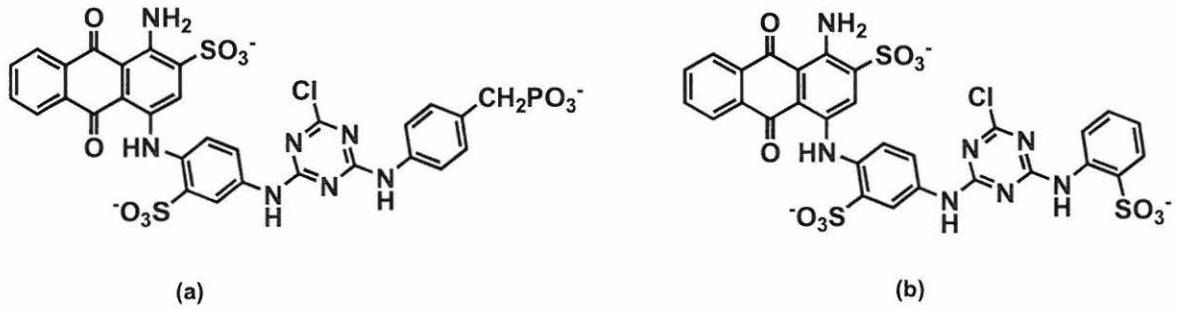

Figure 1.13: Structures of the anthraquinone triazine dyes; (a) phosphono-biomimetic and (b) Cibacron blue 3GA (Clonis et al., 2000)

There have been a substantial number of investigations into incorporation of dyes in various matrices. Dye-polymer systems were of a particular interest to studies conducted for this thesis. The mechanism by which dye solutes specifically interact with a variety of polymer structures has been investigated (Slark and Hadgett, 1999).

1.2.3 Dye-Polymer Systems

Polymers are made of long flexible molecules (macromolecules) which are characterized by a backbone of atoms connected through single covalent bonds. In such chemical bonds electrons reside in low level orbitals with a very large energy gap between bonding and antibonding orbitals. This electronic transition is the reason why natural and man-made polymers are colourless (Ciardelli et al., 2013). The rigid backbone adversely affects the typical viscoelastic behaviour of polymers, which usually leads to the high entropy gain provided by the easy coiling of the flexible chains.

The basic principle of the chromogenic polymer composites is based on colour changes in absorption or in emission associated with the structural modification of the molecular assemblies of dyes dispersed in the continuous polymeric amorphous phase (Pucci et al., 2011). Depending on both the processing conditions and dye-polymer interphase interactions (which are related to the chemical nature of both guest and host components), molecularly dispersed (monomeric, M form) dye molecules can aggregate (A form) in either the ground or excited state to yield stacked structures of at least two molecules (Fig. 1.14).

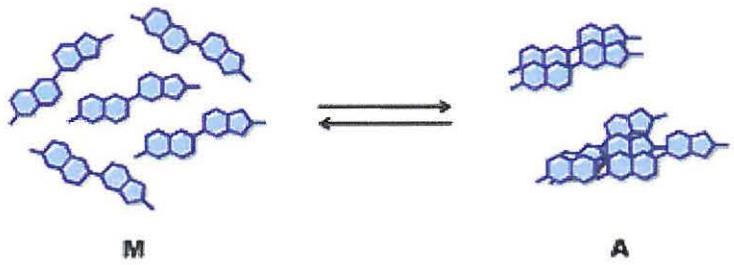

Figure 1.14: Equilibrium between the monomeric form (M) and the aggregated form (A) of a generic dye molecule (Pucci et al., 2011)

There are two possible procedures used to prepare materials showing optical responses to visible light. One approach is based on dispersing the appropriate dye in the bulk of the pristine colourless polymer matrix (Ciardelli et al., 2013). Here, the macromolecules remain structurally unaltered and the system is generally biphasic unless the resulting dyes are fully soluble in the native polymer. The resulting optical behavior of the coloured polymeric material (probe) is driven by specific interactions occurring between the macromolecule and the chromophore providing also innovative characteristics and responsive character upon external stimuli. Once a mechanical force is applied to the polymer–dye system, the macromolecule chain slippage and reorganization promote the break-up of non-covalent interactions among chromophore molecules and their mixing within the polymer matrix (Fig. 1.15).

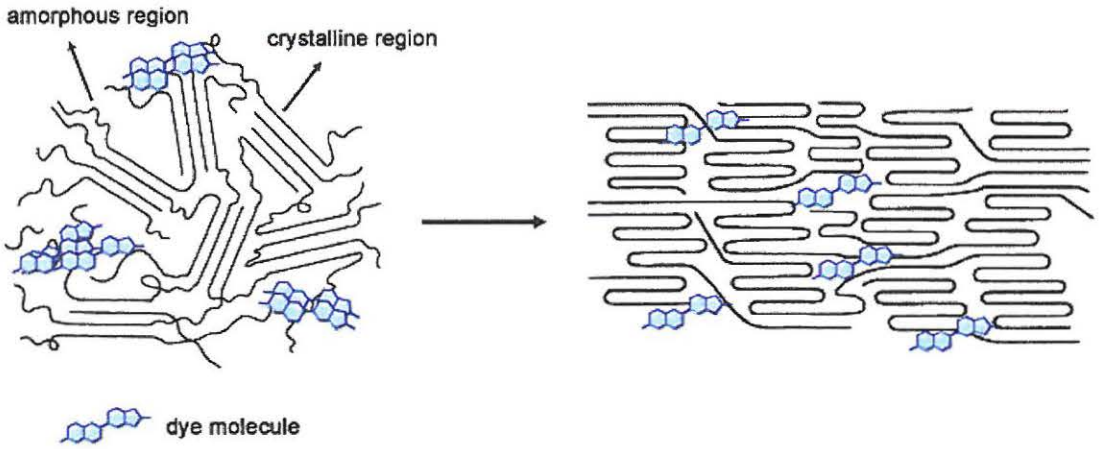

Figure 1.15: Shear induced mixing between a generic aggregachromic molecule and polymer phase caused by the macromolecular reorganization due to a mechanical stress (Pucci, et al., 2011 and Cardelli et al., 2013)

The second approach consists of chromophoric units covalently inserted into the macromolecular chains, allowing the backbone to remain stable and flexible (Ciardelli et al., 2013). The modified macromolecules form a polymeric material with colour and intensity determined, respectively, by the selected chromophore and the extent of chemical modification in terms of chromophore concentration. The resulting coloured macromolecules have the structure of a copolymer, with random or block distribution of colourless and coloured monomer residues. Another very interesting kind of dye–polymer conjugates are polymer chains carrying dyes at specific positions, such as the chain-end or the mid-chain. This type of dye-polymer conjugates is employed where precise location of the dye is crucial to provide a given property to the material or to understand some physicochemical phenomena (Beija et al., 2011).

The vigorous development of polymeric science and extensive utilization of polymeric materials in technology has led in recent years to the increased interest in the preparation and characterization of polymers and their composites (Lagashetty (Ed), 2005). Characterization techniques include X-ray diffraction (XRD), atomic force microscopy (AFM), scanning and transmission electron microscopy (SEM and TEM), ultraviolet visible spectroscopy (UV–Vis), Fourier transform infrared spectroscopy (FTIR) and light scattering technique.

1.3 Diagnostic tests

Diagnostic tests are of paramount importance in many fields. Figure 1.16 is a summary of the various fields and application of diagnostics. Based on application, diagnostic tests employ various techniques such as electrochemistry, photoluminescence, spectrophotometry, colorimetry and fluorescence. In addition, the majority of these diagnostic tests are based on specific interactions between biomolecules, most often antibodies and antigens or between complementary strands of nucleic acids (Slomkowski and Basinska, 2010). However, direct observation of these interactions is difficult due to small dimensions of biomolecules. There have also been developments in a variety of indirect methods suitable for detection of antigen-antibody interactions. However, properties of nano and microspheres make these particles especially valuable as candidates for development of diagnostic tests. For studies conducted in this thesis colorimetric type of diagnostics are of interest. In most diagnostic laboratories, colorimetric analyses employ complex and expensive analyzers requiring large power supplies. Although some of the instruments are automated and able to perform more than 100 runs per hour, still there is a need for development of simple, small and light, low cost, and portable devices for routine analysis particularly in clinical and environmental fields (Sorouraddin et al., 2010).

With the advent of nanomaterials and their base technologies, there has been a rise in new and exciting possibilities for applications in medical, aerospace, catalysts, batteries, nonvolatile memories, sensors, insulators, colour imaging, printing, flat panel displays, waveguides, modulators, computer chips, magneto-optical discs, transducers, photodetectors, optoelectronics, solar cells, lithography, holography, photoemitters, molecular sized transistors and switches, drug delivery, medicine, medical implants, pharmacy, cosmetics, and several others (Chandra et al., 2013). Among the nanomaterials, gold nanoparticles have gained considerable attention in recent years for application in colorimetric analysis. This is mainly due to the interesting properties of Au NPs such as size dependent chemical, electronic and optical properties as well as chemical stability, non-toxicity and easy to functionalize.

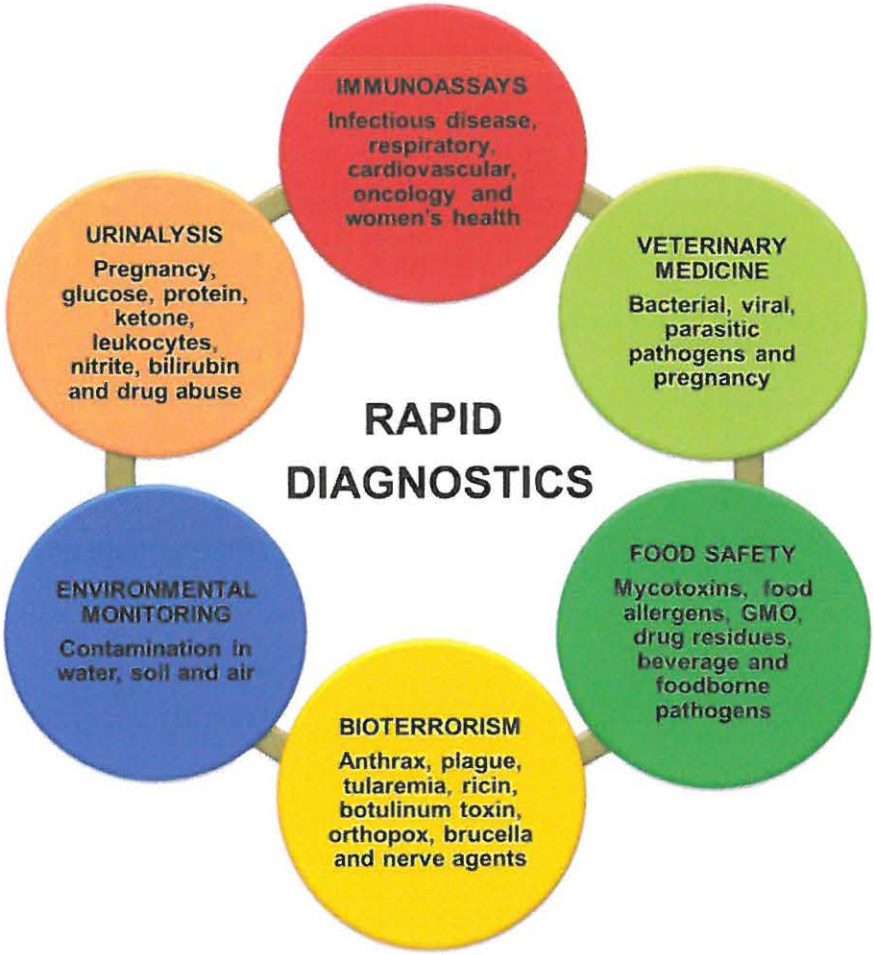

Figure 1.16: The array of rapid tests: urinalysis, immunoassays, veterinary diagnostics, food safety, environmental, biothreats, drug abuse. Rapid diagnostic tests often have lower specificity and sensitivity than their laboratory bench counterparts. The majority of these tests is simple and provides a yes/no answer where response time is critical to the user [Adapted from Yetisen et al.,](Yetisen et al., 2013)

1.3.1 Gold nanoparticles based diagnostic probe

Owing to the ease of functionalization gold nanoparticles are a promising platform for various types of applications. For instance, in sensing and diagnosis, biomolecule conjugated Au NPs provide assays with increased sensitivity and selectivity. With these advantages in diagnostic sensing and therapy, Au NPs have been established as a valuable tool within the realm of life science. The versatile functions (Fig. 1.17) of Au NPs were highlighted in a review on development of Au NP-based sensors (Lu et al., 2012).

Figure 1.17: A graphical highlight on the progress in using gold nanoparticles for the applications in diagnostic sensing and therapy (Lu et al., 2012)

Gold nanoparticles may be a good chromogenic dye for the development of a colorimetric sensing system because Au NPs with extinction coefficients, 3 - 5 orders of magnitude higher than those of organic dye molecules, as well as exhibit unique distance-dependent optical properties that can be programmed chemically using specific host compounds that can induce a dramatic red-to-blue colour change in Au NPs (Klein et al., 2010, Kim et al., 2001). However, dyes are also known to form stable bonds with analytes, in particular reactive dyes and in terms of cost dyes are cheaper than gold.

1.3.2 Dye based diagnostic probes

Organic or inorganic chromophores such as dyes with available delocalized electrons or metal derivatives constitute the basis of the sensing mechanism since they confer to the material a variation in the opto-electronic features in order to be able to respond to stimulus (Ciardelli et al., 2013, Pucci et al., 2011). Among the plethora of dyes, azo dyes provide a whole range of colours from which the most popular are red, orange, brown and yellow. Therefore azo dyes are the most popular group of dyes and have found many applications in industry (Bauman et al., 2009). Additionally, azo dyes have a very high extinction coefficient and give bright, intensive colour by using small concentrations. Because of the large change of the dipole moment at π - π^* electronic transition from the ground to the excited state (charge transfer transition) azo dyes have application in many systems (Inglot et al., 2008). As an example, Zhang's group (Zhang et al., 2006) have developed a simple colorimetric method for the determination of cysteine (Cys) and homocysteine using azo dyes that contain an aldehyde group. The azo dye employed was selective to cysteine and homocysteine over other amino acids. It was demonstrated that upon addition of Cys, the absorption intensity at 515 nm decreased with the concomitant formation of a hypsochromically shifted band peaked at 475 nm, corresponding to a colour change from pink to yellow, which were clearly visible to the naked eye (Fig. 1.18).

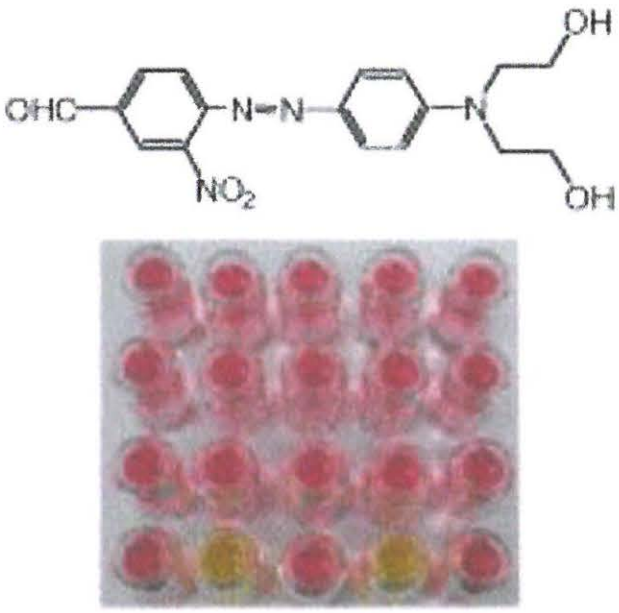

Figure 1.18: Graphic representation of simple colorimetric method for the determination of cysteine and homocysteine using an azo dye with the shown chemical structure (Zhang et al., 2006)

Colorimetric methods for serum aspartate amminotransferase, based on reacting oxalacetic acid with a diazonium salt, have been in widespread use since 1962 (Babson et al., 1962). The dye used then was Fast Violet B salt (6-Benzamido-4-methoxy-m-toluidine diazoniumchloride), with modifications and developments more azo dyes possessing much better qualities are now in use. The dyes include Fast Blue RR salt (4-amino-2.5-dimethoxybenzanilidine diazonium chloride), Fast Red TR Salt hemi(zinc chloride) salt (4-chloro-2 methylbenzenediazonium salt), Fast Red RC salt, (5-chloro-2-methoxyaniline-1-diazonium chloride) and Fast Red Violet LB Salt (5-Chloro-4-benzamido-2-methylbenzenediazonium chloride hemi(zinc chloride) salt).

Regardless of the colorimetric protocol, sensitivity and selectivity are of paramount importance to diagnostic assays. An array of innovative designs has therefore been geared towards highly sensitive and selective detection of a range of analytes in clinical and environmental applications.

Chapter 2

Environmental contaminants and Clinical enzyme biomarkers

2.1 Environmental contaminants

A diverse array of environmental contaminants has been detected in varied matrices such as in food substances, indoor air, workplace air, ambient air, surface and ground water, soil, sediments and aerosols. Examples of these contaminants include pharmaceuticals, dioxins, hormones, synthetic musk fragrances, polycyclic aromatic hydrocarbons, perfluorinated compounds, heavy metals and some of their organo-metallic species. Physicochemical properties of these chemicals are wide-ranging and so are their impact on the global environment and the quality of life of many living species (Seethapathy et al., 2008). This diversity often poses a challenge for their monitoring as the contaminants are usually present in complex and in trace concentrations.

Most aquatic monitoring programmes rely on collecting discrete grab, spot or bottle samples of water at a given time. Often, where pollutants are present at only trace levels, large volumes of water need to be collected. The subsequent laboratory analysis of the sample provides only a snapshot of the levels of pollutants at the time of sampling. However, there are drawbacks to this approach in environments where contaminant concentrations vary over time, thus episodic pollution events can be missed (Vrana et al., 2005).

According to Petty et al. almost all currently employed analytical and biomonitoring based sampling techniques are inherently limited in their ability to provide a holistic exposure assessment because: (1) they lack the capability to integratively sample through time, i.e., sampling represents one or more points in time, (2) analytical sensitivity and selectivity are insufficient to detect and quantify ultra-trace to trace levels of complex mixtures of contaminants in water, (3) site conditions (e.g., water quality) impact the survival of sentinel organisms (e.g., caged fish or bivalves) and exposure information is lost due to species-specific metabolism and depuration of contaminants of interest, and (4) causal links between observed biological effects and environmental contaminant mixtures are seldom established (Petty et al., 2004). To curb the challenges posed by the sampling techniques there has been an increasing number of pocket-sized chemistry equipment based on the so-called lab-on-a-chip approach.

These chips, in combination with portable electronic equipment, are applicable in, for example, "point-of-care" ion analysis of body fluids, forensics, identification of explosives, tracking of pollution in environmental or waste waters, monitoring nutrients in agricultural or horticultural water, controlling quality in food production, or process control in the chemical industry (Gardeniers and van den Berg, 2004). There are however, good alternatives to techniques that employ some form of instrumentation, that offer possibilities for on-site and naked-eye rapid detection to analytes with bio- medical, clinical, food safety and environmental significance (Vilela et al., 2012). The techniques explore the use Au NPs-based colorimetric assays.

For example, a gold nanoparticles based colorimetric assay for direct detection of binding interactions between nuclear hormone receptors and their corresponding DNA-binding elements, the human estrogen receptors (ERα) has been reported (Tan et al., 2010). The colour changes, following a proposed mechanism in Fig. 2.1, were from red to blue for ERα containing solutions.

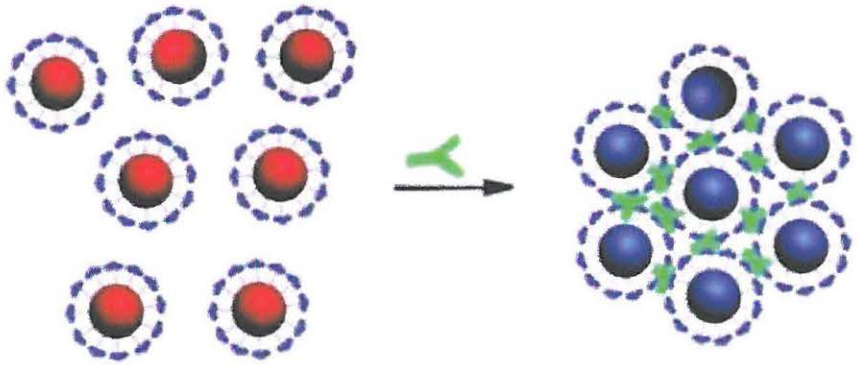

Figure 2.1: Visual detection based gold nanoparticles aggregation induced by chemical interaction between the analyte (e.g. environmental contaminant) and nanoparticles surroundings leading to a change of colour (red to blue for Au NPs) (Adapted from Vilela et al., 2012)

Most of the mentioned contaminants include endocrine disrupting chemicals (EDCs). The potential impact of endocrine disrupting contaminants on aquatic ecosystems has become a subject of vast interest in the scientific community as well as in the general public. Elevated levels of plasma vitellogenin, a biomarker for endocrine disruption, were observed in male fish exposed to effluents from wastewater treatment plants or in rivers downstream of the effluent discharge points (Ying et al., 2009).

2.1.1 Endocrine Disrupting Chemicals (EDCs)

Environmental endocrine disrupting chemicals have been defined by the US Environmental Protection Agency as:

> "exogenous agents that interfere with the synthesis, secretion, transport, binding, action, or elimination of natural hormones in the body which are responsible for the maintenance of homeostasis, reproduction, development, and/or behavior" (US Environmental Protection Agency) (US, 2001).

Studies show that reptiles living in contaminated environments exhibit: (1) population declines due to the lethal and reproductive effects of the contaminants on embryos, juveniles or adults; (2) developmental abnormalities of embryos, including subtle effects in the reproductive system of alligators and (3) abnormalities of the endocrine system (Hopkins et al., 2006). Numerous studies have demonstrated that any environmental pollutant that disrupts the normal steroid milieu of the developing embryo will have significant lifelong consequences on sex determination and on the organization and function of the reproductive and endocrine systems (Guillette et al., 2000). The most prominent classes of chemicals that contain EDCs are natural estrogens, phytoestrogens, pesticides (methoxychlor), surfactants (nonylphenol), plasticizers (diethylphthalate, BPA) and organohalogens (polychlorinated biphenyls (PCBs) and dioxin) (Gültekin and Ince, 2007). Estrogens are a concern because low concentrations (10–100 ng/L) in water can adversely affect aquatic vertebrate species such as fish, turtles and frogs by disrupting the normal function of their endocrine systems (Hanselman et al., 2006).

2.1.1.1 Estrogenic endocrine disruptors

Steroidal estrogens are a large group of lipophilic, low-molecular weight, high estrogenic active compounds, which could be roughly classified as natural and synthetic estrogens. Natural estrogens (also called endogenous estrogens) include estrone (E_1), 17β-estradiol (E_2) and estriol (E_3), while 17α-ethynylestradiol (EE_2) used in oral contraceptives is a synthetic estrogen (Wang et al., 2011a). Figure 2.2 shows the molecular structures of steroidal estrogens. Some industrial chemicals such as non-ionic surfactant degradation products 4-*t*-octylphenol (4-*t*-OP), 4-nonylphenols (4-NP) including their mono- and di-ethoxylates (NPE1-2) and bisphenol-A (BPA), used in the manufacture of epoxy resins and polycarbonate plastics, were also found to posses disrupting trends, but to a lesser extent in estrogenic activities since these xenoestrogens are less potent compared with estrogens (Ying et al., 2009). For instance, bisphenol-A estrogenic potency *in vitro* is 10^{-3} to 10^{-4} relative to that of estradiol, and 4×10^{-4} to 10^{-5}*in vivo* relative to that of diethylstilbestrol (Gültekin and Ince, 2007).

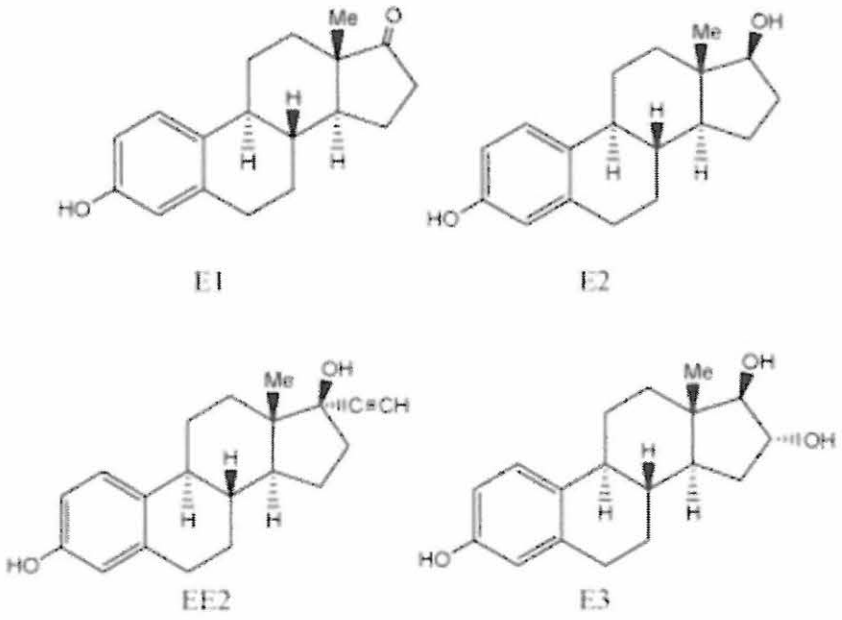

Figure 2.2: Chemical structures of estrone (E_1), 17β-estradiol (E_2), estriol (E_3) and 17α-ethynylestradiol (EE_2)

The physicochemical properties of estradiol, estrone, and estriol as well as 17α-ethynylestradiol are given in Table 2.1. Unconjugated estrogens are known to have low aqueous solubility (0.8-13.3mgL-1) and are moderately hydrophobic (log *K*ow 2.6-4.0). They are also nonvolatile (vapor pressure 9 x 10^{-13} - 3 x 10^{-8} Pa) and weak acids (p*K*a, 10.3-10.8). Estrogen conjugates on the other hand are characterized by much greater aqueous solubility than unconjugated estrogens due to their polar glucuronide or sulfate functional groups (Hanselman et al., 2003). Steroidal estrogens completely ionize in alkaline conditions e.g. in 0.1 N NaOH.

Table 2.1: Physicochemical properties of the analytes, estradiol, estrone, estriol and 17α-ethynylestradiol (Hanselman et al., 2003)

Analyte	Molecular weight (g/mol)	Water solubility (mg/L)	$logK_{ow}$	pK_a
Estrone (E_1)	270.4	12.4	3.13	10.5
17β-Estradiol (E_2)	272.4	13.3	4.01	10.7
Estriol (E_3)	288.4	13.3	2.8	10.4
17α-Ethynylestradiol (EE_2)	296.4	11	3.67	10.4

Estrogens have been described as triple-edged swords (Watson et al., 2011). Insufficient dozes of estrogens leads to complications in women, such as reproductive failure, bone loss, hot flashes, skin changes, some cardiovascular system vulnerabilities and cognitive declines. Excessive estrogens on the other hand lead to more detrimental effects including cancers such as for the breast, uterus, colon and pituitary or other malfunctions such as blood clots and nausea/eating disorders (Tchaikovski and Rosing, 2010). In addition, exposure to the wrong estrogens (xenoestrogenic mimetics) could result in endocrine disruption of functions normally mediated by physiologic estrogens (Colborn et al., 1993).

The impact of environmental estrogens (both natural and synthetic) found in waterways has been intensely investigated due to adverse effects resulting from the ability of these estrogens to mimic or disrupt the natural estrogens found in humans and animals. Estrogenic chemicals of varying potency and persistence originate from agriculture, industry, humans, household products, and other pharmaceuticals (Diamanti-Kandarakis et al., 2009, Arnold et al., 2013). Figure 2.3 illustrates the various points of entry into waterways for estrogenic chemicals.

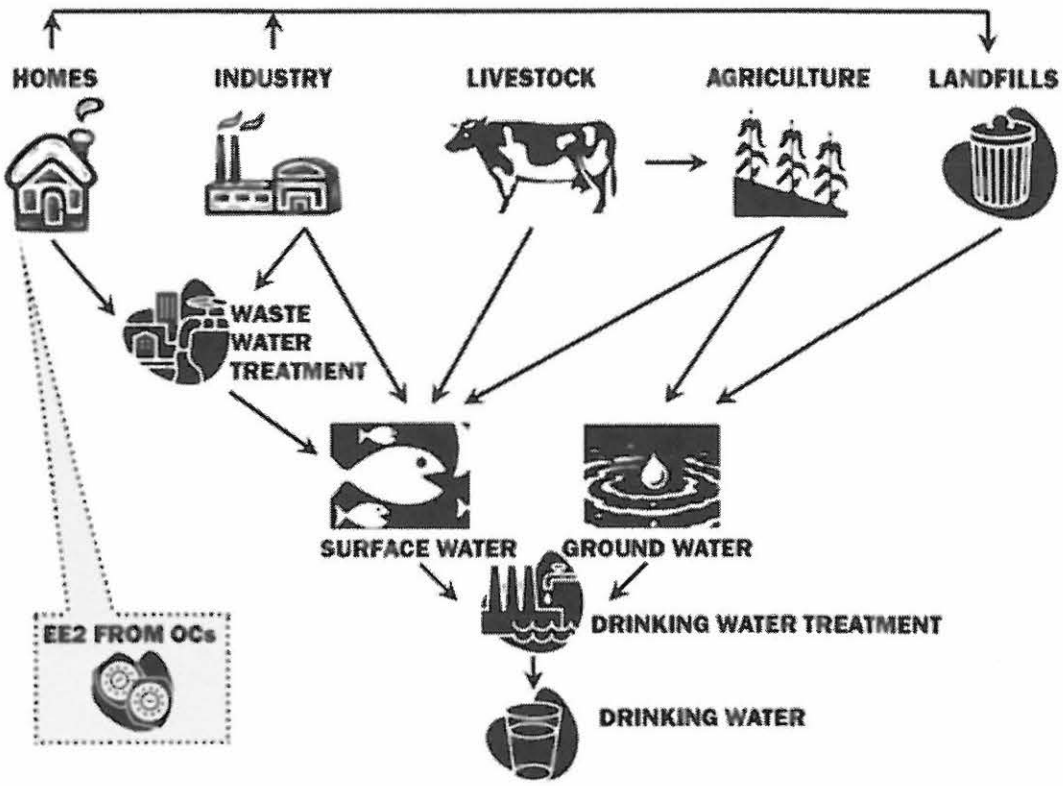

Figure 2.3: The various points of entry into waterways for estrogenic chemicals (Wise et al., 2010)

Livestock excrete the same natural estrogens (E_1, E_2, and E_3) as humans and there is a growing body of research showing elevated estrogen levels in surface and groundwater downstream of farms and agricultural land. The effluents are untreated, and their use as an agricultural fertilizer is growing. In addition to spreading manure for fertilizer, livestock waste can enter the environment when rain causes overflow, or from runoff and leaching into the soils near manure storage facilities. Figure 2.4 shows an example of a typical scenario as to how livestock effluents and runoff from manure are likely to be a significant source of natural estrogens in the waterways. The agricultural studies indicate that livestock effluents and runoff from manure are likely to be a significant source of natural estrogens in the waterways and have the potential to reach drinking water (Hanselman et al., 2006, Wise et al., 2010).

Figure 2.4: A photograph showing a typical scenario of how livestock effluents and runoff from manure are likely to be a significant source of natural estrogens in the waterways

Dairy farming wastewater contains significant concentrations of natural steroidal estrogens such as 17α-estradiol, 17β-estradiol, and estrone that can potentially contaminate surface and ground water (Hanselman et al., 2006, Zheng et al., 2008). Like other estrogenic contamination of surface waters feminization of male fish, reproductive abnormalities and skewed sex ratios is also a major concern (Oishi and Moriuchi, 2010, Gadd et al., 2010). Within the estrogenic contaminants 17β-estradiol (E_2) has emerged as a target for recognition and analysis due to its dual role (Chiu et al., 2008) 17β-estradiol plays an important function during the various stages of mammalian development, including growth and reproduction. However, E_2 is also the most potent naturally occurring estrogen as it has the highest estrogenic activity at ng/ℓ concentrations (Hanselman et al., 2003). Although several detectors, in particular, flame ionization or mass spectrometric detection coupled with GC have had significant achievements in the determination and quantification of estrogenic steroid hormones in aqueous samples (Wang et al., 2011b), they are expensive, sophisticated and require extensive sample handling. Owing to the current detection drawbacks simple, rapid, reliable and cheaper protocols are highly desirable for analysis of estrogenic steroid hormones.

2.2 Clinical enzyme biomarkers

The clinical diagnostic market presents a unique opportunity for the introduction of biosensors on a widespread commercial basis. Successful biosensors have since been launched in this field or many others, with many promising ideas. According to Connolly (Connolly, 1995), the need for biosensors in the clinical diagnosis must be analyzed more critically, to assess in which direction the developing biosensor technology can be most effectively utilized and which areas need a more focused approach from basic research in bioelectronics. In addition, the diagnostics market is already a highly competitive field; from an industrial perspective, some of the critical issues that need to be taken into consideration when evaluating biosensor projects are: costs per test, regulatory requirements, quality control, instrumentation design and test parameter selection (Connolly, 1995).

The International Union of Pure and Applied Chemistry (IUPAC) has defined a biosensor as a specific type of chemical sensor comprising a biological recognition element and a physico-chemical transducer. The biological element is capable of recognizing the presence, activity or concentration of a specific analyte in solution. The recognition may be either a binding process (affinity ligand-based biosensor, when the recognition element is, for example, an antibody, DNA segment or cell receptor) or a biocatalytic reaction (enzyme-based biosensor). The interaction of the recognition element with a target analyte results in a measurable change in a solution property, such as formation of a product. The transducer converts the change in solution property into a quantifiable electrical signal. The mode of transduction may be one of several approaches, including electrochemical, optical and the measurement of mass or heat (Thévenot et al., 2001).

This thesis however, is mainly focused on self-contained sensor types, probes, rather than on sensors used for measurements in biological fluids, comprising a biological recognition element or a physical electronic transducer (e.g. electrodes for measurement of glucose, pH and blood gases).

Development of the single-use, disposable electrochemical test strip for blood glucose has driven the need to develop inexpensive sensor mass fabrication techniques easily adaptable to the sensing technology. However, for most approaches developed there was a necessity to separate analytes free from bound label, requiring washing and separation steps, adding to the complexity of the assay. In one example of a separation-free technique, an immunosensor was developed (Fig. 2.5) where an anti-hCG antibody was covalently immobilized on gold-coated, microporous nylon membrane (pore size 0.2 μm). The membrane served as both the solid support for the sandwich immunoassay and working electrode for the amperometric sensor (D'Orazio, 2003).

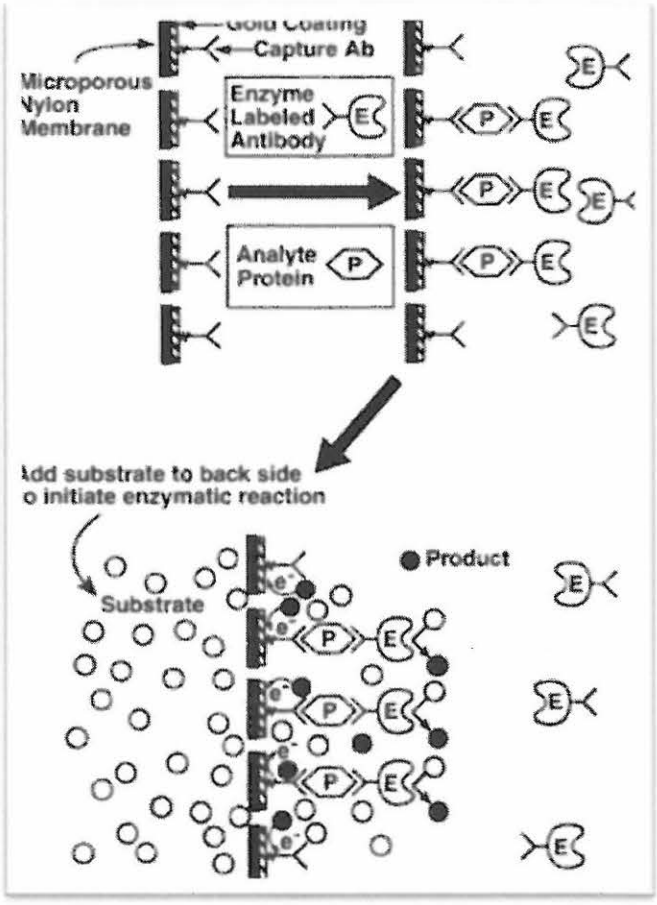

Figure 2.5: Reaction scheme for a non-separation electrochemical enzyme immunosensor for detecting proteins in undiluted samples, based on a gold-coated microporous nylon membrane (D'Orazio, 2003)

Experts claim that leaving an enzyme in its native environment would optimize its biological activity and improve sensor characteristics. Sensitive markers of enzymes/disease are therefore a major necessity. Traditional markers of conventional clinical chemistry and histopathology method were of interest since the markers are normally not region-specific and only increase significantly after serious disease or injury. The ideal biomarkers are those that will identify disease early, resulting in early treatment before irreparable damage has occurred (Zhang et al., 2012).

A biomarker is defined as

"A characteristic that is objectively measured and evaluated as an indicator of normal biologic processes, pathogenic processes, or pharmacologic responses to a therapeutic intervention" (Atkinson et al., 2001).

Biomarkers have further been classified into hierarchical systems based on their ability to assess natural history (type 0: prognosis), biological activity (type 1: response to therapy), and therapeutic efficacy (type 2: surrogate for clinical efficacy) (Mildvan et al., 1997). Broadly, biomarkers may be classified into molecular and imaging biomarkers. In general, molecular biomarkers refer to non-imaging biomarkers that have biophysical properties, which permit their measurement in biological samples (e.g., plasma, serum, CSF, bronchoalveolar lavage, biopsy). Molecular biomarkers include nucleic acids-based biomarkers such as gene mutations or polymorphisms, gene expression analysis, peptides, proteins, lipid metabolites, and other small molecules. Biomarkers are diverse in function, they may be employed for; confirmation of diagnosis; epidemiological screening; predictive testing and monitoring disease progression following diagnosis; drug development and response to treatment as well as learning brain-behavior (Sharma et al., 2013).

In vivo as well as *vitro* diagnostic markers have been developed for various diseases and these biomarkers facilitate early non-invasive and effective treatment. Of interest for this thesis are biomarkers for hepatotoxicity.

2.2.1 Biomarkers for hepatotoxicity

Liver injury may be classified as: acute or chronic hepatitis/cholestasis; zonal or nonzonal primary hepatic necrosis; reversible hepatic changes such as steatosis, glycogen accumulation, or centrilobular hypertrophy due to P450 enzyme induction; preneoplastic/neoplastic patterns of hepatic injury; mixed histological patterns due to a combination of lesions; and nonspecific changes that are secondary to other systemic and metabolic diseases (Ramaiah, 2007). The liver injury classifications guide the mode of liver function tests. The tests are further based on primary liver metabolic and excretory functions under treatment conditions (or disease state). Conventional liver function assays include serum bilirubin, serum albumin, and plasma prothrombin time (PT). In addition to these, selected hepatic enzymes that are representative of cellular disruption or damage to organelles when elevated in the plasma are used routinely as conventional preclinical biomarkers of DILI. These include enzyme biomarkers of cholestasis such as alkaline phosphatase (ALP), 5′-nucleotidase and gamma-glutamyl transferase (GGT); and enzymes that are indicative of hepatocellular cytotoxic effects such as alanine aminotransferase (ALT), aspartate aminotransferase (AST) (Ozcanli et al., 2006, Okafor et al., 2011) and sorbitol dehydrogenase (SDH) (Ozer et al., 2008, Amacher, 2010).

Aspartate aminotransferase (AST) and alanine aminotransferase (ALT) are found mainly in the liver. Their levels are a good indicator of liver function as their concentrations levels reflect its health status (Huang et al., 2006). These hepatic enzymes (alkaline phosphatase, alanine aminotransferase, albumin, gamma-glutamyl transferase and glutathione-S-transferase) including proteins released into the blood stream by damaged liver cells are useful tools available in detecting liver damage/toxicity in a non-invasive manner (Gonzalez et al., 2012).

2.2.2 Catalytic reaction of Enzymes

Since enzymes do not get consumed in the reaction, when transforming a specific substrate molecule into a product, they allow for continuous bio-sensing of a specific compound. Among other advantages enzymes are highly selective and sensitive compared with other catalysts, they are fairly fast-acting in comparison with other biological receptors (Marazuela and Moreno-Bondi, 2002). Additionally the catalytic activity of enzymes also allows lower limits of detection compared to common binding techniques.

Enzymes are very specific to the substrates (reactants) and reactions that they can catalyze. Enzymes work by binding the substrate into a favorable orientation in an enzyme-substrate complex (an intermediate in the reaction), which promotes the making and breaking of chemical bonds. The substrate is bound to the active site (a specific region of the enzyme), then converted to a product and finally be released from the active site. The active site is a three-dimensional crevice, and is usually only a small portion of the total volume of the enzyme (Fig. 2.6)

To be specific, the substrate is "bound" to amino acids in the active site of the enzyme by multiple intermolecular interactions, including charge-charge interactions (electrostatics), hydrogen bonding, and van der Waals forces. Enzymes are often very sensitive to changes in pH and temperature, in part because these changes can affect the shape and charge of the active site, thus changing the interaction with a substrate. If the optimal conformation of the enzyme is lost, the enzyme becomes nonfunctional (*i.e.*, the substrate can no longer bind to active site) (http://science.jrank.org). Among the myriad of enzymes aspartate aminotransferase is one of the most important enzymes for liver toxicity diagnosis and it has a well known clinical significance (Lee et al., 2012).

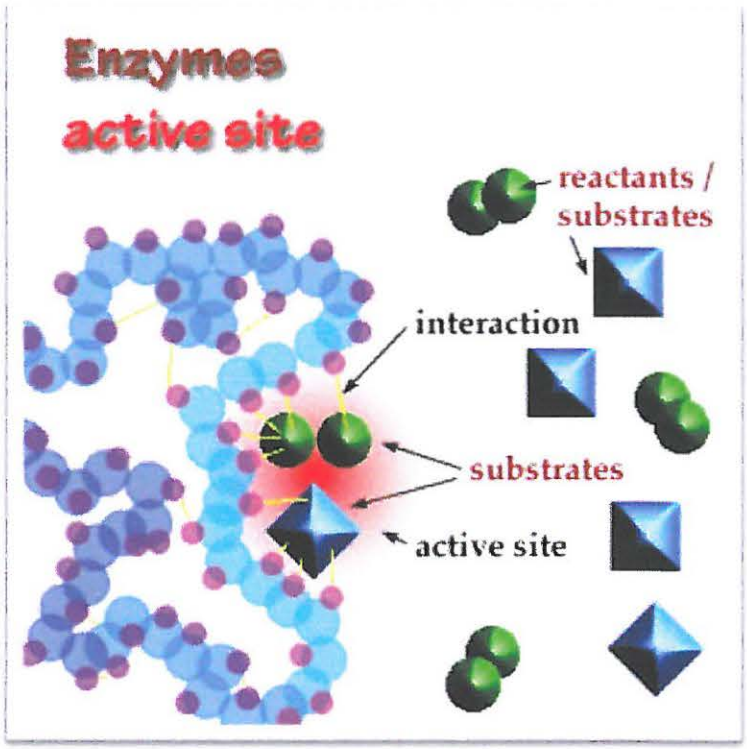

Figure 2.6: A schematic diagram showing the active site of an enzyme

2.2.2.1 Catalytic efficiency of aspartate aminotransferase

Aspartate aminotransferase is a key enzyme of cell metabolism that catalyses the amino group transfer from an amino acid to a keto acid molecule. The study of the physicochemical and kinetic reaction of enzymatic transamination between L-aspartate and 2oxo-glutamate and between L-glutamate and oxaloacetate has shown that the reaction proceeds according to a "ping-pong" mechanism. Aspartate Aminotransferase is a dimer consisting of two sub units identical in primary structure. Figure 2.7 shows an aspartate aminotransferase homo dimer, active sites are highlighted in red and blue.

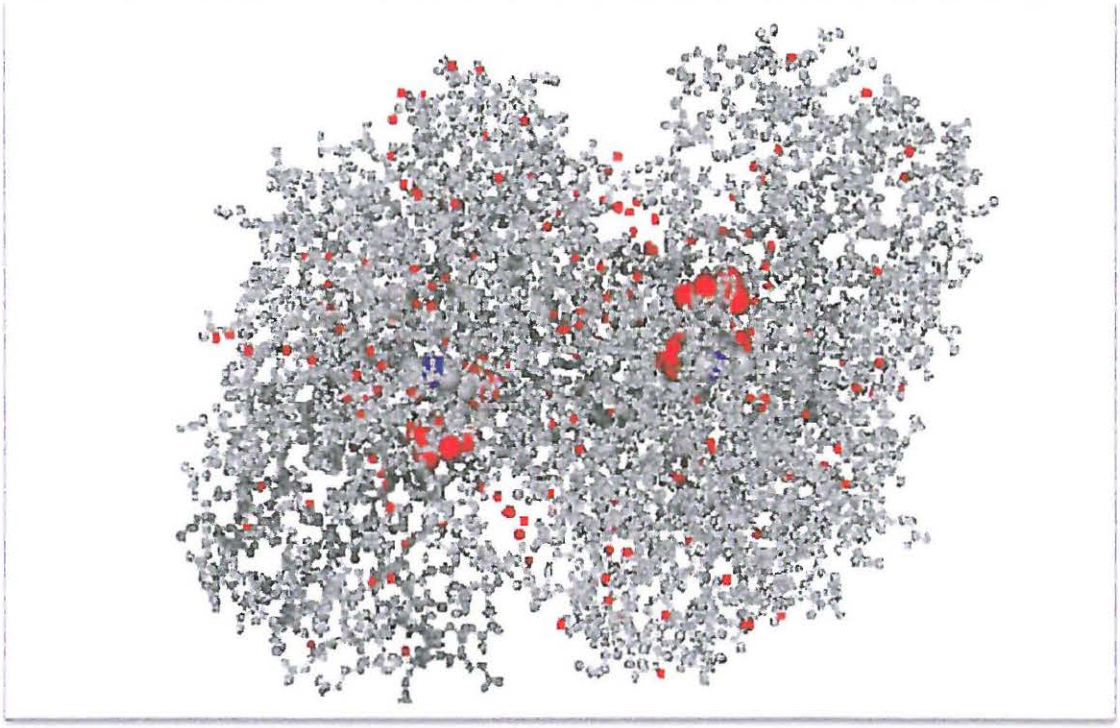

Figure 2.7: Aspartate aminotransferase homo dimer, active sites are highlighted in red and blue (http://www.chemaxon.com/)

Each active site is formed by amino acid residues belonging to both sub units and as a result the dimeric molecule is the catalytic unit of the enzyme (de la Torre et al., 2009).

2.2.3 Aspartate aminotransferase as liver toxicity biomarker

Aspartate aminotransferase can also be found in spinal fluid (Riemenschneider et al., 1997), urine (Wei et al., 2008) as well as in plasma (Howie et al., 1992) hence AST diagnosis is not limited to blood analysis only. Aspartate aminotransferase blood levels are normally low (5 to 40 U/L) and increase more than 10 folds the highest normal level usually due to various clinical conditions that include liver toxicity induced by alcohol abuse (González de Requena et al., 2002) or exposure to drugs.

Elevated serum AST in relation to serum ALT has been proposed as an indicator for alcohol induced liver damage (Nyblom et al., 2004). Furthermore, liver toxicity is prevalent in HIV-positive patients as a result of co-infection with hepatitis B and/or C or antiretroviral therapy (Soriano et al., 2006). Antiretroviral therapy is however beneficial to HIV-infected patients as it results in virus suppression and a significant level of immune recovery (Arnold and Parslow, 1995).

Owing to the important clinical diagnostic value of AST a variety of colorimetric assays for aspartate aminotransferase have been devised (Stejskal, 1994, Pari and Suresh, 2008). Aspartate aminotransferase activity may be monitored based on the following transamination reaction in Fig. 2.8.

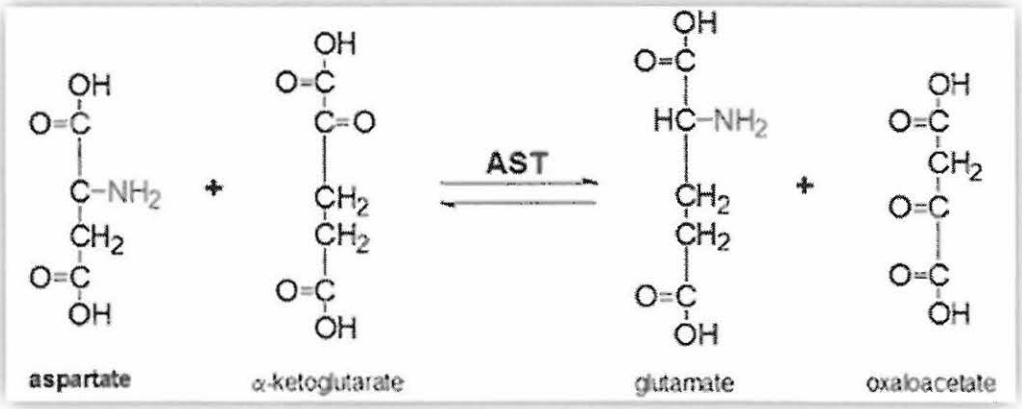

Figure 2.8: Reaction scheme involving aspartate aminotransferase catalysis conversion of L-aspartate and α-ketoglutarate to L-glutamate and oxaloacetate

The rate of reaction is directly proportional to the concentration of AST activity in the sample. The general trend is that the AST reaction may be coupled to a second indicator reaction catalysed by malate dehydrogenase (MDH), which allows AST activity to be monitored spectrophotometrically by measuring the oxidation of NADH to NAD^+ at 340 nm (Huang et al., 2006).

However some of the assays suffer limitations in terms of simplicity and reliability where the defects result mainly from difficulties in preventing interference from the keto acid added as an amino acceptor substrate (Yagi et al., 1985). Furthermore, the spectrophotometer is not only expensive but requires skilled personnel. Thus, it is not everyone who can carry out the assays for diagnostics.

The development of colorimetric probes that allow naked-eye detection without the use of any expensive and sophisticated instrument is of current interest in analytical and clinical fields. As the demand for simple, rapid and low cost point-of-care (POC) diagnostics continues to increase, there is a need to dedicate resources and efforts towards their development. Several diagnostic approaches already exist for enzyme biomarkers. For example, a method has been developed for an approach to biomarker for activated drug release. Enzymes alanine transaminase and aspartate transaminase biomarkers for liver injury were logically processed by a biocatalytic cascade realizing a Boolean AND gate. The system comprised a logically processed biochemical signals with the result that a drug-mimicking material is released only when both biomarker-signals are present at their high pathophysiological concentrations jointly indicative of liver injury (Bocharova et al., 2012). Production of citrate was then indirectly measured for each combination of the inputs using the interaction between the DTNB reagent and a thiol group of CoASH which is produced by the biocatalytic cascade in 1 : 1 stoichiometry to citrate (see Fig. 2.9). However this method is rather complex and requires the use of an expensive instrument to interpret data, which also limits the use of the system by unskilled personnel.

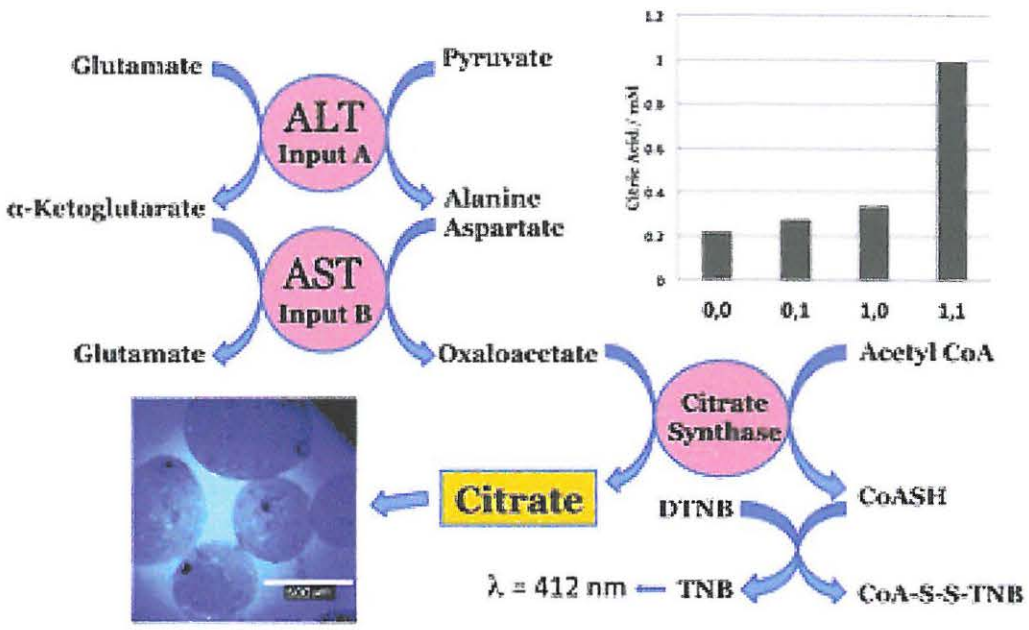

Figure 2.9: Scheme for the biocatalytic cascade mimicking the AND logic gate activated by two input signals, ALT and AST, which are biomarkers for liver injury. The production of citrate, which is the final product of the biocatalytic cascade, is indirectly analyzed by measuring the CoASH byproduct using DTNB-assay for thiol groups. Citrate induces dissolution of the alginate microspheres shown in the micrograph (Bocharova et al., 2012)

Simple and cheaper colorimetric assays are also available for rapid, semiquantitative measurement of AST and ALT in a fingerstick whole-blood specimen. The devices required no external pumps, instrumentation, or power and were both portable and disposable (Pollock et al., 2012). Additionally, the devices have been reported for potential clinical diagnostic applications and have demonstrated both the ability to conduct clinical chemistry, enzymatic, immunoassay, and enzymelinked immunosorbent assay tests on patterned paper, visually and quantitatively, and the viability to sense various analytes, including AST.

Diagnostic platforms based on paper, paper based microfluidic devices, thread and magnetic levitation that are configured to detect simple analytes such as protein, enzymes and glucose, or that employ ELISA to detect and quantify HIV antibodies have been reported. A research group has developed an inexpensive and portable system for measuring the levels of multiple analytes in a drop of blood obtained from a fingerstick (Fig. 2.10). The system comprised a paper chip patterned into hydrophobic and hydrophilic regions, a filter, and self-adhesive laminating sheet. The device is designed to serve four primary functions, to (i) remove red blood cells from plasma; (ii) distribute the resulting plasma into three regions within the paper; (iii) run three simultaneous colorimetric assays; and (iv) display results of the colorimetric assays for quantitative analysis (Vella et al., 2012).

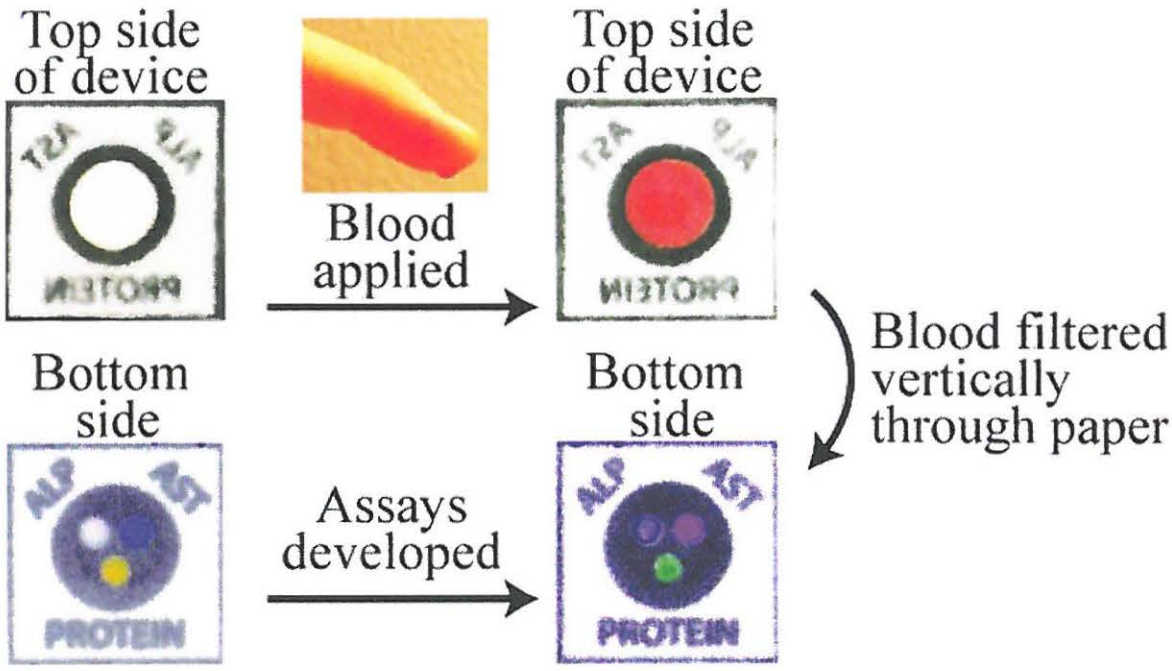

Figure 2.10: System designed for the quantitative measurement of two enzymatic markers of liver function ALP and AST and total serum protein in a drop of blood (Vella et al., 2012)

Among the many colorimetric assays is a method developed by Babson et al., for determining the concentration of AST from biological fluids (Babson et al., 1962). The method entails colorimetric detection for AST, based on reacting oxaloacetate with a diazonium salt in solution state. However, liquid based sensing systems may suffer from volatility and handling issues, meaning their performance suffers over time (Kavanagh et al., 2012). Producing solid-state platforms is of great importance for some applications, as the solid-state removes many of the issues associated with that of the liquid state.

There is therefore, great interest in solid-state sensing devices that can provide reliable signals at a low unit cost, low imprecision, small lot-to-lot variations, high analytical sensitivity, analytical specificity and accuracy with long calibration stability and through careful optimization of the sensitive polymer composites, prevent leaching or removal of key components over time. With the ever evolving technology there are commercial available rapid tests striving to meet the demands of detection suitable for field and bed-site testing.

2.2.4 Commercial rapid tests

Commercially available rapid tests include pregnancy test kits, litmus papers, glucose tests, paper based microfluidic HIV tests, just to mention a few. Figure 2.11 shows pictures depicting examples of some of the commercial test kits, randomly picked from the internet. These kits may use either gold nanoparticles or dyes as colour reagents, with different solid platform and support materials.

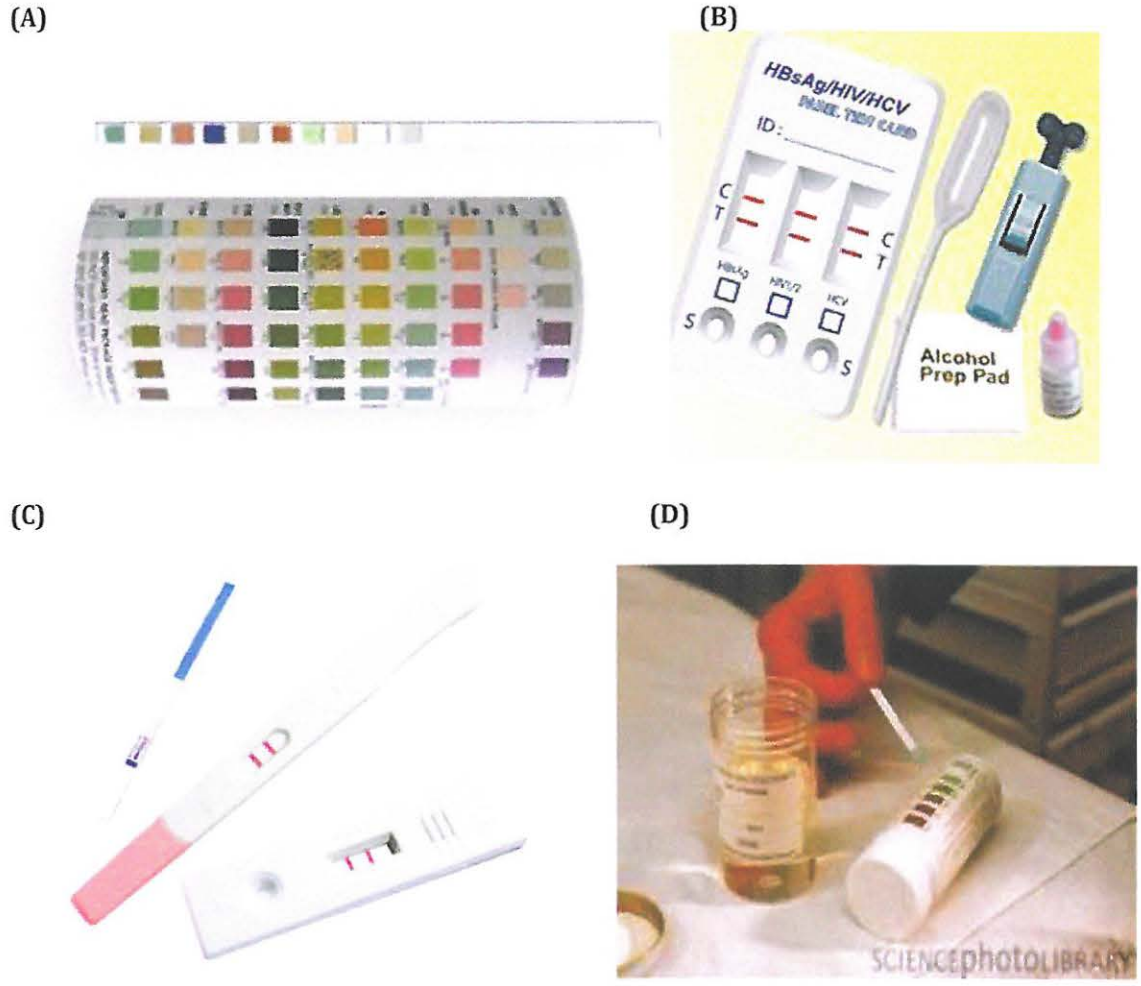

Figure 2.11: Commercial raid tests; A) Multi-stick urine test; B) HIV rapid test; C) Pregnancy test; D) Urine glucose test strip

Among solid substrates such as quartz, ITO glass, sol–gel matrix and paper, polymers are an excellent solid support because of their characteristic properties such as unreactive nature, availability, decay resistance and flexible structure.

2.2.5 Polymer based solid support for diagnostic test

Polymers are commonly used in optical chemical sensors as inert supports for indicator dyes keeping the molecules apart to allow for exposure to analytes and to maintain the peculiar optical properties of the sensitive dyes (Dini et al., 2011) The protocol is based on the principle that a coloured polymeric material can be obtained by dispersing the appropriate dye in the bulk of the pristine colourless polymer matrix. In this case, the macromolecules remain structurally unaltered and the system is generally biphasic unless the resulting dyes are fully soluble in the native polymer (Ciardelli et al., 2013). Examples of polymer based colorimetric assays include a pH sensitive membrane with remarkable colour changes from pale yellow to violet in a wide range of alkaline solutions (pH = 9–14) and a rapid response time as illustrated in a photograph by Zhang, 2011b (Fig. 2.12).

Figure 2.12: The colour change properties of pHS-NF membranes in different pH buffer solution. The pH sensitive membrane (pHS-M) showed a good mechanical integrity (Zhang et al., 2011b)

Diverse factors are also known to affect the stability of gold colloids, such as solvent, stabilizer, surfactant and pH. Low shelf stability of gold colloids, poor portability and matrix interference has resulted in limited number of applications.

In order to overcome the limitations of gold colloids, similar to dyes, solid supports have been introduced. The chromogenic reagents may either be immobilized on to the support that suffers from disadvantages such as the dye/Au NPs leaching at elevated pH conditions or inhomogeneity of the material. The reagent could also be covalently bonded (Mohr, 1994). However it should also be noted that when immobilized on the solid substrate, the strong interaction between Au NPs is reduced preventing the spontaneous agglomeration of particles (Li et al., 2013).

Among the several procedures of incorporating chromogenic reagents into polymer is a facile electrospinning technique. Electrospinning is a relatively simple process to produce nanofibrous structures from polymer solutions and is consequently most commonly applied (Van der Schueren et al., 2010)

Chapter 3

Electrospinning

3.1 Introduction

Electrospinning is a phenomenon that describes a class of fiber forming processes whereby an electrostatic force is employed to produce continuous nonwoven fibers that are unparalleled in their porosity, have high surface area with fineness of surface detail as well as uniformity of the fibers (Shin et al., 2001). The "spinning" here is synonymous with a textile term that is derived from the early use of spinning wheels to form yarns from natural fiber staples like cotton and is commonly used to identify fiber-forming processes for synthetic fibers (Rutledge and Fridrikh, 2007).

3.2 The principle of electrospinning

The fundamental principle underlying the electrospinning process is the effect that high voltage has on a polymer solution. Typically, for an electrospinning process to occur, a polymer solution or melt, held by its surface tension is subjected to an electric field (Chun 1996). The electric field then induces a charge on the liquid surface resulting in a charged repulsion that causes a force directly opposite to the surface tension. With an increase in the intensity of the electric field, the hemispherical surface of the solution at the tip of the capillary tube elongates to form a conical shape known as the Taylor cone (Doshi and Reneker, 1995). When the electric field reaches a critical value at which the repulsive electric force overcomes the surface tension force, a charged jet of the solution is ejected from the tip of the Taylor cone. Since the jet is charged, its trajectory can be controlled by an electric field. As the jet travels in air, the solvent evaporates, leaving behind a charged polymer fiber, which lies randomly on a collecting metal screen (Islam and Karim, 2010). There are various forces acting on the Taylor cone prior to fiber formation. The forces include electrostatic force, drag force, gravity, Coulombic repulsion force, surface tension and viscoelastic force. As shown in Fig. 3.1, the electrostatic force carries the charged droplet from capillary tip to collector while the Coulombic repulsion force causes the droplet to expand.

The surface tension and viscoelastic forces on the other hand induce contraction of charged droplet. An increase in the electrostatic force leads to an increase in acceleration of the moving of charged droplet, which then amplifies the drag force (Wang et al., 2013). The synergic effect of these forces gives nano and porous fibers.

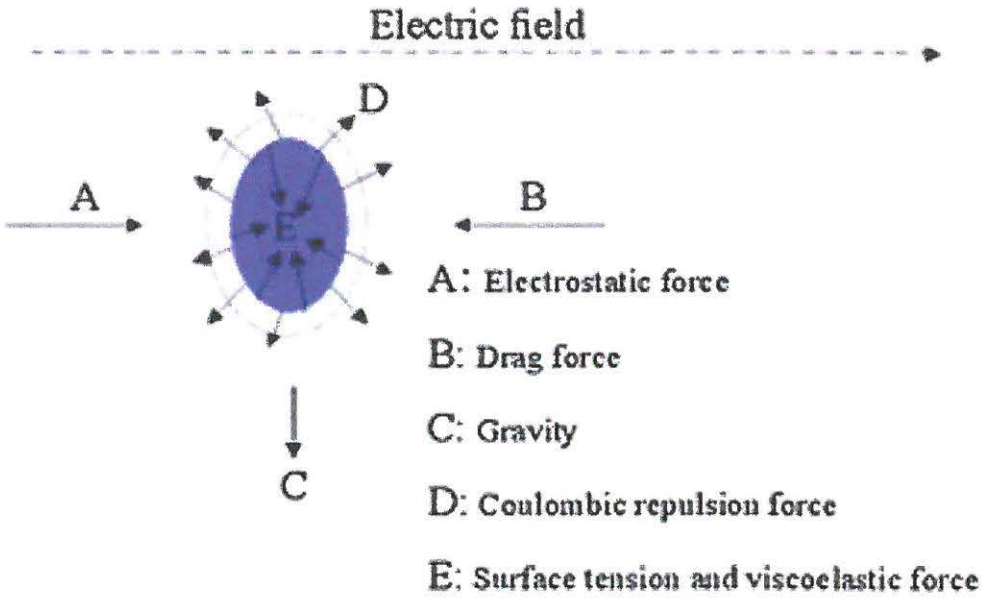

Figure 3.1: Forces acting on a charged droplet which leads to fabrication of nanofibers with high specific surface areas and porosities (Adapted from Wang et al., 2013)

In the simplest form a nozzle based electrospinning setup comprises three parts: a high voltage power supply to generate electric field for spinning, a polymeric solution contained within a capillary tube/syringe pump and grounded collector placed at a distance from the tip of the capillary tube (Fig. 3.2).

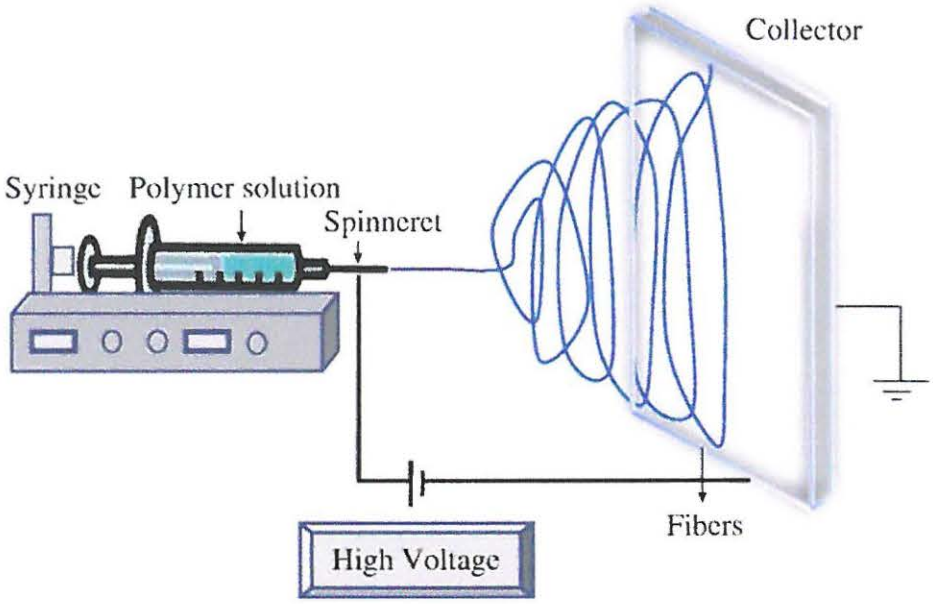

Figure 3.2: Schematic diagram of set up of electrospinning apparatus; a syringe pump containing the polymeric materials, a high voltage source to generate high electric field for spinning, and a collector to collect the fibers (Bhardwaj and Kundu, 2010)

The collector can either be vertical or horizontal to the spinneret. There are various parameters that govern the electrospinning process. The parameters are broadly classified into solution, process and ambient parameters.

3.3 Effects of solution, process and ambient parameters

Transformation of polymer solutions into nanofibers through electrospinning is dependent on various parameters, some of which are summarized in Table 3.1. It is also worth noting that in electrospinning, high molecular weight polymers and high solution concentration, elasticity and relaxation time are generally important since they have an impact on the electrospinnability of solutions (Celebioglu and Uyar, 2013).

Table 3.1: Electrospinning parameters (solution, processing and ambient) and their effects on fiber morphology (Huang et al., 2003, Wang et al., 2013)

Parameters	Effect on fiber morphology
Solution Parameters	
Viscosity	Low-beads generation, high-increase in fiber diameter, disappearance of beads.
Polymer concentration	Increase in fiber diameter with increase of concentration.
Molecular weight of polymer	Reduction in the number of beads and droplets with increase of molecular weight.
Conductivity	Decrease in fiber diameter with increase in conductivity.
Surface tension	No conclusive link with fiber morphology, high surface tension results in instability of jets.
Processing Parameter	
Applied voltage	Decrease in fiber diameter with increase in voltage.
Distance between tip and collector	Generation of beads with too small and too large distance, minimum distance required for uniform fibers.
Feed rate/Flow rate	Decrease in fiber diameter with decrease in flow rate, generation of beads with too high flow rate.
Ambient Conditions	
Humidity	High humidity results in pores on the fibers.
Temperature	Increase in temperature results in decrease in fiber diameter.

Electrospinning provides a very simple, cost-effective and versatile method for generating ultrathin fibers from a rich variety of materials that include polymers, polymer blends (Kim et al., 2007, Charernsriwilaiwat et al., 2010, Prasanth et al., 2012), sol–gels (Ding et al., 2007), emulsions (Yang et al., 2008, Dai et al., 2010), suspensions (Sung et al., 2012, Yang et al., 2011), composite structures and ceramics (Li and Xia, 2004). As highlighted in one review, ultrathin fibers with diameters of submicrons or nanometers ($10 \times 10^{-3} - 100 \times 10^{-3}$ μm) possess several amazing characteristics such as very large surface area to volume ratio (this ratio for a nanofiber can be as large as 10^3 times of that of microfiber), flexibility in surface functionalities and superior mechanical performance (e.g. stiffness and tensile strength) compared with any other known form of fibers (Huang et al., 2003).

With such versatility, electrospinning is attractive to both academic research and industrial application. It is applicable to a wide range of materials such as synthetic and natural polymers, metals as well as ceramics and composite systems (Wang et al., 2009). Electrospinning can, furthermore, allow fabrication of nanofibers at a lower cost and with relatively, a high yield. Over 200 universities and research institutes worldwide are studying the various aspects of electrospinning process and countless benefits offered by electrospun fiber (Ramakrishna et al., 2006). Furthermore, commercial companies such as eSpin Technologies, IME Technologies, NanoTechnics and KATO Tech, Donaldson Company and Freudenberg are known to be actively engaged in electrospinning with Elmarco been probably one of the biggest. In order to meet the ever increasing demands for mass production further developments have been channeled towards commercialization. Several researchers looked into different types of electrospinning such as the single nozzle and multi-nozzle systems.

3.4 Types of electrospinning

The advantage of the electrospinning approach lies in the ability to fine tune the process parameters such as polymeric solution composition, needle-target distance and applied voltage. The technique hence opens a vast scope for researchers to tailor investigations towards achieving high throughput as well as improve on the classic electrospinning process. The diverse range of approaches include single nozzle, multi-nozzle and needless systems.

3.4.1 Mono nozzle electrospinning

Traditionally, the electrospinning process is basically composed of a needle, fed by a polymer melt or solution, and connected to a high voltage generator where by a grounded target is fixed at a certain distance from the needle. As shown in Fig. 3.3, the needle and target can be positioned vertically with the needle set above the target. However, due to the chaotic oscillation of the electrospinning jet, a characteristic feature of the electrospinning process, randomly oriented and isotropic structures in the form of nonwoven nanofiber mats or webs are often generated due to a lack of control over the forces driving fiber orientation and crystallization (Fennessey and Farris, 2004). Nanofibers fabricated with a single nozzle usually have weaker mechanical intensity (Zhang et al., 2011b) and finding common solvents to blend polymers in a solution to the creation of single-polymer material is a challenge for this type of electrospinning.

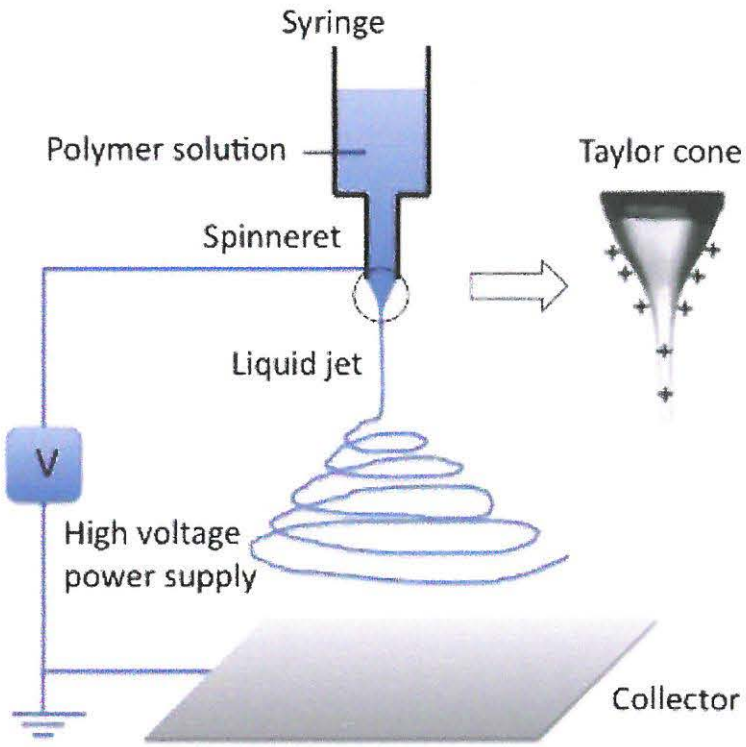

Figure 3.3: The common setup and working principle of electrospinning (Li et al., 2010)

Single nozzle electrospinning systems, in addition, have a low fluid throughput (1-10 ml/min) which may limit the industrial use of electrospinning regarding mass fabrication. Technically, there is also an issue of the needle clogging, causing an interruption on the process. To overcome the limitations arising from single nozzle electrospinning, multi-nozzle electrospinning configurations were introduced. With multi-nozzle electrospinning systems composite membranes made up of two or more different polymers were fabricate. The basic idea was to multiply the number of Taylor cones (see Fig. 3.3) from which fiber jets are emitted and finally collected as fibers with better mechanical properties.

3.4.2 Multi nozzle electrospinning

Hybrid materials with new/ improved properties such as mechanical, thermal and antimicrobial properties offer better characteristics than their single-polymer material counterparts (Tijing et al., 2013). Relative to traditional electrospinning, multi nozzle electrospinning protocols allow for blending of tenacious materials. Blending of polymers could have a profound impact on the superior performance and large-scale applications of the electrospun polymer blends.

Amongst other researchers Zhang's group successfully employed an advanced two nozzle electrospinning approach to fabricated pH-sensitive nanofiber membranes with mechanical integrity. Two types of polymeric fibers solutions were mixed homogeneously in one electrospinning step shown in Fig. 3.4. The simultaneous presence of nanofiber and microfiber generated a novel composite electrospun mat which exhibited greater pH sensitivity. Furthermore, the mechanical property of electrospun sheet, owing to the character of polyamide-66 microfibers, had significantly improved (Zhang et al., 2011a).

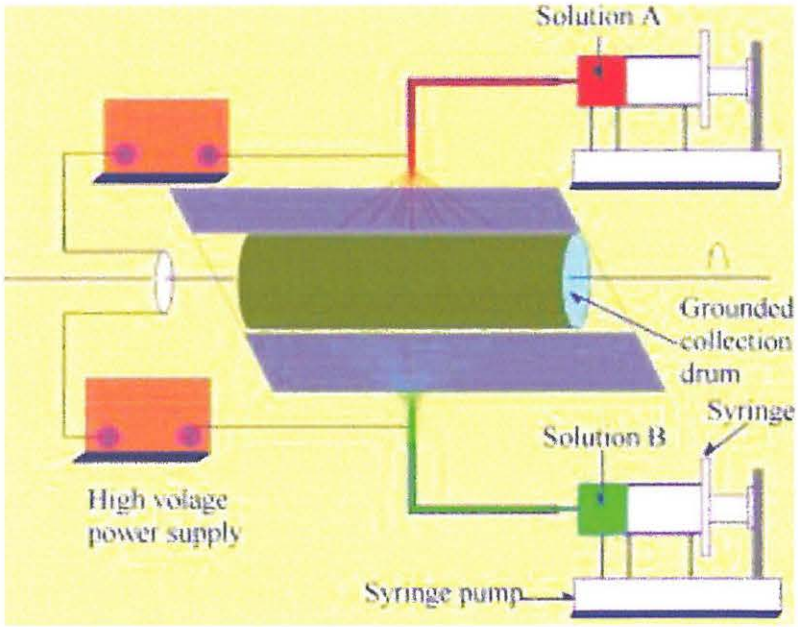

Figure 3.4: Two-nozzle electrospinning equipment (Zhang et al., 2011a)

In another approach, a different configuration, using a stationary collector, was employed to fabricate a simple colorimetric strip for assaying lead. A dual-component alternate distribution multifluidic electrospinning technique was employed (Fig. 3.5). A mechanically stable and selective sensor strip electrospun from polyamide-6/nitrocellulose was fabricated then functionalized with bovine serum albumin-Au NPs.

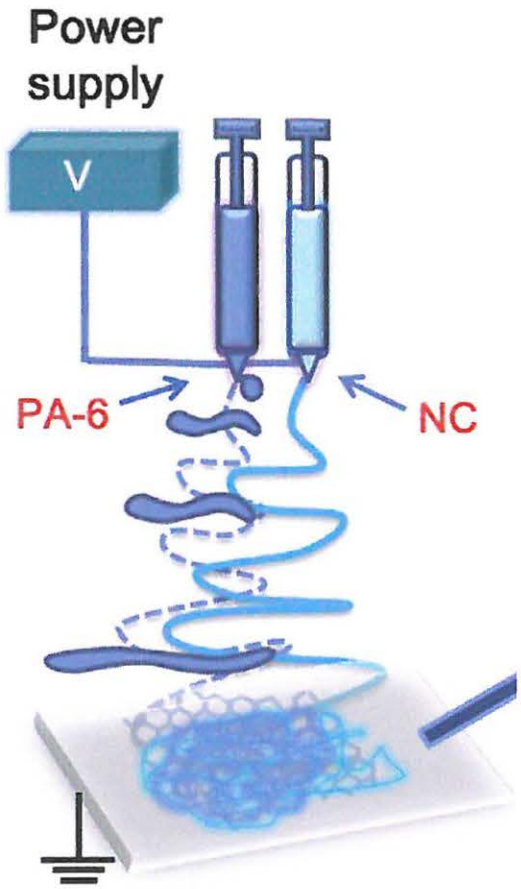

Figure 3.5: Adapted scheme representing the preparation of polyamide-6/nitrocellulose (PA-6/NC) nano-fibers/nets (NFN) membranes assemble bovine serum albumin functionalized Au NPs colorimetric strips (Li et al., 2013)

Although the production rate is improved with the two-nozzle electrospinning the high yield requirements are forever increasing. Therefore, so as not limit the use of multi nozzle systems, it has been imperative to aim for throughput comparable to that of the ever increasing industrial mass production of nanofibers. Systems comprising more than two nozzles have been developed. Kim et al. developed a five nozzle electrospinning protocol (Fig. 3.6) while Theron et al. during a more complex multi-jet electrospinning, demonstrated how both external electric field and mutual electric interaction influence the path and evolution of jets (Fig. 3.7). The multi nozzle approaches however, have some limitations. For instance, dealing with different polymer solutions is not an easy operation, the issue of instability as well as bent jet-motion by the outer nozzles and the interferences by charged fibers of inner nozzles are some of the challenges (Kim et al., 2006).

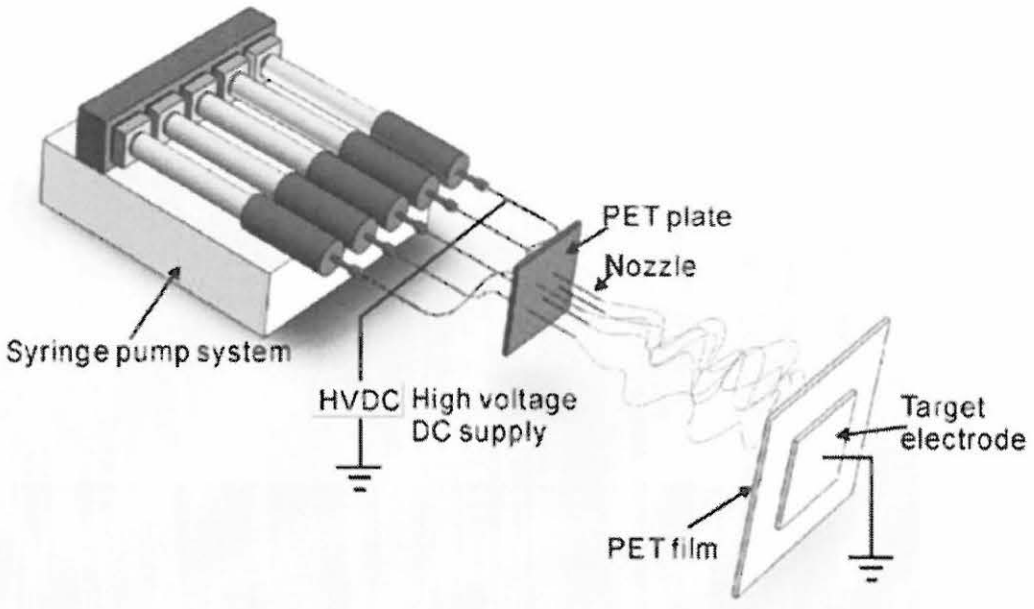

Figure 3.6: Schematic of an electrospinning apparatus with five-nozzles (Kim et al., 2006)

Another disadvantage is due to the electric field interferences generated by the numerous spinning heads. The field interferences have lead to several challenges of non-uniform fiber deposition as a result of mutual repulsion generated by the Coulombic forces of the ejected thread (Varesano et al., 2009). Although multiple jets in electrospinning have proven to be a practical implementation towards increasing the production rate detailed physical understanding of the outcome of jet–jet interaction is yet to be understood (Theron et al., 2005). Furthermore, the challenge of clogging syringes is still persistent.

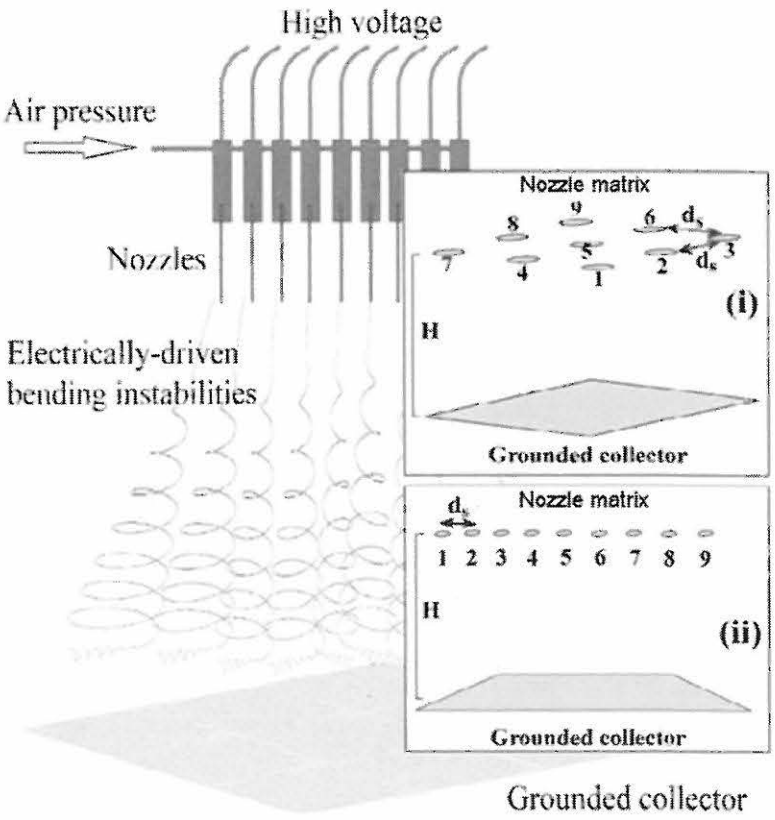

Figure 3.7: Multiple-jet electrospinning setups: (i) The nozzles in the setup were arranged in a 3 x 3 matrix with each nozzle attached to a syringe with polymer solution; (ii) The second multiple-jet arrangement consisted of syringes in a row (a 9 x 1 and a 7 x 1 linear array)(Theron et al., 2005)

Despite the fact that electrospinning setup maybe modified to minimize the drawbacks, for example by using a collector with an opposite charge to that of the syringe/s instead of the traditional target connected to ground, the solution still presents many complexities for industrial utilization. The challenges further include merging of the droplets when the nozzle spacing is narrow (Yamashita et al., 2008). In order to cub the inherent limitations brought about by the use of capillaries and needles, various researchers have devised new forms of spinnerets usually referred to as 'needleless' electrospinning.

3.4.3 Needless electrospinning

One of the remarkable features of the electrospinning process is that jets can be launched, in principle, from any liquid surface (Forward and Rutledge, 2012). Based on this principle needleless electrospinning has emerged as a new electrospinning mode to produce nanofibers on large scales and as the name suggests, needleless electrospinning produces nanofibers without using needle-like nozzles (Fang et al., 2013). Needless electrospinning can broadly be categorized into two; needleless electrospinning with a 'confined feeding system' and with an 'unconfined feeding system'. The significant difference between the two categories is that the former employs setups that have a reservoir for the polymer solution that is subsequently injected into an enclosed nozzle while in the latter Taylor cones are formed instead, on a free liquid surface and no nozzles are needed. Needleless electrospinning has several potential benefits, including simplicity of design, robustness against clogging of a spinneret and increased productivity through the simultaneous operation of numerous jets (Jiang et al., 2013).

Owing to its merits, particular that of no clogging of spinnerets, a variety of needless electrospinning configurations has been reported. Just to mention but a few examples, Thoppey et al. demonstrated an easily-implemented, edge-plate geometry for electrospinning and produced high quality nanofibers from unconfined polymer fluids.

The fabricated nanofibers possessed similar fiber diameter and diameter distributions while operating at comparable voltages and working distance as those from an aperture-based system, yet with more intrinsic flexibility to potentially scale-up the process without openings or nozzles that could potentially clog (Thoppey et al., 2010). While Jian et al., on the other hand, developed a simple and efficient needleless electrospinning setup using one stepped pyramid shaped copper spinneret (see Fig. 3.8). An approach which, when compared with the traditional needle based electrospinning, produced finer nanofibers with an enhancement in productivity of more than 100 times (Jiang et al., 2013).

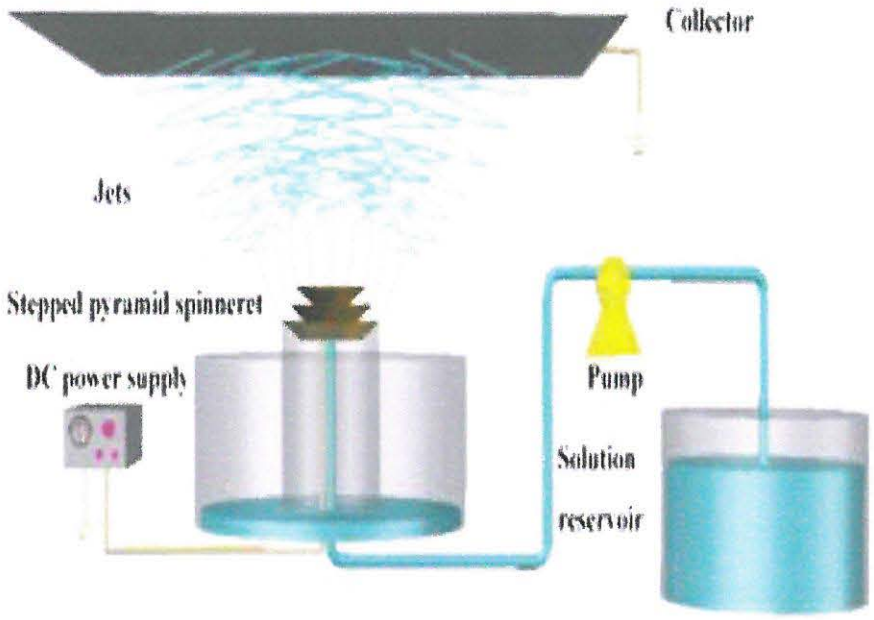

Figure 3.8: Scheme of the electrospinning apparatus using a stepped pyramid spinneret (Jiang et al. 2013)

In another intriguing needless electrospinning approach, Forward and Rutledge analyzed a particular case of free surface electrospinning from a thin wire electrode. The process involved a metal wire electrode swept through an electrified liquid bath. As the bath got charged through the liquid/air interface the liquid got entrapped within the interface leading to formation of liquid droplets on the wire (Fig. 3.9). At a sufficiently high electric field, the charged liquid drops deformed into Taylor-like cones and emitted fiber jets.

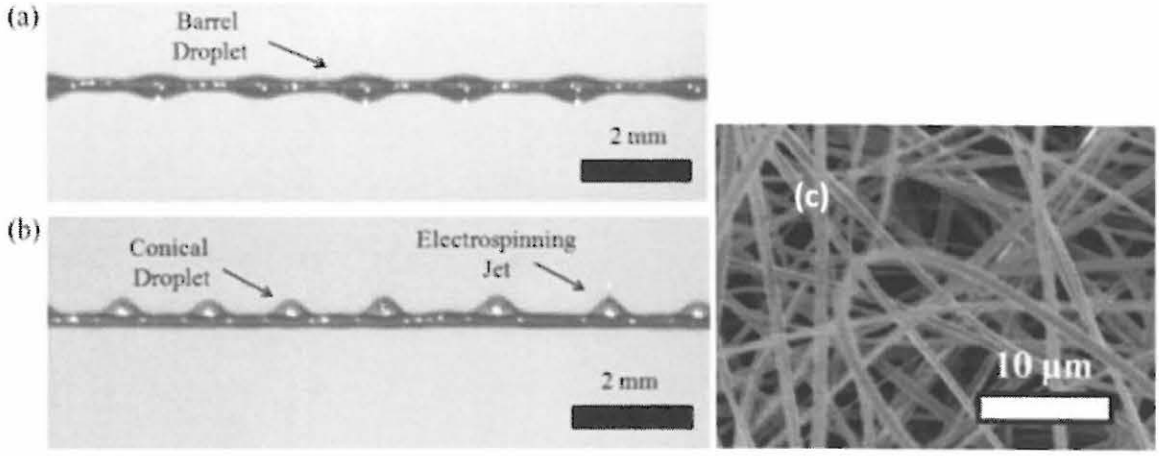

Figure 3.9: A) Optical image of droplets of polymer solution on a rotating wire; B) A photograph showing only one electrospinning jet (as indicated) while other droplets produced a conical shape, attributed to the combined effects of surface charge repulsion (similar to the Taylor cone) and attraction of the charged fluid to the grounded collection plate; C) Scanning electron micrograph of the resulting electrospun+ mat (Forward and Rutledge, 2012)

Examples cited so far include needless electrospinning protocols that basically employ organic solvents. However for bio-related applications such as in tissue engineering scaffolds, life sciences, cosmetic skin masks and military protection clothing toxicity of the organic solvents is a major factor.

Electrospinning with aqueous solvents was therefore an alternative for applications and configurations where toxic solvents are a concern. In 2007 Liu and He developed a bottom-up gas-jet (bubble) electrospinning process for mass production. The bubbles induced on the surface of the polymer solution were equivalent to a Taylor cone in the traditional electrospinning protocol. A hydrophilic polymer, polyvinyl alcohol (PVA), dissolved in water has been used to produce environmentally benign nanofibers through this bubble electrospinning (Yang et al., 2009). A compressed gas is released inside the solution producing one or several bubbles on the free surface of the solution as shown in Fig. 3.10.

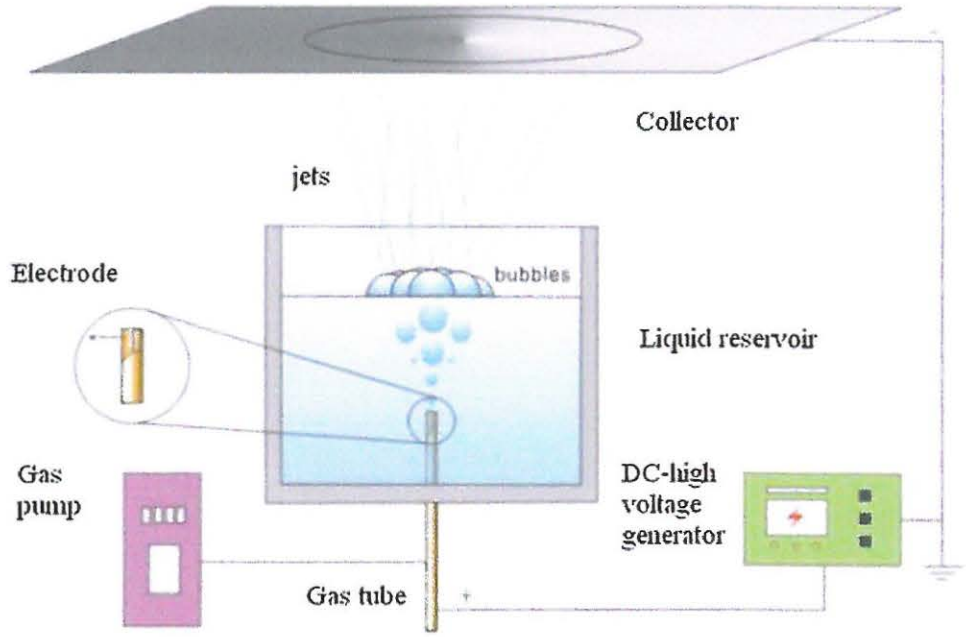

Figure 3.10: Sketch of the set-up used in bubble electrospinning (Agarwal et al., 2013)

Establishing the integrity of the electrospun fibers is of great importance in ensuring that the fibers have the necessary properties to perform their proposed functions. To evaluate structure elucidation of the electrospun fibers it is necessary to perform characterization on the fibers.

3.5 Characterization of electrospun polymers and polymer composites

The important aspects of characterization are chemical composition and compositional homogeneity (chemical homogeneity), structure (including crystal system where possible atomic coordinates, bonding and ultra structure) and identification and analysis of defects and impurities influencing the properties of the materials (Lagashetty, 2005). Characterization, besides, describing features of composition also allow investigations on the structure of a material that would suffice for reproducing the material. The different ways of characterizing fibers include geometrical, chemical, physical and mechanical as well as spectroscopic characterization.

3.5.1 Geometrical characterization

Typical geometric properties of nanofibers include fiber diameter, diameter distribution, fiber orientation, and fiber morphology (e.g. cross-section shape and surface roughness). Techniques such as scanning electron microscopy (SEM), field emission scanning electron microscopy (FE-SEM), transmission electron microscopy (TEM), and atomic force microscopy (AFM) (Shirazi et al., 2013) are used for the characterization of geometric properties. Porosity also falls under geometric parameter and can be evaluated using Brunauer, Emmett, and Teller (BET) method (van Erp and Martens, 2011). These methods include X-ray diffraction, both wide angle and small angle (WAXS and SAXS) (Graewert and Svergun, 2013) and differential scanning calorimetry (DSC) (Said et al., 2011). Some techniques such as X-ray photoelectron spectroscopy (XPS), contact angle measurements and Attenuated total reflectance Fourier transform infra red spectroscopy (ATR-FTIR) are also being used to determine the surface chemistry of the electrospun nanofibers (Tu et al., 2013).

3.5.2 Chemical and physical characterization

Energy dispersive X-ray spectroscopy (EDS or EDX) is a standard analytical technique for element identification or chemical characterization in material analysis (Utsunomiya and Ewing, 2003). Energy dispersive X-ray spectroscopy systems are usually mounted on scanning electron microscopes (SEM-EDS) for chemical composition analysis (Hollerith et al., 2004).

TEM and X-ray diffraction (XRD) are complimentary techniques usually employed as effective means of developing insights into the surface morphology, internal structure and spatial distribution of various components, through direct visualization.

3.5.3 Mechanical characterization

The mechanical properties of the nonwoven mat with randomly distributed nanofibers depend more on the assemblage of these fibers rather than the structural characteristics of a fiber molecule. The fiber diameter is the most important factor to affect mechanical properties of nanofiber mat and a smaller fiber diameter leads to better mechanical properties (He et al., 2011). Mechanical characterization is achieved by applying tensile test loads to specimens prepared from the electrospun non-woven fiber mats. The breaking stress, for electrospun nonwoven mats with known width (mm) and length (mm), may be calculated according to the Eqn. (3.1). A variety of approaches has been applied towards mechanical characterization of nanofibers and nanowires by employing nanoindentation, bending tests, resonance frequency measurements, and microscale tension tests (Naraghi et al., 2007).

$$Breaking\ stress\ (MPa) = \frac{Tensile\ strength\ (N)}{Thickness\ (mm) \times Width(mm)} \qquad \ldots (3.1)$$

Mechanical strength of the nanofibers is crucial in biomedical applications. For example, as scaffolds, nanofibers must be able to withstand the forces exerted by growing tissue or during physiological activities. Owing to their mechanical stability, electrospun nonwoven nanofibrous structures have been widely used in multiple biomedical applications, such as tissue engineering, wound dressing, drug delivery, and medical implants (Aghdam et al., 2012).

3.5.4 Spectroscopic methods

Spectroscopic methods are widely used to reveal valuable information regarding the constituent elements and chemical structure near the surface region of a sample (Merrett et al., 2002). Infrared (IR) spectroscopy has been employed for mapping the porosity of polymer membranes where the conventional transmission IR spectroscopy was employed to assess the bulk porosity across the entire thickness of a polyethersulfone (PES) membrane, while attenuated total reflection IR (ATR-IR) provided information about the porosity of a thin layer at the membrane surface (Kiefer et al., 2014). Traditionally, nuclear magnetic resonance (NMR) has also been regarded as a technique of choice for studying polymeric materials, especially in the solid state, because of its ability to yield highly informative spectra in a nondestructive way. Several methods have been proposed in the literature to boost the NMR sensitivity, including dynamic nuclear polarization (DNP). With further developments, DNP has been modified into DNP solid-state nuclear magnetic resonance (SSNMR) with remarkable advances in high-resolution (Ouari et al., 2013, Sullivan et al., 2012, Bhardwaj and Kundu, 2010).

As highlighted in a review by Merrett et al., characterization techniques utilized in the biomaterials field include scanning transmission X-ray microscopy (STXM) and photoelectron emission microscopy (PEEM). Both techniques require synchrotron light sources and advanced instrumentation. Scanning transmission X-ray microscopy has the advantages of not being affected by sample charging or topography and has the ability to image the sample in solution. Photoelectron emission microscopy on the other hand requires ultra high vacuum and no sample charging. Both techniques, STXM and PEEM, have a high lateral spatial resolution on the order of 50 nm and excellent chemical sensitivity. Much more commonly utilized in the surface characterization of biomaterials, the traditional spectroscopic techniques used include:

- Auger electron spectroscopy (AES)
- X-ray photon spectroscopy (XPS)
- Secondary ion mass spectrometry (SIMS)

Auger electron spectroscopy (AES) has been used for investigating surface morphology and in particular elemental analysis (Mercado-Pagán et al., 2013). No special sample preparation is required and data collection is rapid (i.e. a few minutes) and reproducible. X-ray photoelectron spectroscopy (XPS), also called ESCA (electron spectroscopy for chemical analysis) is widely used in biomaterial applications to determine the elemental composition of solid surfaces. Special sample preparation is generally not required for XPS, although surface contamination upon storage or during transport from the research laboratory to the XPS facilities may certainly have an adverse effect on the XPS results obtained (Diplas et al., 2001, Merrett et al., 2002).

Static SIMS using time-of-flight (TOF) mass spectrometer has proven to be a powerful technique for the chemical characterization of the constituents in the upper monomolecular layer of various industrial materials. From the analytical viewpoint, its capability of the detection of molecular secondary ions as well as structural fragments with high sensitivity has a big potential for the evaluation of low-levels of organic contamination on the sample surface: identification of the molecules, the study of segregation of additives, and the detection of surface functionalities are commonly applicable to wide variety of materials (Karen et al., 2003).

Surface matrix-assisted laser desorption/ionization mass spectrometry is another powerful analytical technique for the analysis of polymeric materials. The advantages of this technique for such analyses include low sample consumption; ease of sample preparation, short analysis times and soft ionization which leads to negligible or no fragmentation of analytes. It has demonstrated to provide absolute, fast and accurate molecular masses for polymers with narrow polydispersity as opposed to relative masses provided by other techniques. In addition it provides masses for the entire polymer distribution instead of the average value, hence providing molecular mass information which can be used to obtain the mass of the end-groups, mass of the repeat unit (monomer) and chemical modifications on the polymer (Macha and Limbach, 2002, Chen et al., 2011). Applications of matrix-assisted laser desorption/ionization time-of-flight mass spectrometry (MALDI-TOF MS) to the quantification of synthetic polymers is relevant. The addition of different components presents a challenge as the components have an impact on the polymer properties (Chen et al., 2002).

Hence MALDI-TOF is a routine analytical tool for the structural analysis of polymers, complementing NMR and other traditional techniques (Montaudo et al., 2006). There are many other equally good techniques, not mentioned in this thesis, employed for characterization of electrospun polymers prior to application in various fields.

3.6 Applications of electrospun polymer nanofibers

Electrospun fibers have a wide range of applications such as in nanocomposites, filtration, medical prostheses, tissue templates, wound dressings, cosmetics, drug delivery and pharmaceutical compositions, protective clothing electrical and optical use (Tan et al., 2007).

To date, the polymer composites reinforced with electrospun nanofibers have been developed mainly for providing some outstanding physical (e.g. optical and electrical) and chemical properties while keeping their appropriate mechanical performance. Some composites are carbon based. Carbon nanofiber composite also has potential applications as filters for separation of small particles from gas or liquid, supports for high temperature catalysts, heat management materials in aircraft and semiconductor devices, as well as promising candidates as small electronic devices, rechargeable batteries, and super-capacitors. Nanocomposites, however, suffer some limitations including lack of superior structural properties. It is well known from composite theory and practice that the superior structural properties can be achieved only when fibers are arranged in pre-determined directions such as in unidirectional laminae, multidirectional laminates and woven or braided fabric reinforced composites. To make these composites, continuous fiber bundles are necessary. The non-woven or randomly arranged nanofiber mats, as collected from electrospinning, generally cannot result in a significant improvement in the mechanical properties of the composites with their reinforcement (Huang et al., 2003).

Electrospun nanofibers are broadly applied in biomedical applications, as tissue engineering scaffolds, in wound healing, drug delivery, filtration, as affinity membrane, in immobilization of enzymes, small diameter vascular graft implants, healthcare, biotechnology, environmental engineering, defense and security, and energy storage and generation as well as in various researches that are ongoing (Fang et al., 2008, Bhardwaj and Kundu, 2010). Figure 3.11 shows a summary of some of the most potential applications of electrospun polymer nanofibers.

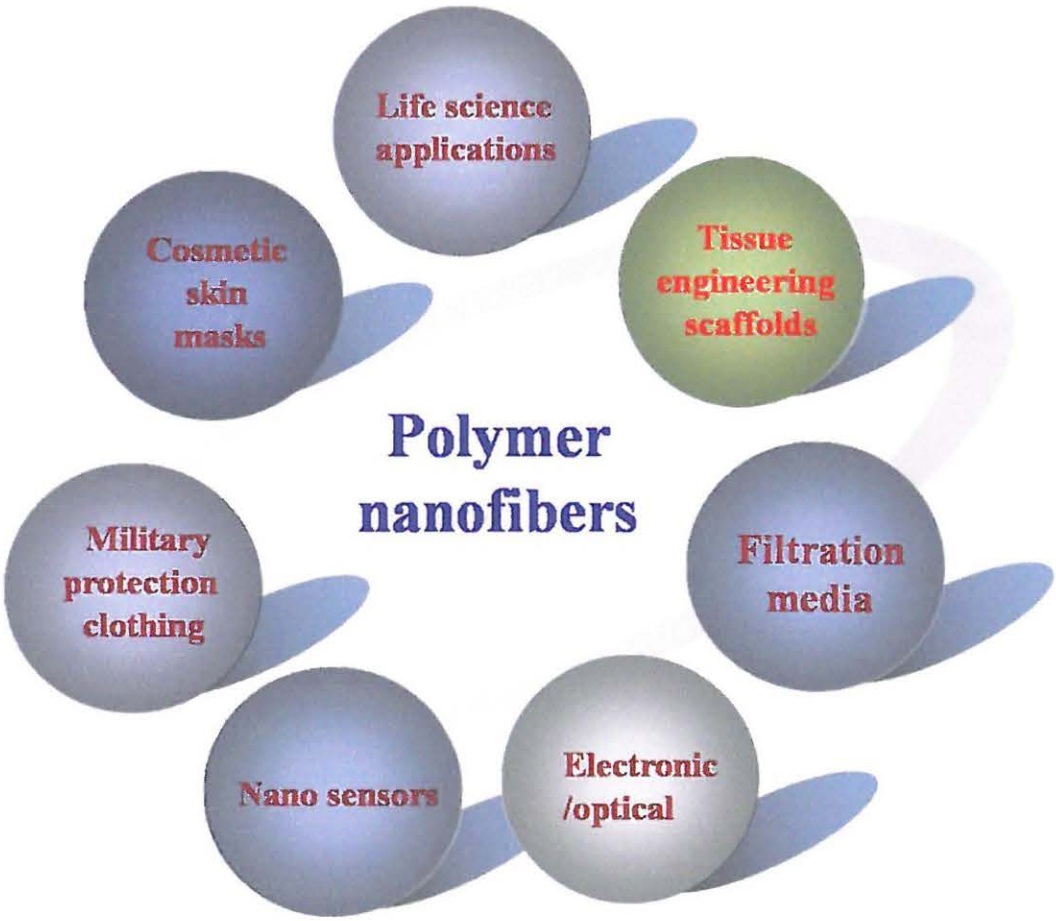

Figure 3.11: Summary of a wide range of some applications of nanofibers in different fields, taking advantage of the facile production of nanofibers with high specific surface areas, high porosities, and controllable compositions (http://faculty.ksu.edu.sa)

There is a general need to develop simple, rapid, inexpensive, portable and easy to operate devices for diagnostic applications in the different sectors. The simplest and thus most interesting of the non invasive analytical devices are colorimetric based as colour changes rely on naked eye detection and therefore no affiliated instruments are required (Zhao et al., 2008, Chigome and Torto, 2011).

3.6.1 Polymer based colorimetric devices

For this thesis, the main focus was on detection systems channeled towards the development of simple and easy to use colorimetric analytical devices. Unlike other nanofiber fabrication techniques, electrospinning is straightforward, versatile, and very cost-effective for producing nanofibers from variety of materials such as polymers, polymer blends, sol–gels, emulsions, suspensions, and composite structures (Zhao et al., 2012). Due to their unique properties, electrospun polymer nanofibers have gained recognition as supports for colour signaling reagents such as dyes and metal nanoparticles.

The use of inorganic nanoparticles into the polymer matrix is known to provide high-performance novel materials that find applications in many industrial fields. With this respect, frequently considered features are optical properties such as light absorption (UV and colour) (Li et al., 2010). A variety of electrospun polymer-metal nanoparticles based colorimetric systems have since been developed for different applications (Scampicchio et al., 2010, Si et al., 2012, Liu et al., 2012, Ignatova et al., 2012). For example, a colorimetric strip based on BAu probe immobilized PA-6/NC NFN membranes that were both swift and simple for real-time lead detection was reported (Li et al., 2013).

Among the many polymer based colorimetric probes are the dye-incorporated devices. Reactive dyes such as the azo and cyanine dyes possess large extinction coefficients and therefore have been successfully used to develop sensitive colorimetric assays (Van der Schueren et al., 2010, Niu et al., 2009). A label-free colorimetric sensor strip for real-time formaldehyde detection was developed based on Methyl Yellow-impregnated nylon 6 NFN membranes that comprise common electrospun nanofibers and ultrafine nano-nets (Wang et al., 2013).

Colorimetric probes are therefore a promising dynamic technique for qualitative, quantitative and semi-quantitative analysis of different analytes in clinical diagnosis, environmental monitoring, as well as food and process control among other applications.

Chapter 4

Experimental

The approach adopted was twofold - evaluation was done in solution, thereafter a solid state platform was developed for practical purposes such as ease of handling and storage as well as stability of the solid probes.

4.1 Materials

4.1.1 Chemical and Reagents

Gold (III) chloride trihydrate ($HAuCl_4.3H_2O$) and sodium borohydride ($NaBH_4$), all of purity more than 99%, were purchased from Sigma-Aldrich, (St. Louis, MO, USA). All reagents were of analytical or HPLC grade. Tetrahydrofuran, THF (98%) and N, N-dimethylformamide, DMF (99%) were purchased from Merck Chemicals (Wadeville, South Africa), methanol (MeOH) from Merck KGaA (Darmstadt, Germany) while formic acid and glacial acetic acid (HAc) were from Sigma-Aldrich (St. Louis, MO, USA). 17β-estradiol, p,p'-DDE (1,1-dichloro-2,2-bis(p-chlorophenyl)ethylene), deltamethrin (D), 4-tert-octylphenol, nonylphenol and cholesterol were also purchased from Sigma-Aldrich. α-Ketoglutaric acid, L-aspartic acid, aspartate aminotransferase (lyophilized powder of recombinant AST from *E.coli*), L-glutamic acid monosodium salt monohydrate, oxaloacetic acid, mercaptosuccinic acid, maleic acid, sodium pyruvate, L-alanine, Fast Blue BB salt hemi (zinc chloride) dye with formula (Fig. 4.1.1) content ≥80% and tris(hydroxymethyl) aminomethane were also purchased from Sigma-Aldrich (St. Louis, MO, USA).

Primary steroid, pesticides, alkylphenols and cholesterol stock solutions were each prepared at nominal concentrations of 1000 µg/ml in MeOH. Stock solutions for the dye and different substrates were also prepared at nominal concentrations of 1000 µg/ml but in 0.5 M tris base buffer pH 7.4.

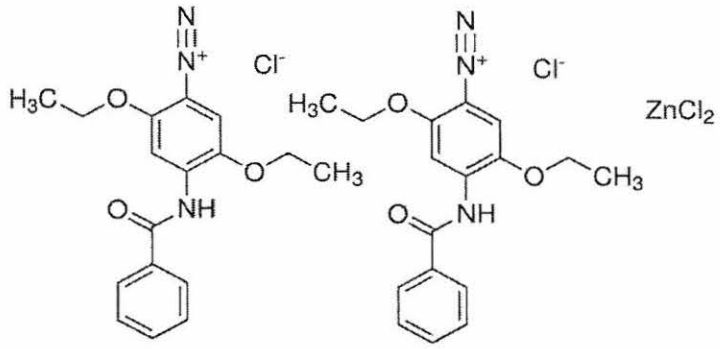

$ZnCl_2$

Linear Formula: $C_{17}H_{18}N_3O_3Cl \cdot 1/2\ ZnCl_2$
Molecular weight: 415.94
Physical appearance: Dark yellow to yellow-green crystalline powder
Composition: Dye content ≥ 80%
Storage temp: -20 °C

Figure 4.1: The diazonium salt, Fast Blue BB salt hemi (zinc chloride) dye contains azo groups, -N=N- and are linked to sp^2-hybridized carbon atoms

4.1.2 Polymers

Pellet type polystyrene (M_w = 192,000, melting point 240 °C, refractive index 1.5916) and polyamide, nylon 6 (M_w = 10,000, melting point 220 °C, refractive index 1.5300) were purchased from Sigma-Aldrich, (St. Louis, MO, USA). Both polymers were used as received. Polymer solutions were prepared by dissolving predetermined masses of the polymer pellets in appropriate volumes of solvents by slowly agitating the solution using Stuart SB-162 magnetic stirrer (Staffordshire, UK). Solutions were prepared in glass vials with air-tight lids to avoid evaporation of solvents at room temperature.

4.2 Synthesis and fabrication of polymer composite

4.2.1 Gold nanoparticles incorporated polystyrene composite

In a typical procedure (depicted generally in Fig. 4.2), predetermined quantities of PS and Au salt were dissolved in DMF/THF (8:2 v/v) in a sealed vial. The PS mixture was left to stir for 3 to 4 h to ensure complete dissolution, after which $NaBH_4$ was added to effect the reduction of the metal salt precursor at ambient conditions. The solution was left to stir overnight to eliminate air bubbles and then it was electrospun. The electrospinning set-up included a syringe pump operated at a flow rate of 0.300 ml/h and a high voltage power supply with a positive polarity. The optimum voltage applied was 22.2 kV.

4.2.1.1 Optimizing concentration of reducing agent

Prior to electrospinning, optimal synthesis conditions were obtained at ambient conditions (temperature and humidity) by evaluating synthesis at different concentrations of the reducing agent. For an efficient use of $NaBH_4$ the following concentrations were evaluated; 0.05, 0.1 and 0.2 mol/l. The polystyrene-gold nanoparticles solutions were further characterized by UV-Vis spectroscopy and TEM.

4.2.1.2 Solution Parameters

Preliminary experiments were carried out regarding concentration of polystyrene in 8:2 v/v N,Ndimethylformamide (DMF) and tetrahydrofuran (THF) mixture, see Table 4.1 for the physical characteristics of these solvents. Different polystyrene concentrations of 10, 12, 16 and 20% wt/v were investigated while other parameters were kept constant. The flow rate was kept at 0.300 ml/h and positive voltage at 22.2 kV.

Table 4.1: Physical characteristics of solvents DMF and THF to dissolve PS-Au NPs prior to electrospinning

Solvent	Boiling Point (°C)	Vapor Pressure @ 20 °C (mmHg)	Volatility	Dielectric constant
N,N dimethylformamide	153	2.6	Non-volatile	37
Tetrahydrofuran	66	129	volatile	7.5

4.2.1.3 Conductivity and surface tension tests for PS-Au NPs

Gold at 0.055, 0.025, 0.025 and 0.002% w/v was added to 16% w/v PS in DMF/THF (8:2 v/v). The effect of Au NPs on conductivity and surface tension of polystyrene polymer solutions was measured using MeterLab CDM 210 conductivity meter (Lyon, France) and Kruss School Tensiometer K6 respectively. Accuracy and precision of the conductivity meter and tensiometer were demonstrated by the data standard deviations after measuring each solvent six consecutive times.

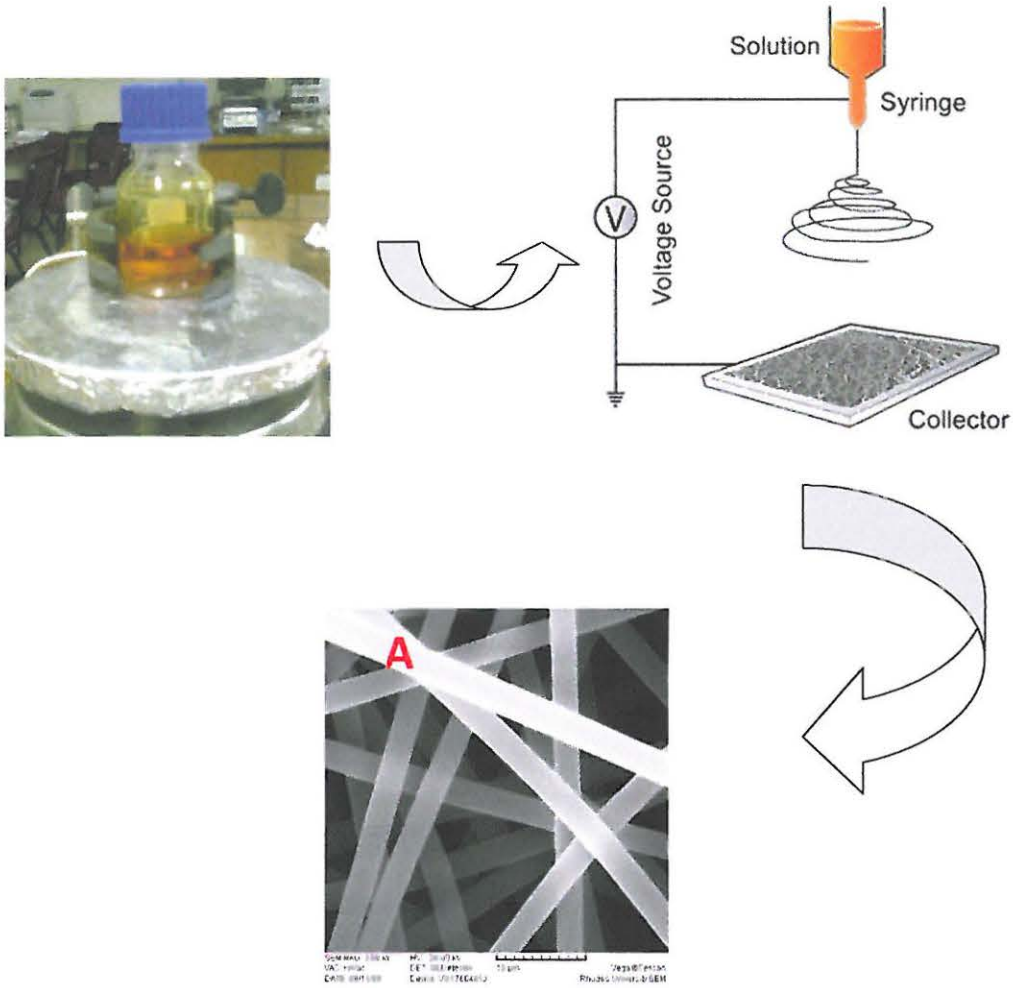

Figure 4.2: Representation of the preparation of Au NPs/diazonium dye-incorporated polymer colorimetric probe using a single nozzle electrospinning set-up; A) Typical SEM image of the electrospun polymer composite fiber

4.2.1.4 Effect of Au NPs concentration on colour intensity of the probe

Besides investigating the effects of nanoparticles concentration on conductivity and surface tension the aspect of colour intensity was also looked into. This was to determine if the electrospun fibers would give faint or intense shades of colour changes for the colorimetric detection. In order to attain intense changes in colour of PS-Au NPs toward E_2, the effect of concentration of Au NPs in polymer solution on the morphology of the electrospun fibers was investigated. The nanoparticles to polystyrene weight ratios were 1:40, 1:20 and 1:10 approximately corresponding to gold concentrations 0.002, 0.015 and 0.025% w/v respectively.

4.3 Application of PS-Au NPs probe

4.3.1 Standard solutions

The probe strips were exposed to increasing E_2 concentrations; 50, 300 and 700 ng/mℓ then 100, 800 and 1000 µg/mℓ). The optical behavior was evaluated with UV-Vis.

4.3.2 Matrix Spike Experiments

The dairy effluents were collected from a local cattle farm. Grab samples were collected from the milking shed drains and preserved by adding concentrated sulphuric acid (pH 3). The dairy water samples were stored at <4°C overnight, then thawed gradually to room temperature and used within 24 h. The sample matrix was spiked with 17β-estradiol and other environmental chemicals with estrogenic activity that included p,p'-DDE, deltamethrin, 4-tert-octylphenol and nonylphenol as well as with cholesterol so as to evaluate the colorimetric response of the PS-Au NPs probe strips. Although cholesterol does not have estrogenic activity it has been found at higher concentrations relative to estrogens, from dairy wastewater treatment plants (Oishi and Moriuchi, 2010).

4.4 Diazonium dye-incorporated nylon 6 composite

4.4.1 Buffer selection

A selection was made between phosphate and tris base buffers, at pH 7.4 and ambient temperature, pressure and humidity, to make standard solutions. The interaction of the dye with various concentrations of oxaloacetate (50, 100, 150, 200, 300, 350 and 400 μg/mℓ), in phosphate or tris base, was then evaluated with UV-Vis.

4.5 Designing the enzymatic assay: Kinetic studies

Varying concentrations of L-aspartic acid (0.8, 2.8, 6.8, 10.8, 20.8, 60.8 and 100.8 mM) were prepared in clearly labeled epperndorf tubes and to each of these epperndorf tubes constant concentrations of α-ketoglutaric acid (0.4 mM) and Fast blue BB salt hemi (zinc chloride) salt dye (2 mM) were added then dissolved with a buffer (100 μl). The reaction was initiated by adding standard solution (100 μl) of AST enzyme and absorbance over time was recorded using Capture 96 at 550 nm. The aspartate concentration was selected such that it was of the order 5-20 times K_M or greater, so that substrate concentrations were saturated and used in excess, equal/greater than10-15 fold of aspartate over α-ketoglutarate in the assay mixture. This was to help drive the reaction to the right (AST is usually competitively inhibited by high α-ketoglutarate concentrations). The Beer-Lambert equation (Eqn. 1.2) was used to calculate the absorption coefficient of the oxaloacetate-diazonium dye chromophore. The concentration of AST activity in units of μg/ml of oxaloacetate was determined using Eqn. 4.1:

$$Activity\ (U/L) = \frac{A \times Vol_{(total)}}{\varepsilon \times b \times Vol_{(sample)}} \times 1000 \qquad \ldots (4.1)$$

4.6 Optimizing electrospinning conditions

4.6.1 Effect of dye on conductivity and surface tension of polymer composite

The dye at 0.5, 2.5 and 5% w/v was added to 16% w/v N 6 in formic/acetic acid (1:1 v/v). The effect of the dye on conductivity and surface tension of nylon 6 polymer solutions was measured using MeterLab CDM 210 conductivity meter (Lyon, France) and Kruss School Tensiometer K6 respectively. Accuracy and precision of the conductivity meter and tensiometer were demonstrated by the data standard deviations after measuring each solvent six consecutive times.

Small molecular weight components have been known to alter the process conditions and fiber morphology (Li, 2004). It was therefore important to investigate whether incorporation of the dye had any effect on the conductivity, surface tension and overall fiber morphology.

4.6.2 Electrospinning conditions for dye-N6 composite

In a typical procedure (Fig. 4.1.3), predetermined quantities of the dye salt; 0.14, 0.07, 0.035 g and nylon 6 with concentration of 14 wt% were dissolved in formic/acetic acid (1:1 v/v) in a sealed vial 12. The polymer mixture was left to stir for 6 h to ensure complete dissolution as well as to eliminate air bubbles and then it was electrospun. The electrospinning set-up included a syringe pump (containing the nylon 6/dye salt solution 18) operated at a flow rate of 0.800 ml/h, a high voltage power supply with a positive polarity at 25 kV, and a collector.

4.7 Application of dye-N6 probe

4.7.1 Standard solution

The electrospun colorimetric probe strips were exposed to 10 mM standard solutions of aspartate, ketoglutarate, alanine, pryruvate, oxaloacetate and glutamate. Exposure time was 5 min @ pH 7.4 and ambient temperature for each. The optical behavior was evaluated with UV-Vis. To further evaluate the selectivity of the colorimetric probe, the test strips were exposed to a variety of dicarboxylic acids, including glutamic, malaic and succinic, known to compete and interact identically as amino, aldehyde and keto acid substrates.

4.7.2 Application in biological matrix

The colorimetric probe strips were introduced to different reaction mixtures in spiked plasma matrices. The conditions were such that aspartate concentrations varied over 0.8 – 100.8 mM concentration range while α-ketoglutarate was kept constant at 10.8 mM and that levels of oxaloacetate produced represented the AST levels in the sample. The activity of AST (U/L) equivalent to μg/ml of oxaloacetate was determined using Eqn. 4.1.

4.8 Instrumentation used for characterizing the electrospun probes

The polymer composites formed were characterized using UV-Vis spectroscopy (UV-Vis), duNouy ring tensiometer, conductivity and pH meters, Atlas Suntest CPS+ model, Brunauer–Emmett–Teller (BET), transmission electron microscope (TEM), scanning electron microscopy (SEM), X-ray diffraction (XRD) and energy dispersive X-ray spectroscopy (EDS or EDX).

4.8.1 Solution studies characterization

4.8.1.1 pH, tension and conductivity meters

The pH of the solutions was determined using the Jenway (3510) pH meter (Essex, UK). While the effect of the dye and Au NPs on conductivity and surface tension of nylon and polystyrene polymer solutions was measured using MeterLab CDM 210 conductivity meter (Lyon, France) and Kruss School Tensiometer K6 (GmbH, Hamburg) respectively.

To measure the surface tension between a liquid and the air, the duNouy ring was placed below the surface of the dye or Au NPs polymer composite solution. This test was performed by pulling the ring upward through the surface of the liquid, for at least six individual samples. The force needed for the ring to break the surface (overcome the surface tension) was then determined in Dynes/centimeter. Conductivity, in microsiemens per centimeter (μS/cm) and pH measurements were determined by just dipping the probe in the in individual solutions.

4.8.1.2 Ultraviolet-visible spectroscopy (UV-Vis)

Ultraviolet-visible absorption spectra were acquired using a double-beam instrument, a Perkin Elmer Lambda 25 UV/Vis spectrophotometer. Samples were placed in cuvettes with an internal width of 1 cm. The instrumental procedure was that the light was split into two beams before it reached the sample. One beam was used as the reference while the other beam passed through the sample. The reference beam intensity is taken as 100% Transmission (or 0 Absorbance), and the measurement was cancelled out by running a blank sample.

UV-Vis spectra were acquired to gain insight on the surface plasmon resonance (SPR) characteristics of Au NPs, in which the highly concentrated samples were diluted pro rata to adapt the measurement limitation. The spectra were also used to evaluate for the presence of oxaloacetate formed from the AST catalyzed reaction of aspartate and alpha-ketoglutarate. The production of oxaloacetate was coupled with the diazonium dye indicator to produce a chromophore that absorbs light between 500 and 630 nm.

4.8.1.3 Transmission electron microscopy (TEM)

Transmission electron microscopy was used complimentary to UV-Vis. Optical absorption studies were carried out with UV-visible while TEM allowed probing into the internal structure and spatial distribution of Au NPs, through direct visualization. In transmission electron microscopy a beam of electrons is transmitted through an electronically transparent specimen interacting with the atoms to produce one image. Due to the small *de Broglie* wavelength of electron image, atomic resolution is possible to be captured by TEM. TEM samples were prepared by dropping the diluted gold colloids on carbon-coated copper grids, followed by natural drying and then samples were observed on a JEOL-JEM 2010 (JOEL Ltd, Tokyo, Japan) electron microscope operating at 100 kV. Polystyrene-gold composite solution TEM characterization was carried out prior to electrospinning.

4.8.2 Solid state probe: fabrication and characterization

4.8.2.1 Electrospinning

A typical electrospinning process employed a single nozzle setup (Fig 4.2.2) comprising an infusion pump (KD Scientific Syringe Pump Series 100 or New Era Multi-phaser NE-1000) and a high voltage source (Glassman High Voltage Series EH). A polypropylene 25 ml syringe and a 21 gauge needle connected, through polytetrafluoroethylene (PTFE) tubing to a 90° blunt end stainless steel needle was clamped horizontally on the syringe pump. The needle was then connected to the anode of the high voltage power supply. The grounded static collector system was a flat aluminum sheet placed on a support. All polymer solutions were delivered by a syringe pump at controlled flow rates. Electrospinning was carried out at ambient conditions.

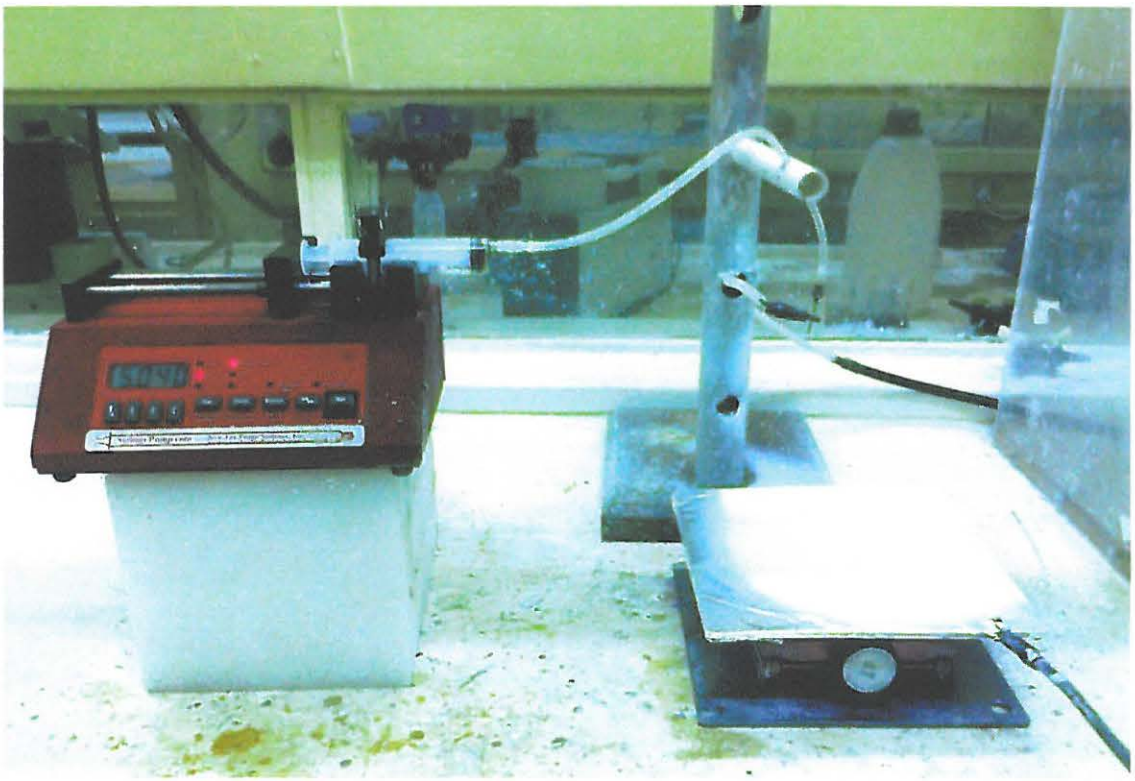

Figure 4.3: Electrospinning setup

4.8.2.2 Scanning Electron Microscope (SEM)

Morphology of the electrospun fibers was studied using two scanning electron microscopes; a low-resolution Tescan TS5136ML (Brno, Czech Republic) and a high-resolution Jeol JSM–700F Field Emission Scanning Electron Microscope (FE-SEM). Samples were air dried, attached to a metallic stub and then sputter coated with gold prior to insertion into the SEM using Balzers SCD 030 (Liechtenstein, Germany). Upon insertion of the sample into SEM, acquisition of the micrographs was achieved fairly quickly allowing images to be obtained with varying magnification ranges between 1000 and 150000.

In addition to imaging the surface morphology of the electrospun polymeric fibers, the SEM was combined with energy dispersive X-ray analysis (EDX) to determine elemental composition of the Au NPs.

4.8.2.3 Energy dispersive x-ray spectroscopy (EDX/EDS)

Similar to the SEM sample preparation, the samples were air dried and attached to a metallic stub. The stubs were loaded into a TESCAN Vega TS 5136LM SEM with an Oxford Instruments EDS analysis system. Preliminary SEM studies were necessary to establish the optimal operating conditions to obtain images of the fiber surfaces for subsequent image analysis for elemental/composition analysis. The data were processed using Scandium software as well as the image analysis capabilities of the SEM. The software had an XPP (extended Puchou/Pichoir) correction procedure, mainly in order to deconvulate peaks where peak overlaps exist.

4.8.2.4 X-ray Powder Diffraction (XRD)

Further evidence for the formation of gold nanoparticles was provided by X-ray diffraction (XRD) analysis. X-ray diffraction studies of the Au NPs-elctrospun polymer fiber were carried out in the transmission mode on a Philips PW 1830 instrument operating at 40 kV voltage and a current of 30 mA using a Cu anode-based powder diffractometer operating in the Bragg–Brentano focusing geometry, and a curved crystal monochromator in the diffraction beam. The sample pressed into the sample holder to get a smooth plane surface and the diffraction pattern was recorded over a 2θ range of 30-100°. All the parameters that could potentially interfere with the analysis were refined and these included scale factor, zero correction, background and half-width parameters along with mixing parameters, lattice parameters, positional coordinates and thermal parameters.

4.8.2.5 Brunauer–Emmett–Teller (BET) surface analysis

The Brunauer–Emmett–Teller (BET) specific surface area and porosity parameters were calculated using nitrogen adsorption analysis with a Micromeritics (Norcross, GA, USA) ASAP 2020 accelerated surface area and porosity analyzer. Prior to analysis, samples were preconditioned to remove any physically bonded impurities. Basically, the samples were exposed to elevated temperatures in the presence of either a vacuum or continuously flowing inert gas. For this study, samples were first degassed at 105 °C under vacuum overnight to remove any adsorbed solvent. The adsorption isotherms of the degassed samples were then acquired using nitrogen as the adsorbate at a temperature of 180 °C. The specific surface areas, total pore volume and pore size distribution were calculated from N_2 gas adsorption–desorption isotherms. The process was carefully controlled and monitored in order to generate accurate and reproducible results.

4.8.2.6 Photostability

For each sample, one gram of the electrospun fiber was placed in a petri dish and kept in a photo stability chamber, Atlas Suntest CPS+ model for seven days. The irradiance was set at 200 Wh/m^2 in ultraviolet (UV) light. Conditions were set such that only light would be the stressful conditions exposed to the fiber sample.

After developing and characterizing of colorimetric probes we then considered the logistics of shelf life of the colorimetric probe. Shelf-life depends on a variety of factors such as leaching of nanoparticles from the electrospun colorimetric probe, packaging, electrospinning process and environmental conditions during transport, storage and use.

Chapter 5

Results and Discussions

This section is divided into two major parts, gold nanoparticles and the dye based categories. For each component the first results are from the solution studies followed by findings from the solid probe development.

5.1 Polystyrene-Au NPs based colorimetric probe

5.1.1 Synthesis of Au-PS composite

Polystyrene stabilized gold nanoparticles were synthesized by *in situ* reduction of Au^{3+} with sodium borohydride. It has been shown that in a system where species do not have a high affinity towards Au, BH_4^- ions bind to the surface of gold nanoparticles and form a negatively charged layer that contributes towards stabilizing the nanoparticles (Fig. 5.1). However, due to secondary interactions with the environment BH_4^- ions are generally not efficient stabilizers (Olenin and Lisichkin, 2011, Uehara, 2010). For instance, BH_4^- ions adsorbed on the surface of nanoparticles usually react with water molecules resulting in aggregation of nanoparticles. For the study in this thesis, polystyrene was used to stabilize the nanoparticles against aggregation.

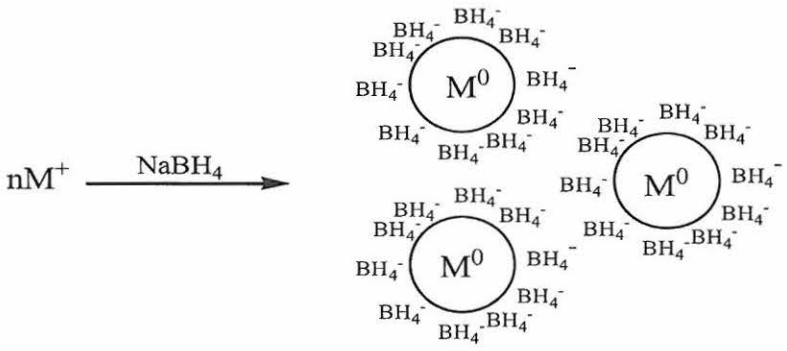

Figure 5.1: Schematic illustration for synthesis and stabilization of metal nanoparticles by tetrahydroborate ions (BH_4^-) (Adapted from Olenin and Lisichkin, 2011)

Polymers (e.g. polystyrene), including small molecules and polyelectrolytes are known to stabilize nanoparticles through steric, electrostatic and electrosteric (a combination of electrostatic and steric) interactions, respectively (Zhang et al., 2011b, Seo et al., 2009). Properties such as concentration of reducing agent, weight ratio of gold salt to the stabilizing agent and temperature are known to have an impact on the stability of Au NPs. One of the prerequisites for a successful use of an analytical probe, PS-Au NPs, developed in this thesis, was achieving colloidal stability of nanoparticles, which can affect the spectroscopic signature of surface plasmon resonance wavelength.

5.1.1.1 Optimizing concentration of reducing agent

Other parameters kept constant, a yellow solution turned green upon addition of $NaBH_4$ at concentration 0.05 mol/l. The green polymer composite solution showed no discernible absorption in the 500-600 nm regions even after a week indicating that reduction of Au (III) ions did not occur. This assertion was consistent with TEM as only crystals were observed. The crystals could be the gold salt that usually absorb in the 200 - 350 nm region. The UV-Vis absorbance for gold (III) chloride ions was observed at ~ 314 nm maximum peak in one study (Peck, 1991). Figure 5.2 shows the optical absorbance spectrum with an intense band at ~ 319 nm and TEM image for the green solution.

When the $NaBH_4$ concentration increased to 0.1 mol/l a brown colour was observed which also confirmed the likely stability of Au NPs against aggregation. The narrow SPR band at ~ 570 nm (Fig. 5.3A) indicated spherical and dispersed Au NPs which was in agreement with the TEM image shown in Fig 5.3B. The colloidal stability of Ps-Au NPs changed when $NaBH_4$ concentration increased from 0.1 to 0.2 mol/l. A dark blue solution was given and it had a broad SPR band with a shoulder at a higher wavelength (~ 680 nm), see Fig. 5.3A. Transmission electron microscope image exhibited aggregated Au NPs (Fig. 5.3C) that was consistent with the UV-Vis findings; a broad SPR band and a shoulder at higher wavelengths usually indicates aggregated nanoparticles.

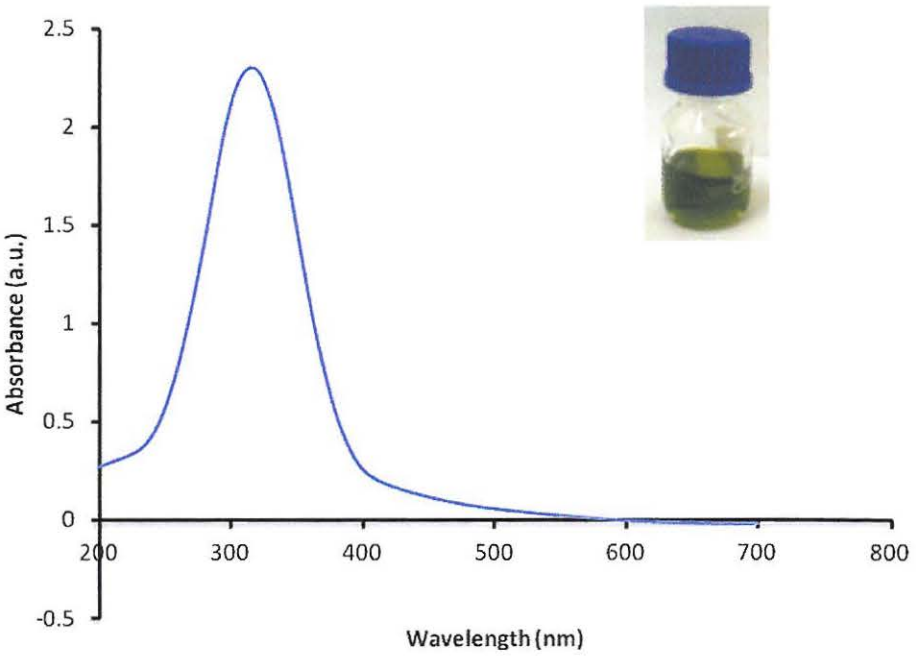

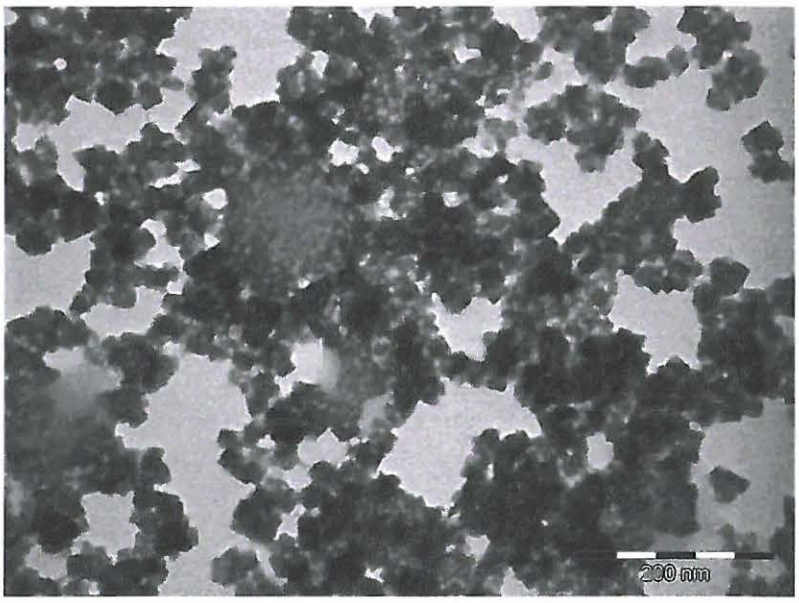

Figure 5.2: UV-Vis absorption spectra for the green polymer composite solution after reduction with 0.05mol/l $NABH_4$ and the corresponding TEM image

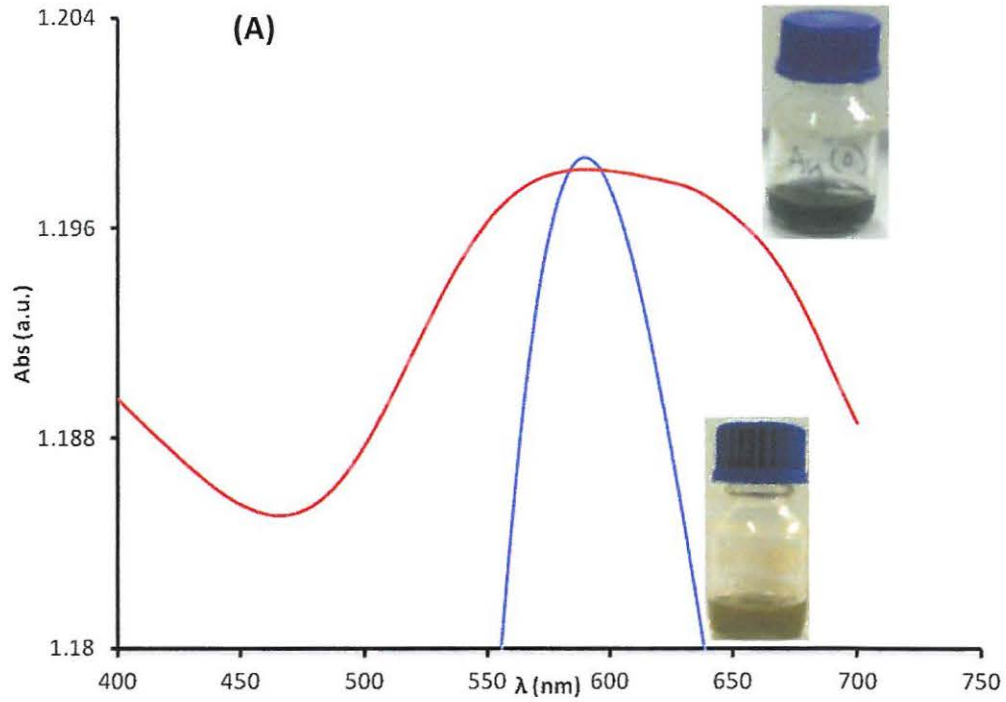

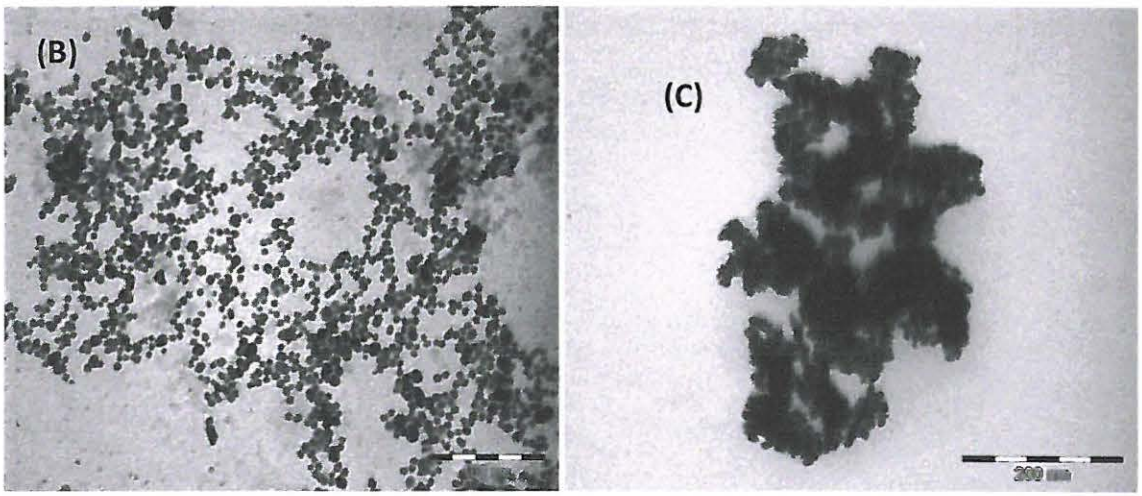

Figure 5.3: (A) UV-Vis absorption spectra of the PS-Au NPs with 0.1 mol/l $NaBH_4$ (brown solution and blue narrow SPR band) and PS-Au NPs with 0.2 mol/l $NaBH_4$ (dark blue solution and brown coloured SPR band); (B) TEM images of PS-Au NPs for the brown solution and (C) TEM showing aggregated Au NPs (dark blue solution)

5.1.1.2 *Effect of gold concentration on conductivity and surface tension of PS-Au NPs solution*

One of the major challenges in fabricating metal-polymer composites has been the uniform dispersion of nanoparticles in the polymer matrix, since van der Waals forces between individual nanoparticles cause agglomeration. The ratio of the nanoparticles to the polymer matrix and dispersion of nanoparticles may alter conductivity of the polymer composite. At a low percentage of nanoparticles, the distance between particles is large, resulting in a lower conductivity. The percolation threshold exists at higher nanoscale inclusions, however, at high percentage of nanomaterials, particles tend to agglomerate due to the lack of dispersion and interfacial interactions and subsequently impede the formation of conductive pathways (Wang et al., 2012).

Therefore, for this thesis the effect of different gold concentrations on the conductivity and surface tension of the PS-Au NPs solution were investigated. A summary of the results is shown in Table 5.1. The results revealed that with increasing concentration of gold, the conductivity values of the corresponding solutions also increased while there was minimum effect on the surface tension.

Table 5.1: Conductivity and Surface tension as a function of gold concentration on PS-Au NPs solution

Gold Concentration % w/v	Conductivity µS/cm	Std Dev (n=6)	Surface Tension mN/m	Std Dev (n=6)
0.002	153.8	0.5	36.5	0.1
0.015	307.0	0.3	36.5	0.2
0.025	920.8	0.3	36.6	0.1
0.055	1535	0.5	36.7	0.1

- Conductivity for 16% w/v polystyrene = 102.3 µS/cm @ 28 °C and 36.5 mN/m surface tension

At low concentrations of gold (0.002, 0.015 and 0.025% w/v) PS-Au NPs solution could be electrospun without clogging. However, at high gold concentrations (0.05 up to 0.30% w/v) it was a challenge to electrospin the PS-Au NPs solutions, which could have been due to excessively high conductivity, resulting in the clogging of PS-Au NPs solution at the capillary tip during the electrospinning process. 153.8 µS/cm was chosen as the operative conductivity of PS-Au NPs solution for fiber structures.

5.2 Colorimetric detection of 17β-Estradiol

Under optimal conditions, dispersed Au NPs, regardless of shape and size, were synthesized. The assumption was that the colorimetric mechanism was based on the aggregation of Au NPs resulting in nanoparticle clusters upon the interaction of the probe with the analyte (Fig. 5.4).

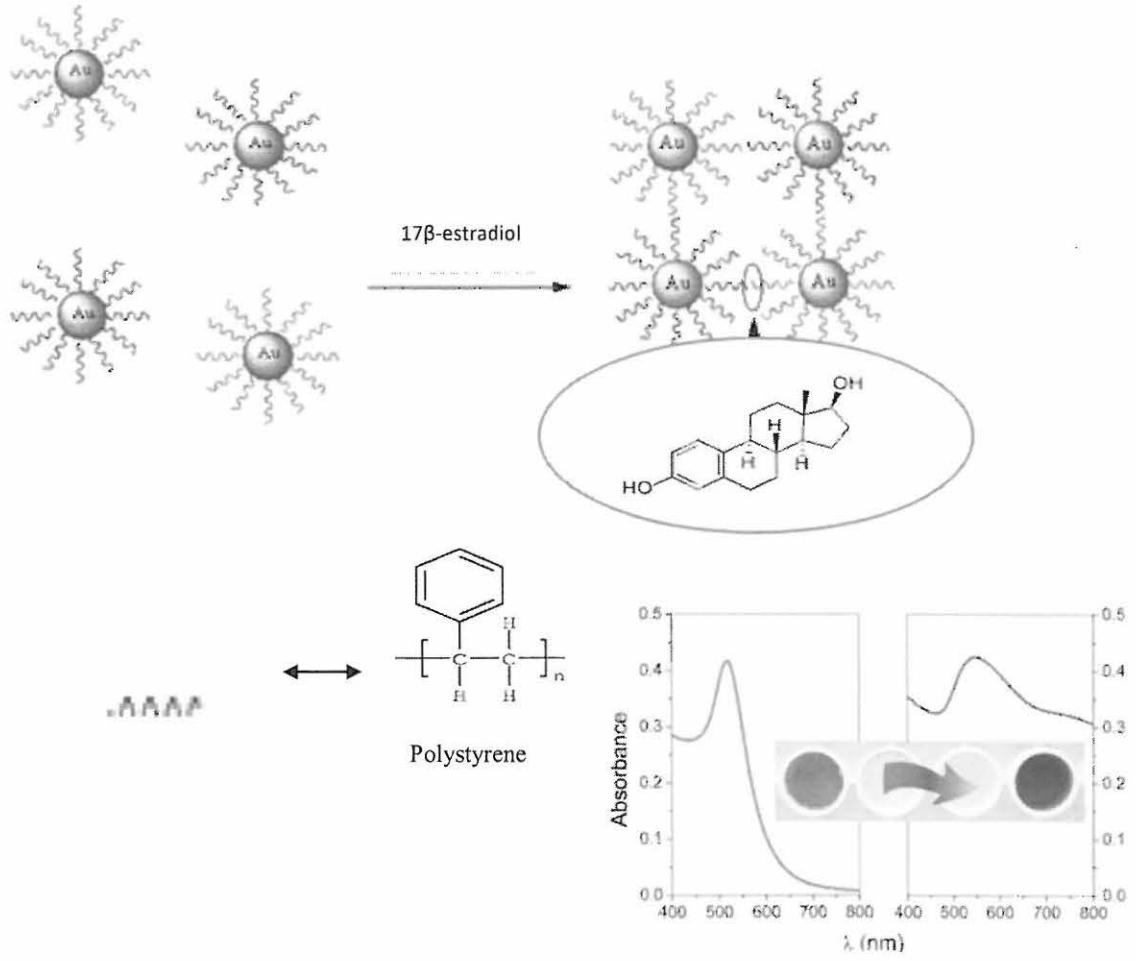

Figure 5.4: Schematic representation of PS-Au NPs colorimetric mechanism for 17β-estradiol detection [Adapted from Zhang et al., and Chen et al.,] (Zhang et al., 2010, Chen et al., 2012)

The prepared PS-Au NPs showed an absorption band at 542 nm, which is characteristic to the surface plasmon resonance of Au NPs. The interaction of E_2 with PS-Au NPs induced aggregation of PS-Au NPs and resulted in the SPR absorption band shifting to a longer wavelength (Fig. 5.5).

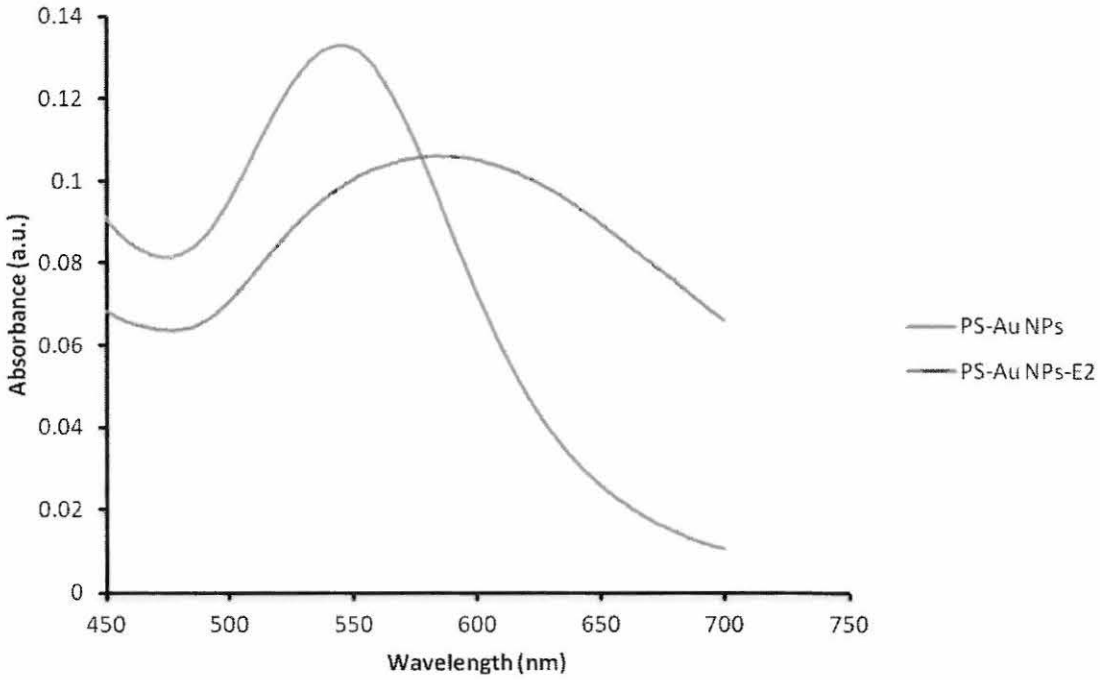

Figure 5.5: Typical absorption spectra of the PS-Au NPs in the absence and in the presence of 17β-estradiol (PS-Au NPs-E_2)

The TEM images verified dispersed, spherical and triangular plate PS-Au NPs (Fig. 5.6A), while a significant 17β-estradiol stimulated aggregation of PS-Au NPs was further evidenced in Fig. 5.6B.

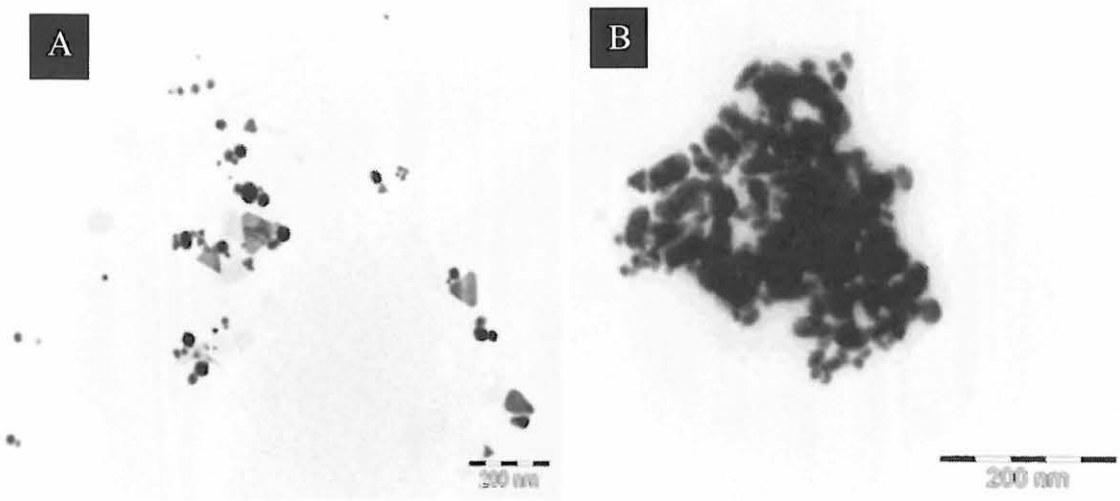

Figure 5.6: (Typical TEM images of PS-Au NPs (A) in the absence and (B) in the presence of 17β-estradiol (PS-Au NPs-E2)

For further evaluation of the analytical performance of the probe, different concentrations (5, 10, 25, 50, 100, 150 and 200 ppb) of E_2 from one stock solution exhibited a concentration dependent absorbance. Absorbance gradually increased upon addition of increasing concentrations of E_2 as shown in Fig. 5.7. A good linear correlation was attained at E_2 concentration in the range 5 to 50 ppb. The regression equation was $Y = 0.0011x + 0.1716$ and $R^2 = 0.9934$. The lowest detection limit was calculated using Eqn. 5.1 and found to be 0.5 ppb.

$$LOD = 3\sigma \qquad \ldots (5.1)$$

Although lower LODs have been attained in other studies, it should be noted that our probe was used without further functionalization. Just to site one example, Olowu *et al.* developed DNA aptasensor with high affinity for endocrine-disrupting 17β-estradiol and obtained a detection limit of 0.02 nM (~0.5 x 10^{-14} ppb) (Olowu et al., 2010).

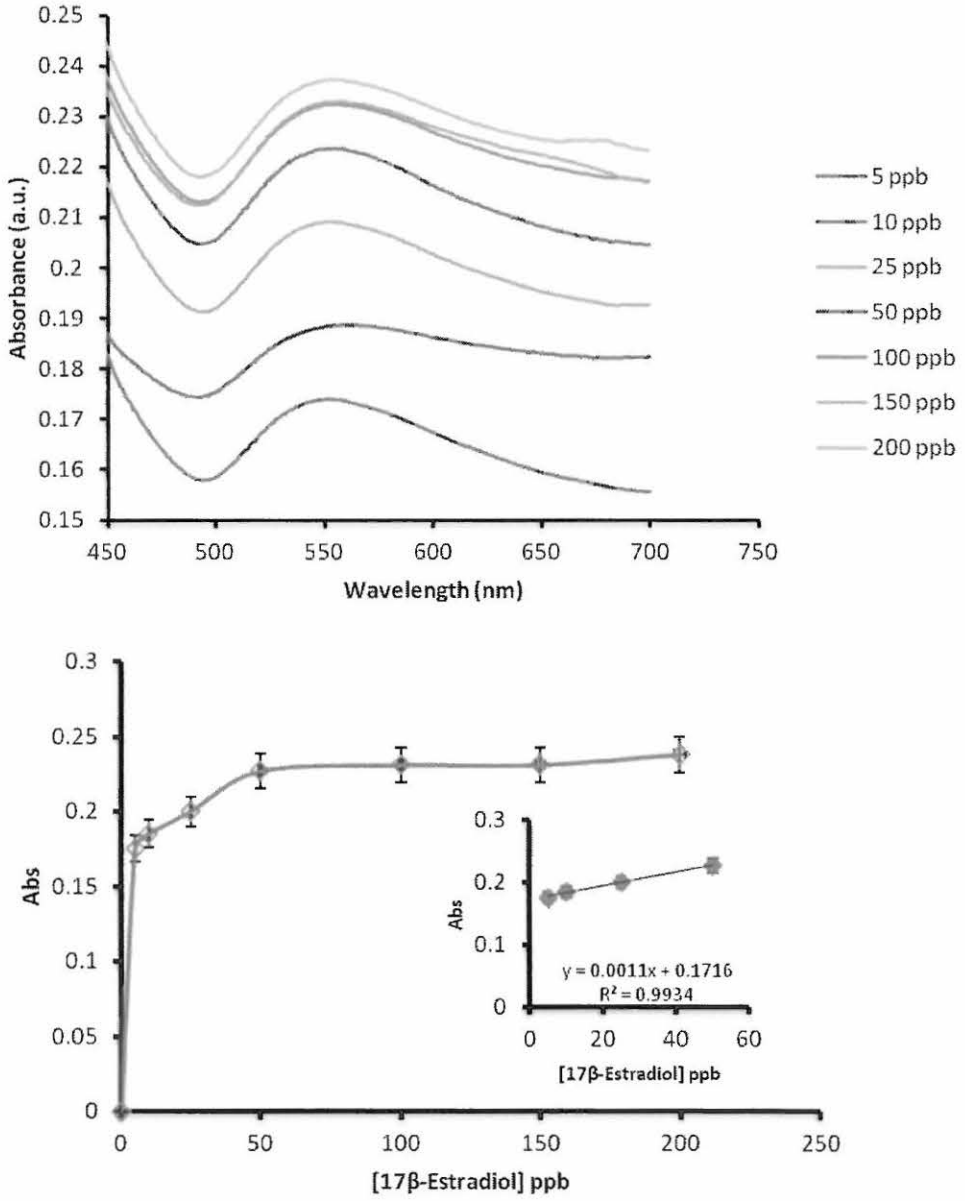

Figure 5.7: Relationship between the UV-Vis absorbance and the concentration of 17β-estradiol

5.3 Electrospinning of the PS-Au NPs polymer composite solution

At 10 and 12% w/v PS solution, bead-on-string structures were observed, probably due to the high content of the solvent that had not evaporated completely before the fibers were collected. Increasing PS concentration from 12 to 20% w/v decreased the amount of bead-on-string structures. The bead-free fibers were observed at 16 and 20% w/v PS in DMF/THF 8:2 v/v. It was also observed that average diameter of fibers increased when PS concentration increased from 10 to 20% w/v. Figure 5.8 summarizes the changes in the fiber diameter and morphology as a function of the polystyrene concentration as observed by a low-resolution Tescan TS5136ML SEM. The results were consistent with previous studies that revealed that the average diameter of the fibers increased with increasing polymer concentration. The increase in fiber diameter is normally due to high resistance of the polymer solution to be stretched by electrostatic force during the electrospinning process (Nitanan et al., 2012, Patel et al., 2012). The optimal concentration was 16% w/v PS. This was because 20% w/v PS showed a larger average fiber diameter that could be attributed to insufficient stretching of the highly viscous PS solution.

It is worth noting that for the DMF:THF mixed solution of PS, DMF is usually the main charge carrier because DMF has a dielectric constant of about 37, which is much higher than that (2.5) of PS and that (7.5) of THF (Fu et al., 2008). Tetrahydrofuran was therefore added to enhance the electrical conductivity toward achieving fabrication of bead free fibers, by allowing maximum effect of the electrical forces and minimizing the effect of surface tension.

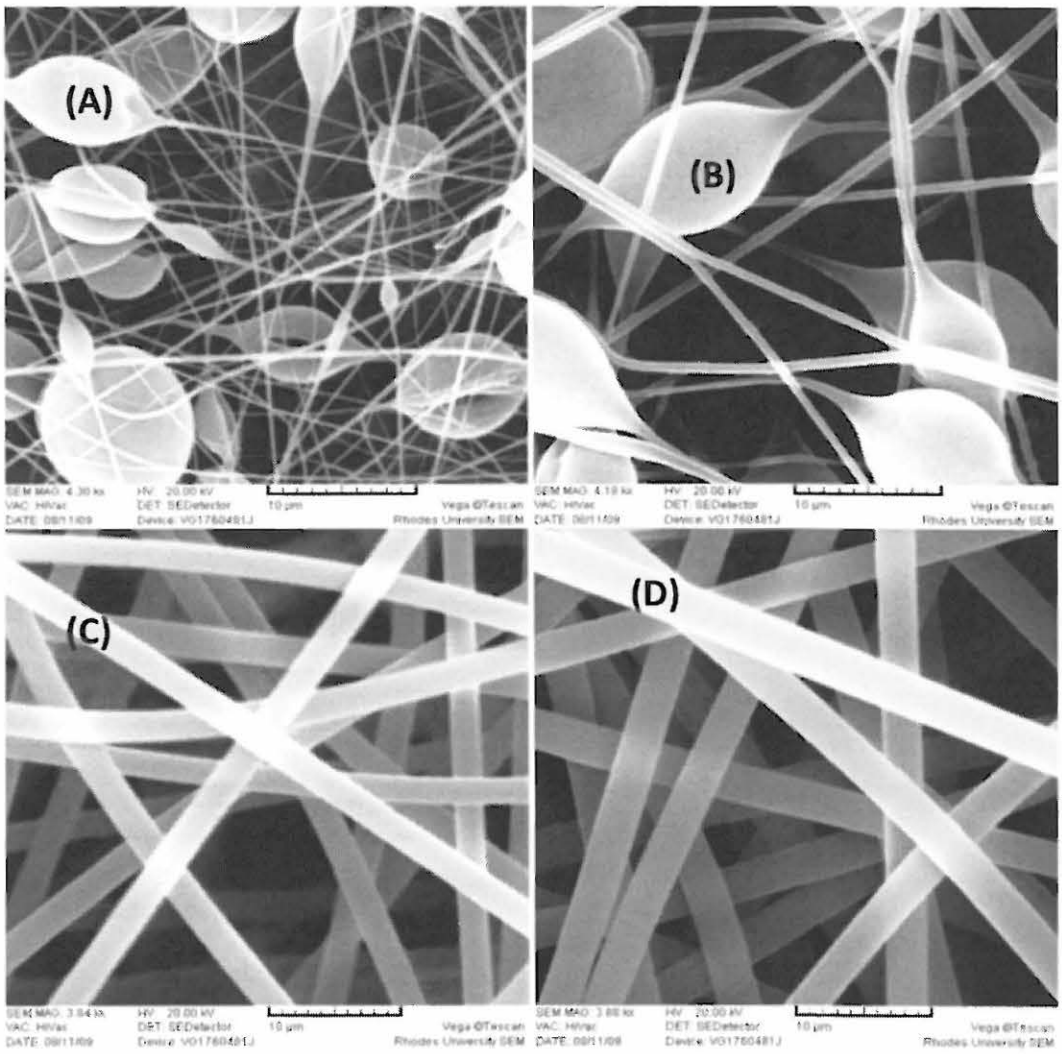

Figure 5.8: Summarizes the changes in the fiber diameter and morphology as a function of the polystyrene concentration; A) 10, B) 12, C) 16 and D) 20% wt/v were investigated while other parameters were kept constant; flow rate was kept at 0.300 ml/h and positive voltage at 22.2 kV

5.3.1 Optimizing concentration of gold nanoparticles for colour intensity of the colorimetric probe

The ratio 1:40 gave the best colour changes (Fig. 5.9A insert) and was therefore chosen to give the optimum Au NPs concentration.

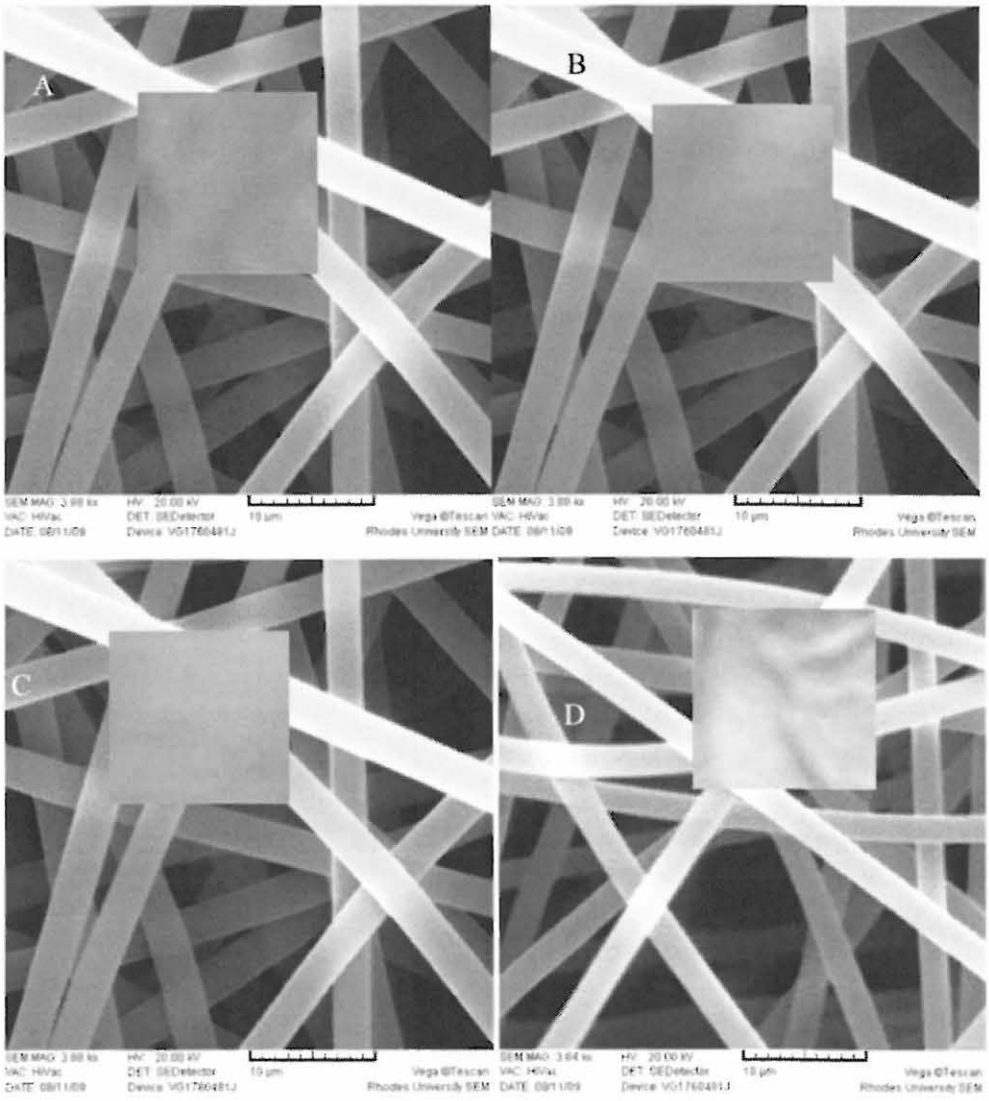

Figure 5.9: Scanning Electron Microscope images of 16 wt% PS-Au NPs electrospun fibers at raito (A) 1:40; (B) 1:20; (C) 1:10; (D) Control. The inserts show corresponding photographs of PS-Au NPs electrospun fibers upon interaction with 100 ppb (ng/mℓ) 17β-estradiol

At a higher magnification, a high resolution, FE-SEM, image confirmed the non-beaded morphology of electrospun PS-Au NPs composite fibers (Fig. 5.10). The insert in Fig. 5.10 exhibit encapsulated and dispersed Au NPs within the PS electrospun fiber. The assumption is that the Au NPs are dispersed as small clusters rather than as individual nanoparticles. The instability of these gold nanoparticle clusters drove the colorimetric mechanism for the naked eye detection of 17β-estradiol.

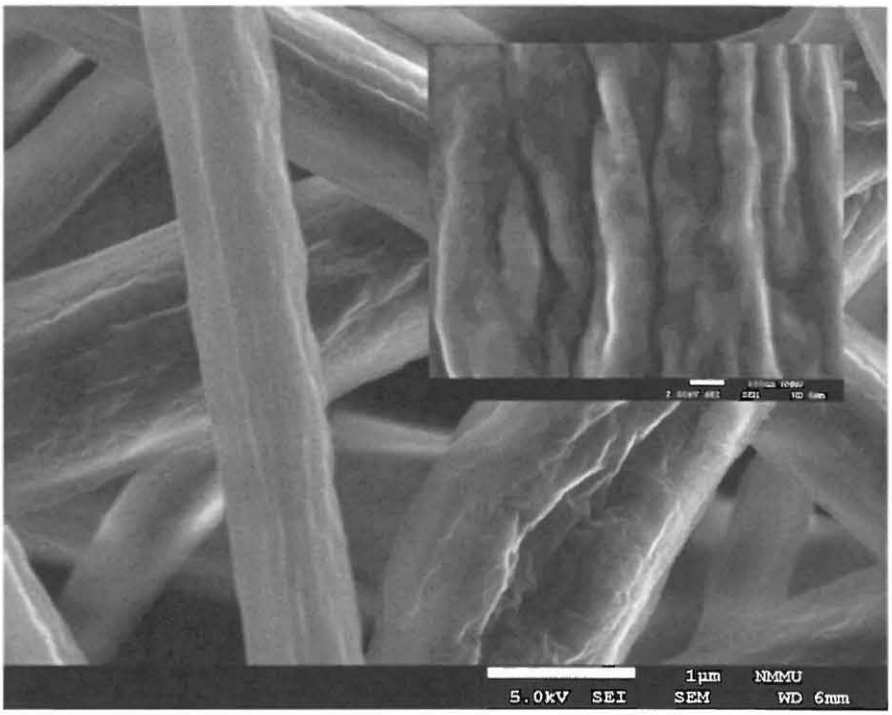

Figure 5.10: FE-SEM image of PS-Au NPs fibers electrospun from 16 wt% PS with molar ratio of 40: 1 w/w

It is believed that during the electrospinning process, particles having diameter less than the diameter of the polymeric nanofibers will be embedded within the nanofibers, see Fig. 5.11 for a conceptual illustration. The big particles on the other hand will stick on the polymeric nanofibers (Barakat et al., 2010). This maybe explains why the nanoclusters could be observed on the surface of the electrospun composites in Fig. 5.10.

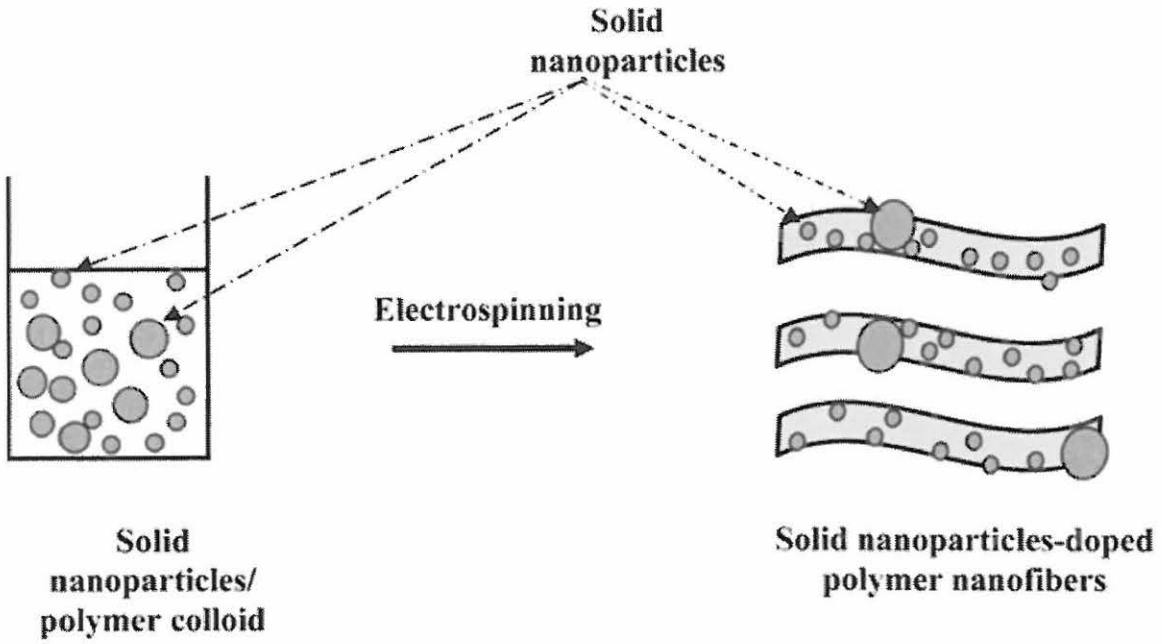

Figure 5.11: Conceptual illustration showing electrospinning of the colloidal solution (Barakat et al., 2010)

5.4 Characterization of PS-Au NPs colorimetric probe

Figure 5.12 shows that the electrospun fibers were composed of various elements. The elements Cu and C detected were from the carbon coated copper grid used as a sample holder while Cl, O, F could just be impurities from the solvent, polymer pellets or the equipment.

5.4.1 Energy dispersive X-ray spectrum (EDS)

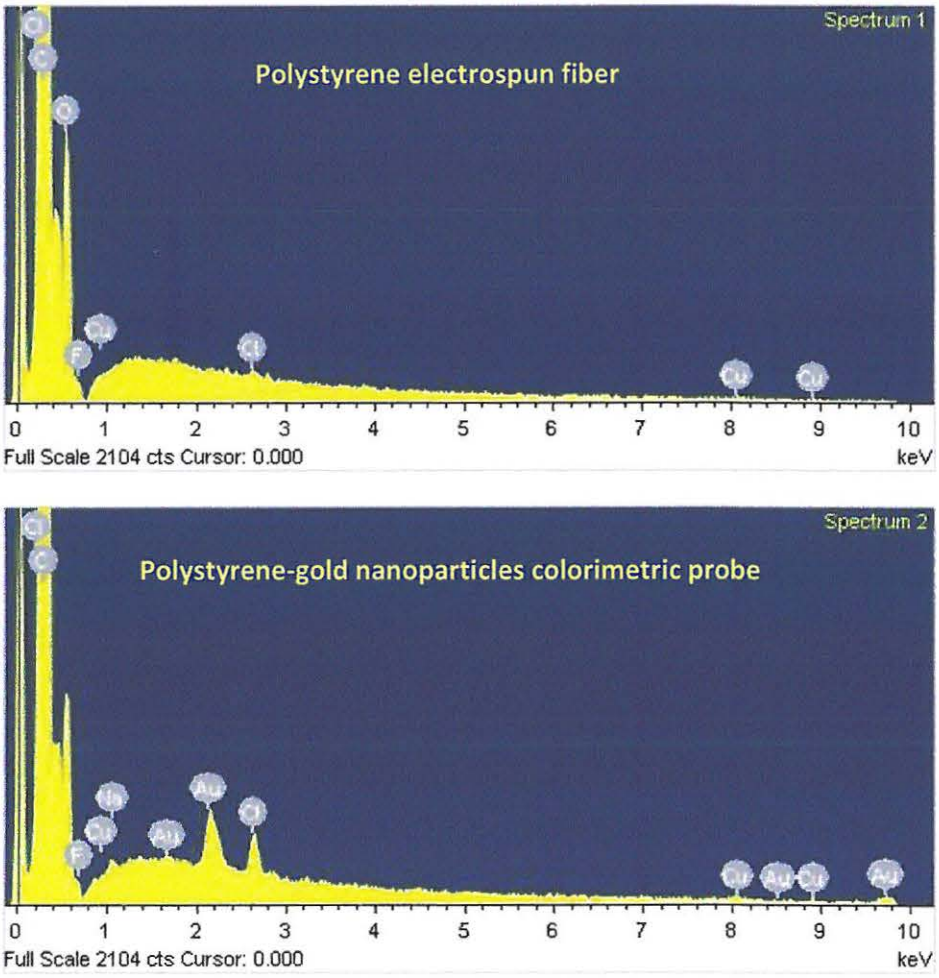

Figure 5.12: Energy dispersive X-ray spectrum (EDS) of polystyrene electrospun fibers and polystyrene-gold nanoparticles composite electrospun fibers

The weak Cl signal could also indicate the presence of a small fraction of $AuCl_4^-$ ions in the region being investigated. Figure 5.12 (spectrum 2) presents the results obtained from the EDS analysis to determine the chemical composition on the PS-Au NPs electrospun fibers, the colorimetric probe. Here, the spectrum consisted of different peaks for gold and those for copper, carbon, and chlorine, fluorine and oxygen found on the EDS spectrum for polystyrene without the Au NPs. The gold displayed two major peaks of Lα and Mα shells at 9.72 and 2.16 keV, respectively. The Au peaks found in this thesis are in agreement with studies that have suggest that major peaks at around 9.72 and 2.16 are characteristic of metallic gold (He et al., 2011, Medina-Ramírez et al., 2009, Kundu and Liang, 2008).

5.4.2 X-ray diffraction (XRD)

X-ray diffraction (XRD) analysis further confirmed the formation of gold nanoparticles. After thermally annealing the probes at 300 °C for 30 min, the XRD pattern of the gold nanoparticles diffraction peaks at $2\theta = 38$, 44, 65, and 78° corresponding to the diffraction planes (111), (200), (220) and (311) were shown (see Fig. 5.13). These diffraction peaks are usually indexed to the gold metal with face centered cubic structures. The peaks are ascribed to four strong Bragg reflections that showed that the Au NPs formed within the fiber were crystalline. These XRD findings were consistent with literature (Jiang et al., 2007, Mukherjee et al., 2001, Yazid et al., 2010).

Strong signals were attributed to the gold atoms in the nanoparticles, while the signals are usually from the substrate materials or could be weaker signals from C and O atoms.

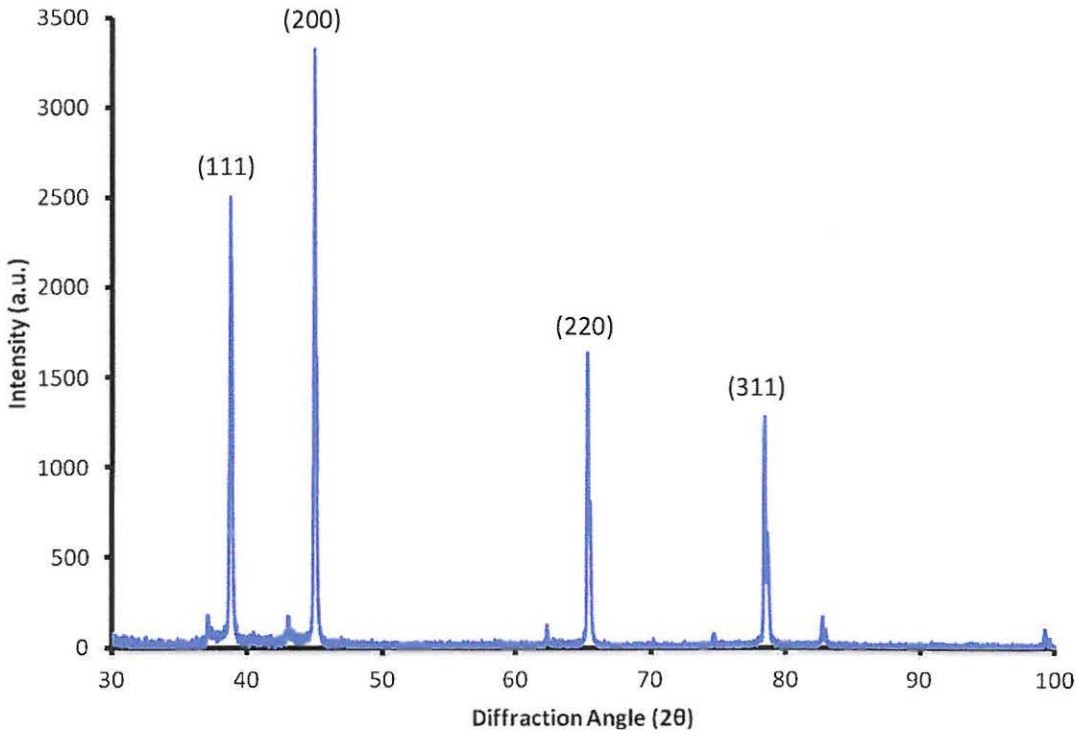

Figure 5.13: X-ray diffraction (XRD) of the PS-Au NPs composite exhibiting patterns of the gold nanoparticles prepared by *in situ* chemical reduction technique

5.4.3 Stability tests for PS-Au NPs probe

Polymer–inorganic composite nanofibrous structures are known to have intriguing properties which combine the advantages of polymers such as structural flexibility and lightweight with the properties of inorganic materials such as high mechanical strength, high thermal stability and excellent electrical, magnetic, optical and catalytically properties (Kayaci et al., 2012). However the probe is also liable to chemical decomposition by hydrolysis, oxidation, isomerization, polymerization, or photochemical degradation that may lead to physical changes. For instance, altering physical appearance (discolouration) hence mess up colour interpretations for the probe. For this thesis, the colorimetric strips were tested for photostability. After placing the strips in a photo stability chamber at 200 Wh/m^2 in UV-Vis light and 1.2 million lux h for seven days, there was no observable difference in terms of colour change for the strips exposed to irradiance and those which were not upon, interaction with 17β-estradiol at 300 ng/mℓ, 700 ng/mℓ, 100 μg/mℓ, and 800 μg/mℓ at 60 sec exposure time for each concentration (see Fig. 5.14).

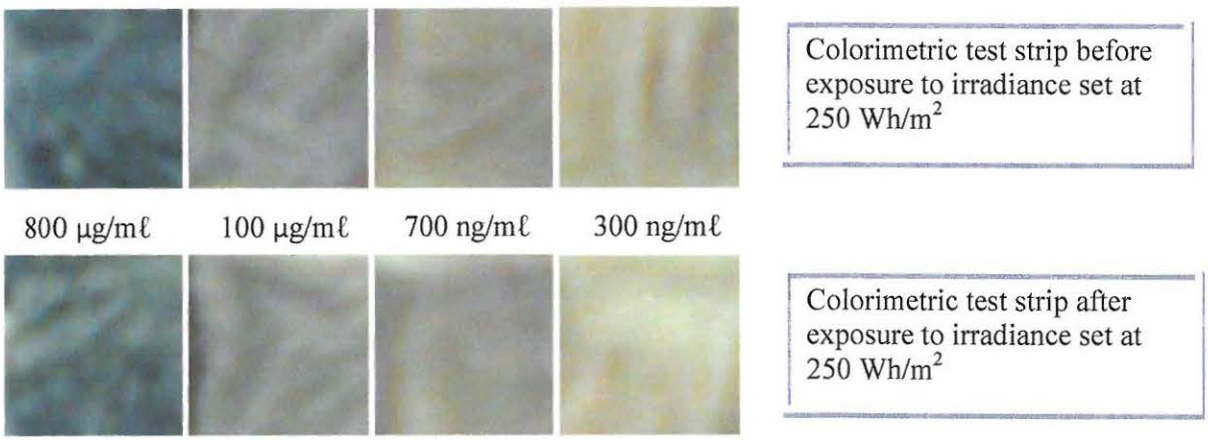

Figure 5.14: Photographs showing polystyrene-Au NPs probe strips before and after irradiance set at 250 Wh/m^2 upon exposure to 17β-estradiol concentrations; 300 ng/mℓ, 700 ng/mℓ, 100 μg/mℓ and 800 μg/mℓ at 60 sec exposure time for each concentration

Finally, fibers that were electrospun and kept for about 12 months were visually inspected and they seemed to be intact in terms of colour and texture.

5.5 Application of PS-NPs probe

5.5.1 Standard solutions

Figure 5.15 presents a profile of the colorimetric response of the probe strips towards various E_2 concentrations. It was observed that with increasing E_2 concentrations (50 ng/mℓ to 1000 μg/mℓ) the colour of the probe changed gradually from white to shades of pink and eventually to shades of blue at higher E_2 concentrations. With an increase in E_2 concentration the surface plasmon resonance (SPR) band shifted to a longer wavelength (Fig. 5.15). The surface plasmon resonance band shift is usually accompanied by a visual colour change, from pink to blue.

The high resolution FE-SEM images (Fig. 5.16) revealed that upon interaction of the probe strip, even at ng/mℓ 17β-estradiol concentrations, the clusters tended to agglomerate further and became more visible on the fiber surface. Figure 5.16A illustrates typical agglomeration of Au NPs upon interacting with 800 μg/mℓ E_2 while the inset depicts a blue shade indicative of higher E_2 concentrations. Figure 5.16B on the other hand, is a typical SEM image showing that lower E_2 concentrations induced relatively less visible Au NPs agglomerates (as shown by the white clumps). Figure 5.16B inset is an optical photograph for the probe showing a typical pink colour for lower E_2 concentrations. The probe showed an excellent performance towards colorimetric detection of E_2 using standard solutions.

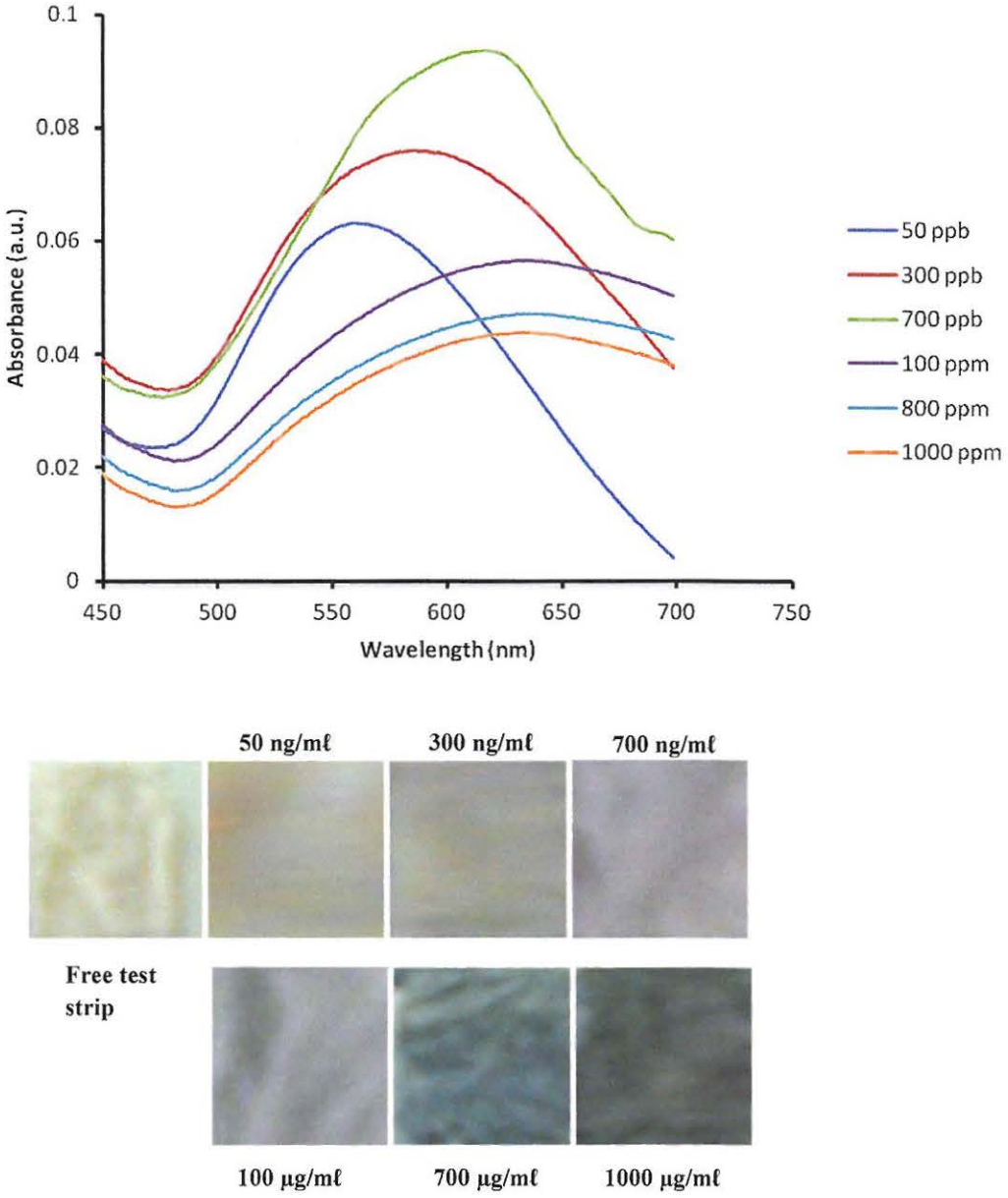

Figure 5.15: UV–Vis absorbance spectra and photographs showing polystyrene-Au NPs probe strips upon exposure to increasing 17β-estradiol concentrations; 50 ppb (ng/mℓ), 300 ppb, 700 ppb, 100 ppm, 800 ppm and 1000 ppm (µg/mℓ) at 60 sec exposure time for each concentration

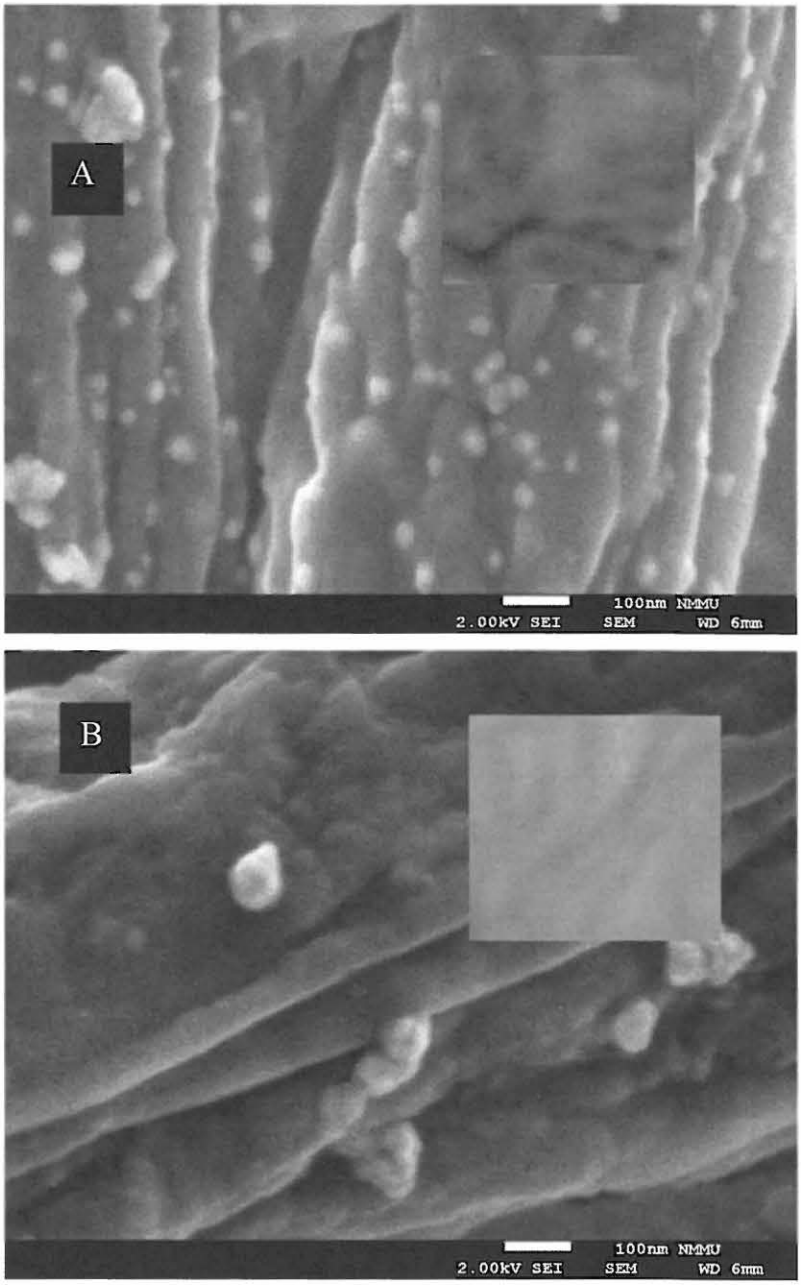

Figure 5.16: FE-SEM images of A) Au NPs agglomerates after interacting with E_2 @ 800 µg/mℓ (inset is a typical blue probe indicative of higher concentrations of E_2) B) Au NPs agglomerates upon interaction with E_2 @ 500 ng/mℓ while the inset shows a pink strip typical of E_2 at lower concentrations

5.5.2 Application in dairy effluents

The spiked dairy effluents allowed analyses without any further sample treatment. 17β-estradiol and cholesterol, selected as representatives of estrogens and other steroids while p,p'-DDE and deltamethrin, 4-tert-octylphenol and nonylphenol representing pesticides and alkylphenols respectively interacted differently with PS-Au NPs probe the strips. It was observed that the probe changed from white to a brown shade on exposure to the unspiked dairy matrix. Upon interacting with the different analytes the probe strip turned pink with E_2 while with p,p'-DDE, deltamethrin, 4-tert-octylphenol, nonylphenol and cholesterol the probe showed a similar brownish colour as with the free matrix (Fig. 5.17). After 120 seconds exposure time and the observed colour changes, the developed probe showed good selectivity towards E_2.

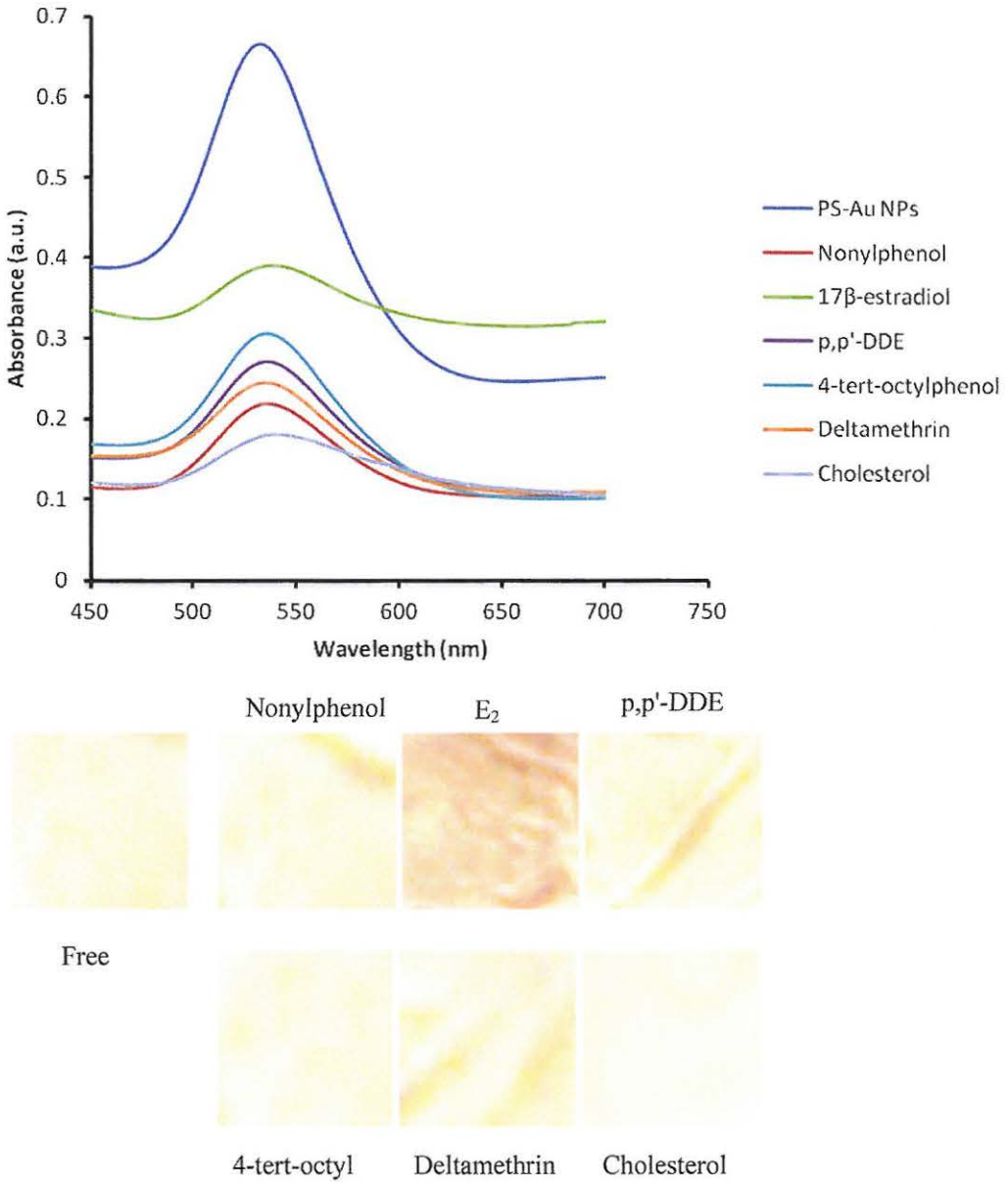

Figure 5.17: UV–Vis absorbance spectra and photographs showing colorimetric responses of strips upon exposure to 200 ng/mℓ 17β-estradiol, p,p'-DDE, deltamethrin, 4-tert-octylphenol, nonylphenol and cholesterol for 120 sec at ambient temperature

5.6 Diazonium dye-incorporated nylon 6 based colorimetric probe

5.6.1 Buffer selection

Initially, a phosphate buffer at pH 7.4 and ambient conditions was used but a precipitate was formed with oxaloacetate that might have lead to fluctuation in the optical absorbance (Fig. 5.18). Because of this fluctuation in absorbance there was no relation between absorbance and the various concentrations of oxaloacetate (50, 100, 150, 200, 300, 350 and 400 µg/mℓ). It was therefore, not possible to determine the molar extinction/absorption coefficient or perform kinetic studies with a phosphate buffer.

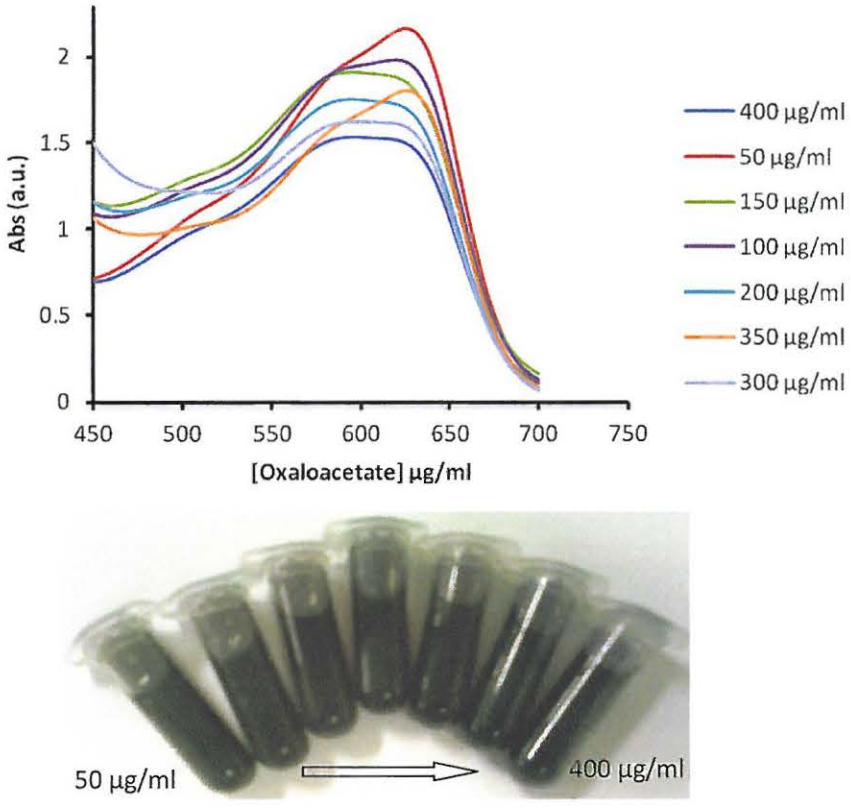

Figure 5.18: UV-Vis absorbance spectra and photograph showing colorimetric responses of various concentrations of oxaloacetate in phosphate buffer @ pH 7.4

A tris (hydroxymethyl) aminomethane (Tris base) buffer was used to replace the phosphate at the same pH and ambient conditions (temperature and humidity). With the tris base buffer, as shown in Fig. 5.19, there was no precipitate formed.

Figure 5.19: Photograph showing colorimetric response of the dye at different oxaloacetate concentrations; 50, 100, 150, 200, 300, 350 and 400 µg/mℓ in tris base buffer @ pH 7.4

According to Dolin, the basic form of tris(hydroxymethyl)aminomethane (Tris base) has been used, during the kinetic studies of an optical assay in which oxaloacetate was formed, to catalyze the oxaloacetate formation (Dolin, 1968). This catalysis may be the reason why a clear solution of oxaloacetate is obtained with the tris base. Here, the absorbance at varying oxaloacetate concentrations were recorded in triplicates per concentration (n = 3) using a microplate reader LEDETECT 96 with a measuring Filter at 450 nm (Fig. 5.20). A linear relation was attained between oxaloacetate concentration and optical absorbance with R^2 value of 0.9978 (Fig. 5.20).

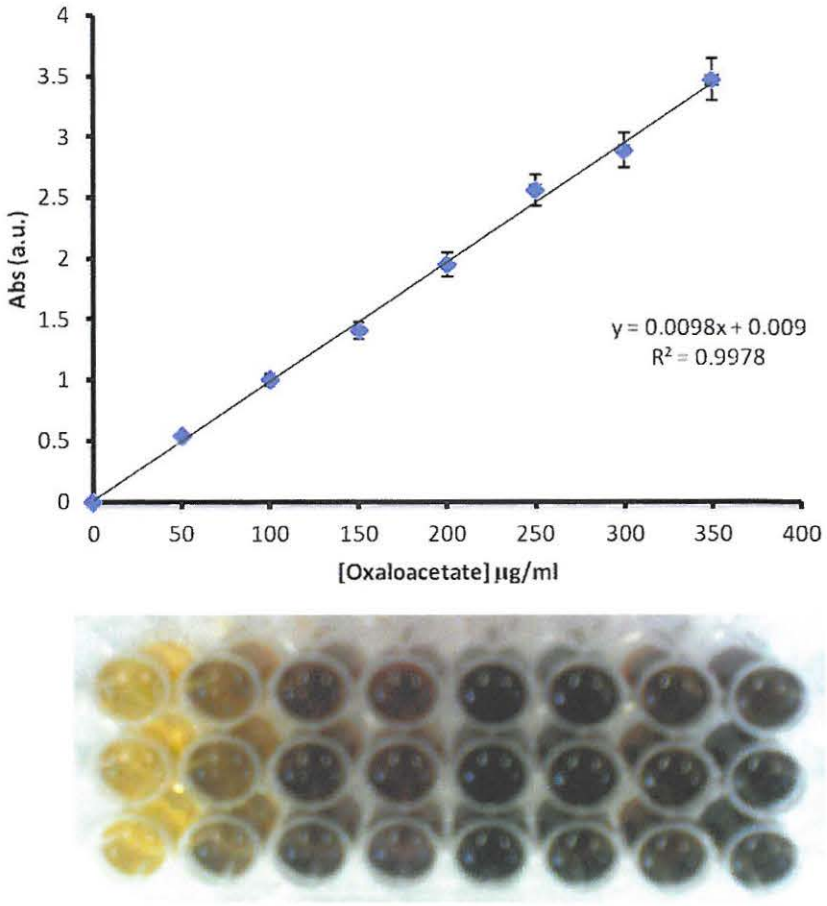

Figure 5.20: A linear calibration curve showing concentration dependent optical absorbance for oxaloacetate

At pH 7.4 the absorption coefficient of oxaloacetate was found to be 1.80 mM cm^{-1}. Even though the absorption coefficient was relatively small we were able to obtain reliable initial velocities at low substrate concentration, during the kinetic studies. For easy calculations and use of conventional units for the kinetic parameters, concentration units were converted from µg/mℓ to mM.

5.6.2 Enzymatic assay: Kinetic studies

Aspartate aminotransferase, one of the group-transferring enzymes that operate exclusively through binary enzyme substrate complexes, was able to catalyze the reaction as shown by the colour scheme in Fig.5.21. Figure 5.21 also shows the UV-Vis spectrum for the coloured reaction scheme used to detect the AST enzymatic activity. The scheme is based on the conversion of aspartate and α-ketoglutarate to glutamate and oxaloacetate respectively. Oxaloacetate then reacted with a diazonium salt to form a chromophore that absorbed light between 550 and 630 nm.

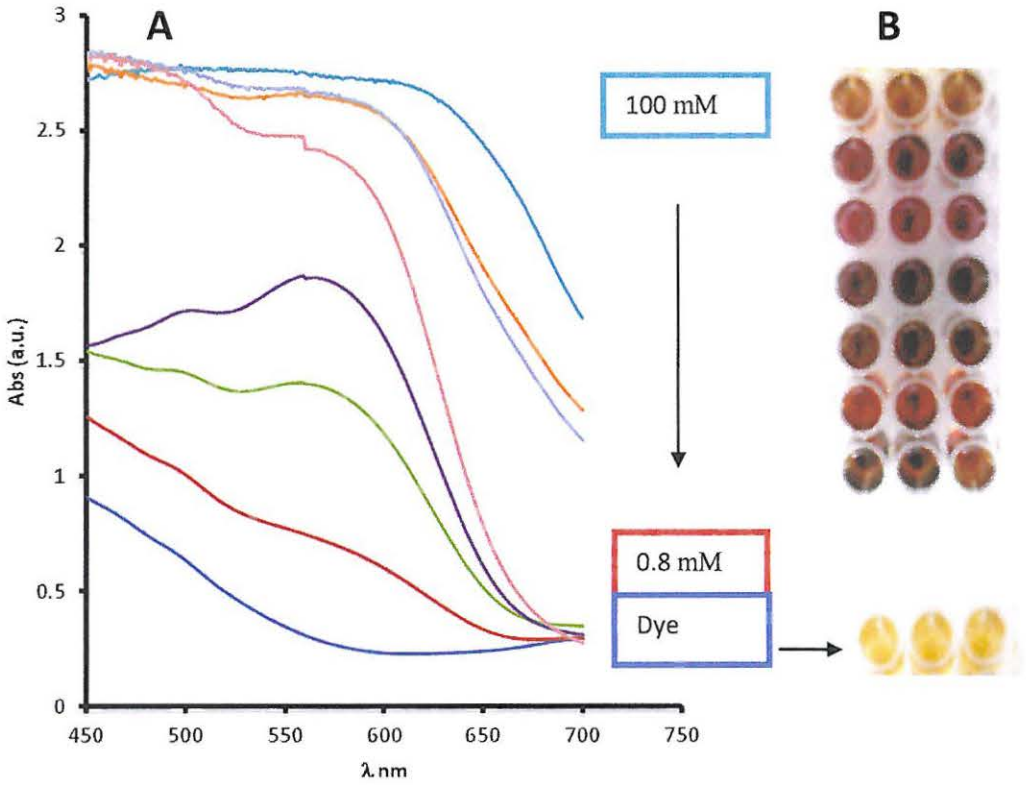

Figure 5.21: UV-Vis spectrum for the coloured reaction scheme used to detect the AST enzymatic activity at varying concentrations of aspartate

The assumption was that enzymatic reaction followed the scheme shown in Fig. 5.22. The diazonium dye, in this thesis, changed colour from yellow to brown upon interacting with oxaloacetate.

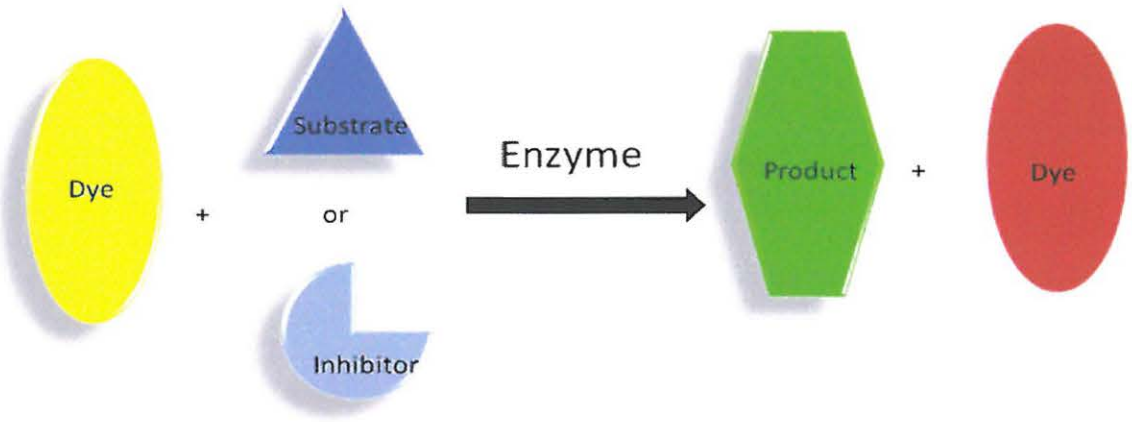

Figure 5.22: Schematic representation of a product- and substrate/inhibitor-selective reaction involving dyes for 'naked eye' detection of enzymes [Adapted from Guo et al., 2011]

Figure 5.23 illustrates the result of the time course progression for varying concentration of aspartate. For the time progression data of each aspartate concentration [*S*], the gradient after the start of reaction (abs/min) was calculated as the velocity *v* shown in Table 5.2.

Table 5.2: Aspartate Concentration [*S*] and Velocity (*v*)

[S] (mM)	v (Abs/min)
0.8	0.211
2.8	0.551
6.8	0.938
10.8	1.10
60.8	1.20
80.8	1.21
100.8	1.22

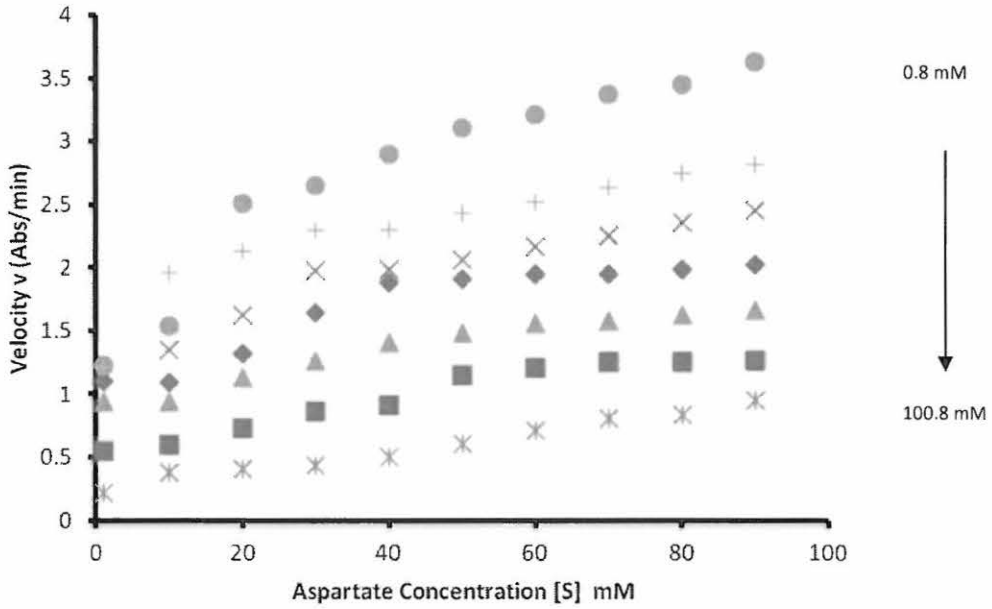

Figure 5.23: A time course progression for varying concentration of aspartate

The data in Table 5.2 were used to generate the Michaelis-Menten curve (A) and also expressed as Lineweaver-Burk (B), Hofstee (C), and Eadie (D) linear plots to determine V_{max} and K_M (see Figure 5.24). The K_M and V_{max} are compiled in Table 5.3.

Table 5.3: K_M and V_{max} values

Substrate (n = 3)	K_m (mM)	V_{max} (µmol/ml/min)
L-aspartate	2.60 ± 1.74	1.23 ± 0.143
α- Ketoglutarate	0.59 ± 0.18	1.18 ± 0.131
Oxaloacetate	0.066 ± 0.010	0.132 ± 0.101

From the K_M values it was possible to determine the concentration of oxaloacetate, in µg/ml, equivalent to normal or more than 10 times the highest normal AST activity level. With the appropriate concentrations of the substrates, the solid-state colorimetric probe was successfully developed.

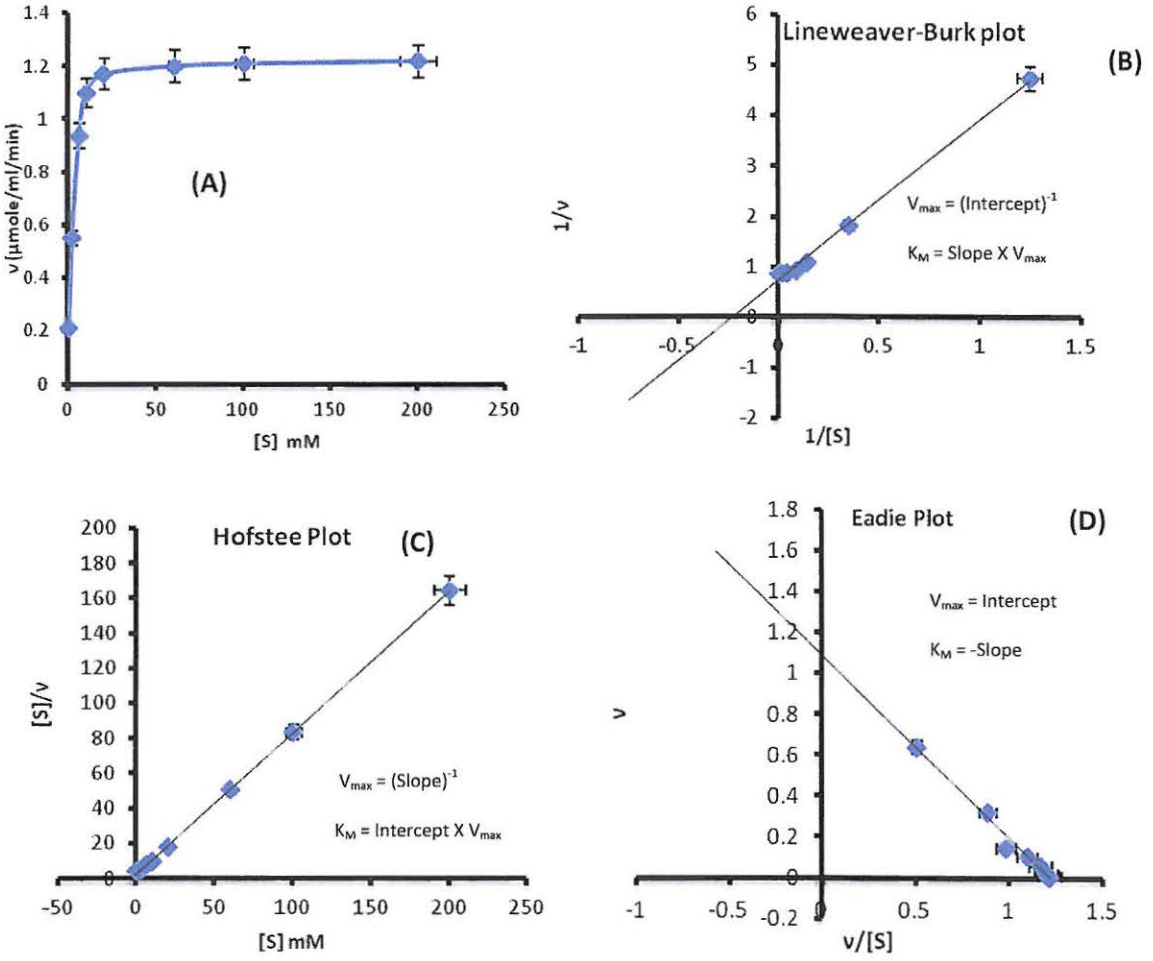

Figure 5.24: A) Michaelis-Menten curve obtained from change in absorbance from assay (v) vs substrate concentration [Substrate]; B) Lineweaver-Burk; C) Hofstee; D) Eadie plots linear plots used to determine V_{max} and K_M

5.6.3 Evaluation of dye concentration on conductivity and surface tension of polymer composite

A summary of the results is shown in Table 5.4. The results revealed that there were minor differences in both conductivity and surface tension of the polymer composite solution with increasing concentration of the dye.

Table 5.4: Conductivity and surface tension as a function of dye concentration on dye-nylon 6 solution

Dye Concentration % w/v	Conductivity µS/cm	Std Dev (n=6)	Surface Tension mN/m	Std Dev (n=6)
0.5	9.30	0.4	36.2	0.1
2.5	9.54	0.5	36.5	0.2
5	9.61	0.3	36.9	0.1

- Conductivity for 16% w/v = 9.28 µS/cm @ 19 °C and 36 mN/m surface tension

5.7 Development of the electrospun diazonium dye incorporated nylon 6 colorimetric probe

Figure 5.25 is a typical FE-SEM image depicting nonwoven fibrous diazonium dye incorporated nylon 6 membranes. The dye-nylon probe strip was pink in colour (inset) before exposure to analytes or any matrix.

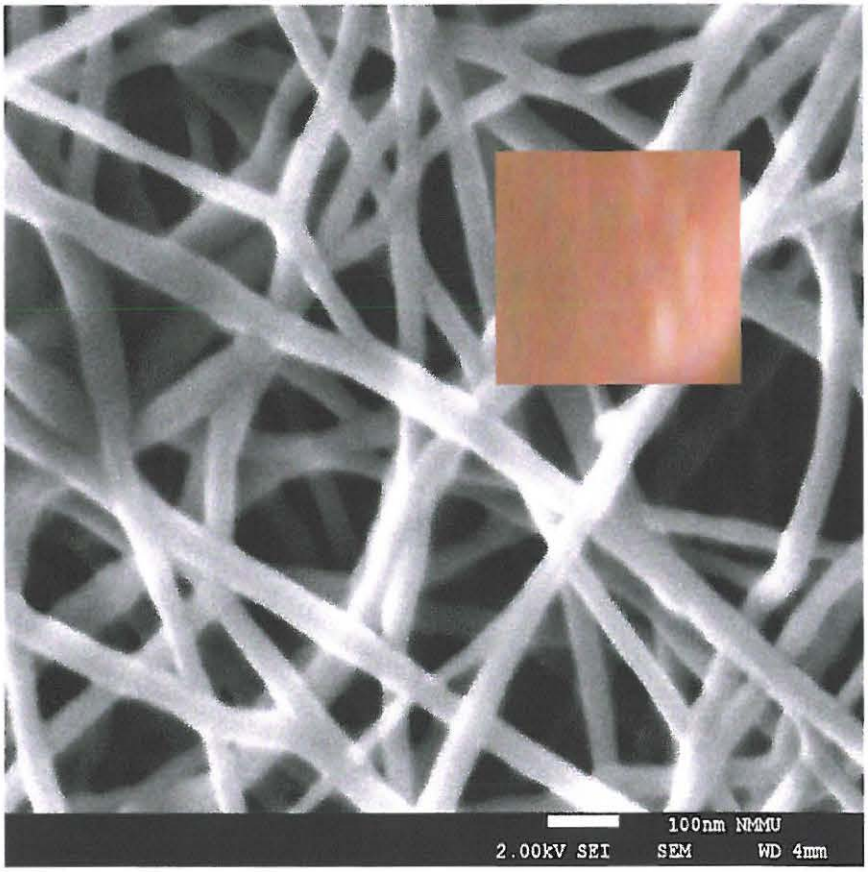

Figure 5.25: FE-SEM image of an electrospun diazonium - nylon 6 probe while the inset represents a typical probe strip before interaction with analytes

5.7.1 Effect of the dye concentration on dye-N 6 morphology and colour intensity

Figure 5.26 shows that the morphology of the dye incorporated nanofibers B), C) and D) corresponding to dye concentrations 0.5, 2.5 and 5% wt/wt respectively, was generally similar to that of the reference sample without the added dye (A).

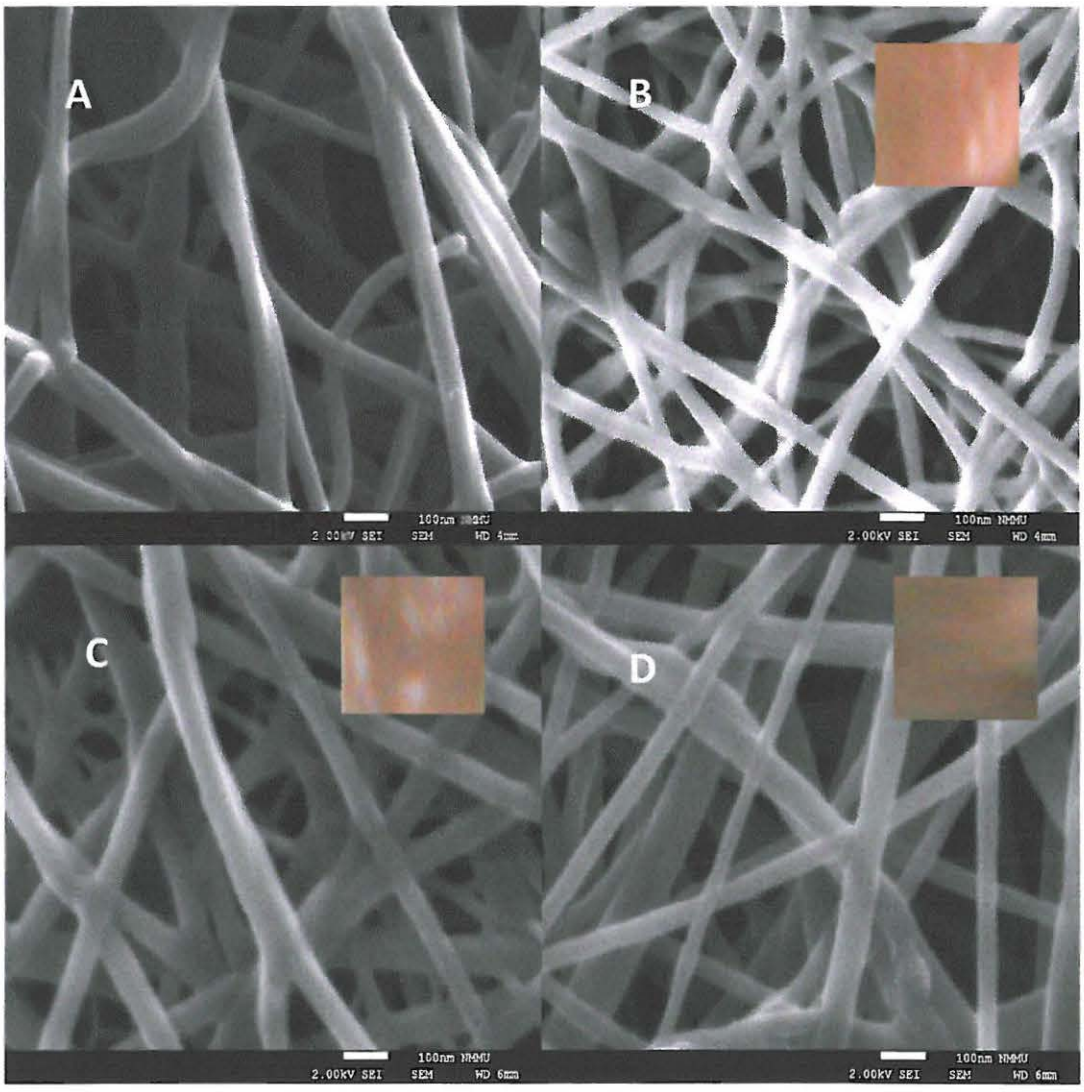

Figure 5.26: SEM images of electrospun nylon 6: (a) reference sample without the dye (b) 0.5 (c) 2.5 and (d) 5% wt/wt

As per expectation, it was also observed from Fig. 5.26 that the colour intensity of the colorimetric probe was concentration dependent. Investigating the different dye concentrations, therefore, allowed for evaluation of the contribution of each concentration to the overall discriminating capabilities, in terms of colour intensity, of the colorimetric system. Figure 5.27 shows different colour intensities elicited. At the highest dye concentration, 5% wt intense shades were given while moderate to faint shades were attained from the probe with 0.5% wt.

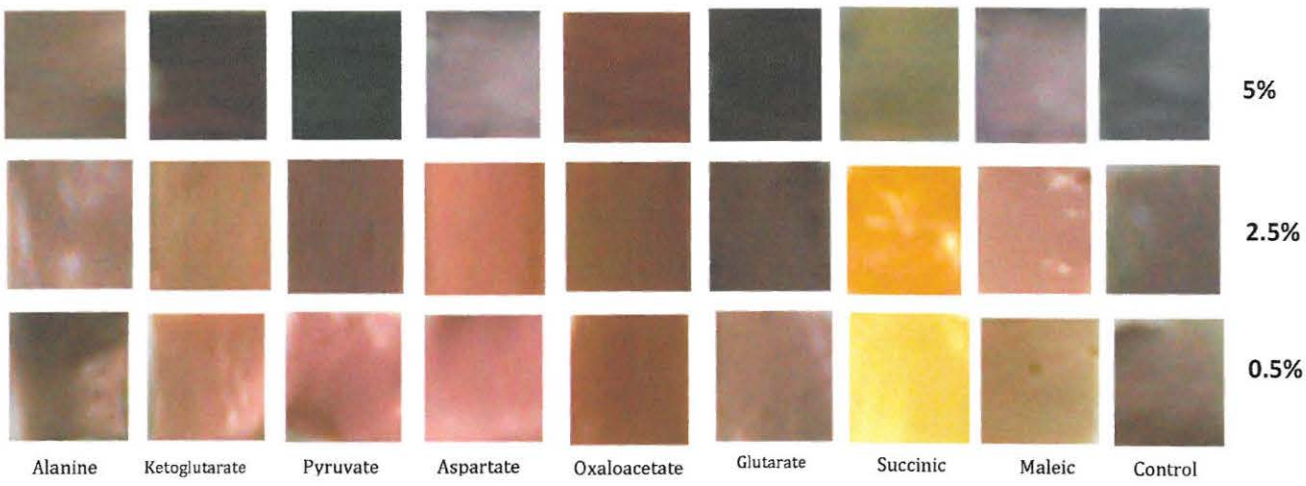

Figure 5.27: Colorimetric interaction of the probe strips at different dye concentrations

Owing to the porous structure of the electrospun fibers the assumption was that the fibers typically had retained the dye within their porous networks, while allowing the reaction product access through the pores to interact with the dye.

5.7.2 Characterization of diazonium dye-nylon 6 colorimetric probe

5.7.2.1 Brunauer-Emmett-Teller (BET) surface characterization

The surface area and porosity values obtained showed that the incorporation of diazonium dye into nylon 6 matrix enhanced its composite properties because a different phase relative to the matrix material was created. Table 5.5 shows the pore characteristics of the fibers. BET analysis showed that N 6 and dye-N 6fibers had average pore diameters of ~ 20 and 22 Å , respectively, which established the markedly mesoporous nature of the newly prepared sorbent materials. Surface area measurements revealed that the surface area of the dye-N 6 fiber was much higher than that of the N 6 fiber (by about 22 %), thus confirming an improvement on the binding sites on the dye-N 6 fiber. There was also a slight difference on the pore volume between the two fibers.

Table 5.5: Pore characterization of nylon 6 and diazonium incorporated nylon 6

Porosity parameter	Measurement	
	Nylon 6	Diazonium-Nylon 6
Surface Area (m^2/g)	3.6002 ± 1.0863	16.5534 ± 0.3557
Pore Surface Area (m^2/g)	0.6474 ± 1.031	7.9971 ± 1.4121
Pore Volume (cm^3/g)	0.000330 ± 0.0200	0.004348 ± 0.01
Ave. Pore Diameter (Å)	20.3867 ± 1.00011	21.7456 ± 1.01010

- Specific surface area was calculated using the BET method
- Average pore diameter, pore surface area and pore volume were calculated using the Barret, Joyner and Halenda (BJH) method

5.7.2.2 *Energy dispersive X-ray spectra (EDS)*

The elemental composition of the colorimetric probe analysed at two different dye concentrations 0.5 and 5% w/w showed that both EDS spectra had zinc as one of the main elements (Fig. 5.28).

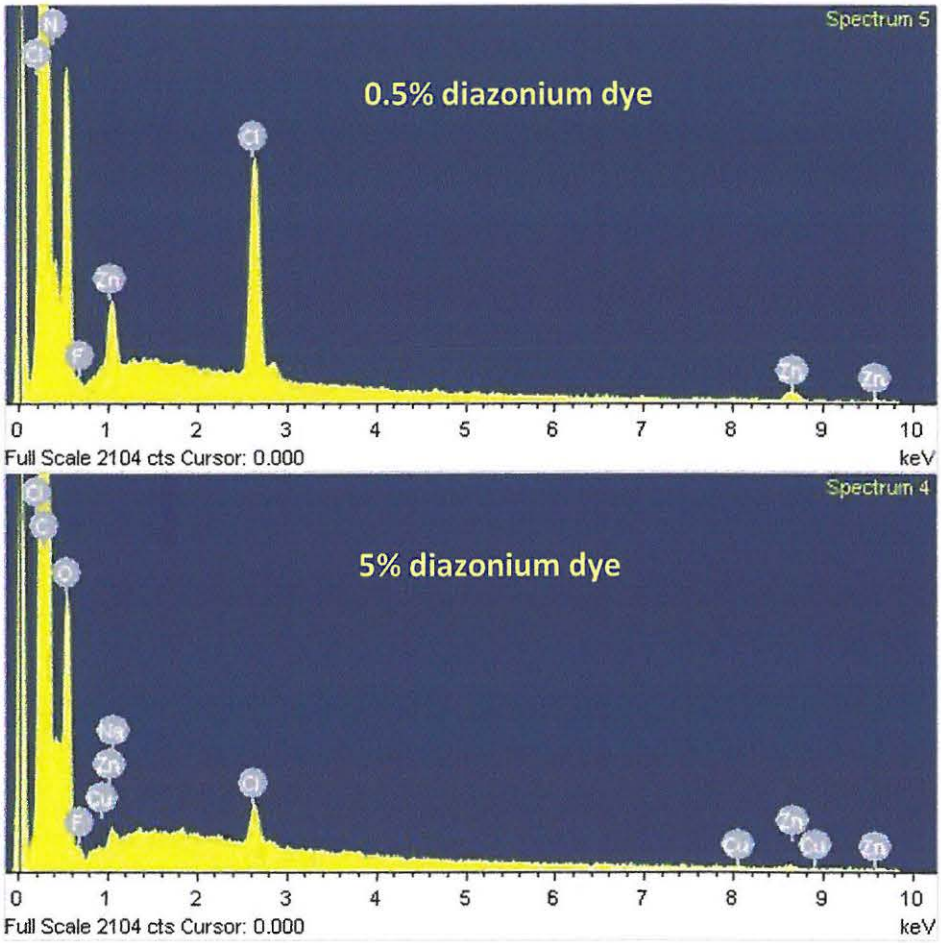

Figure 5.28: Energy dispersive X-ray spectra (EDS) of diazonium dye-nylon 6 fibers at dye concentrations 0.5 and 5% w/w

The elements Cu and C detected were from the carbon coated copper grid used as a sample holder while F and Na could just be impurities from the solvent, polymer pellets or the equipment.

The nitrogen (spectrum 5) Cl, O and Zn observed in Fig. 5.28 were from the diazonium dye, the nitrogen could also be from nylon 6 polymer.

5.7.2.3 Photostability

There was no observable difference, in terms of colour change for the strips exposed to irradiance and those which were not, after exposure of the colorimetric strips to succinate, aspartate, α-ketoglutarate and oxaloacetate at 300 ng/mℓ and 120 sec each substrate (see Fig. 5.29).

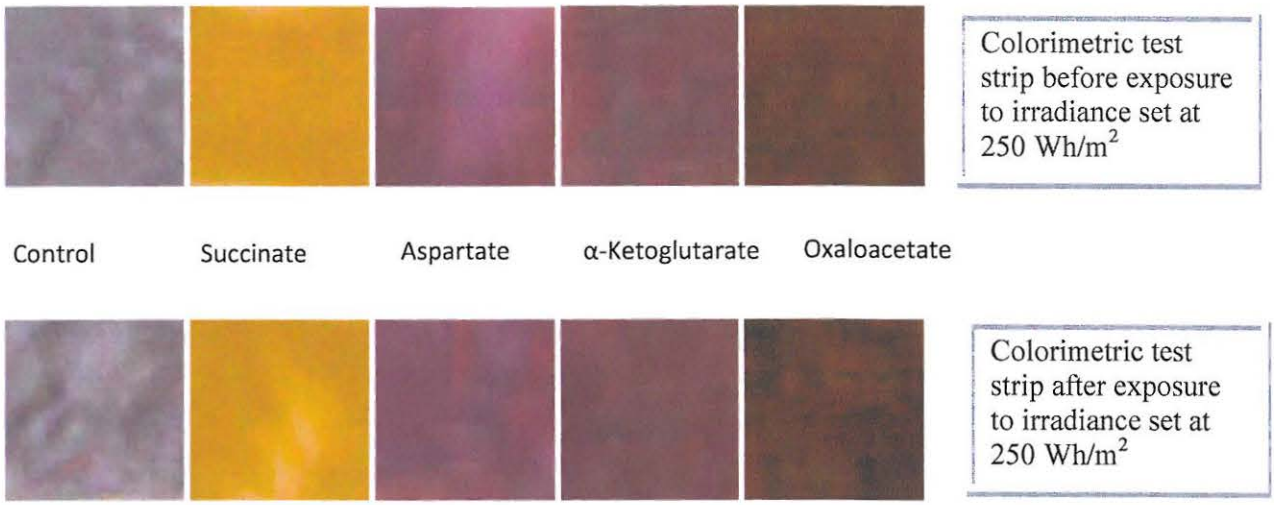

Figure 5.29: Photostability of the colorimetric probe. Photographs showing diazonium-nylon 6 probe strips before and after irradiance set at 250 Wh/m² upon exposure to succinate, aspartate, α-ketoglutarate and oxaloacetate at 300 ng/mℓ and 120 sec exposure time for each substrate

Finally, an inspection on the storage of the dye-nylon 6 colorimetric probe at ambient conditions (temperature and humidity) has shown a significant stability of the probe based on colour and texture of the probe. The fibers were kept in the locker for 12 months.

5.8 Application of dye-N6 probe

5.8.1 Standard solutions

The electrospun colorimetric probe strips upon interacting with 10 mM standard solutions gave distinct colour changes for the different substrates that included aspartate, ketoglutarate, alanine, pryruvate, oxaloacetate and glutamate (Fig. 5.30).

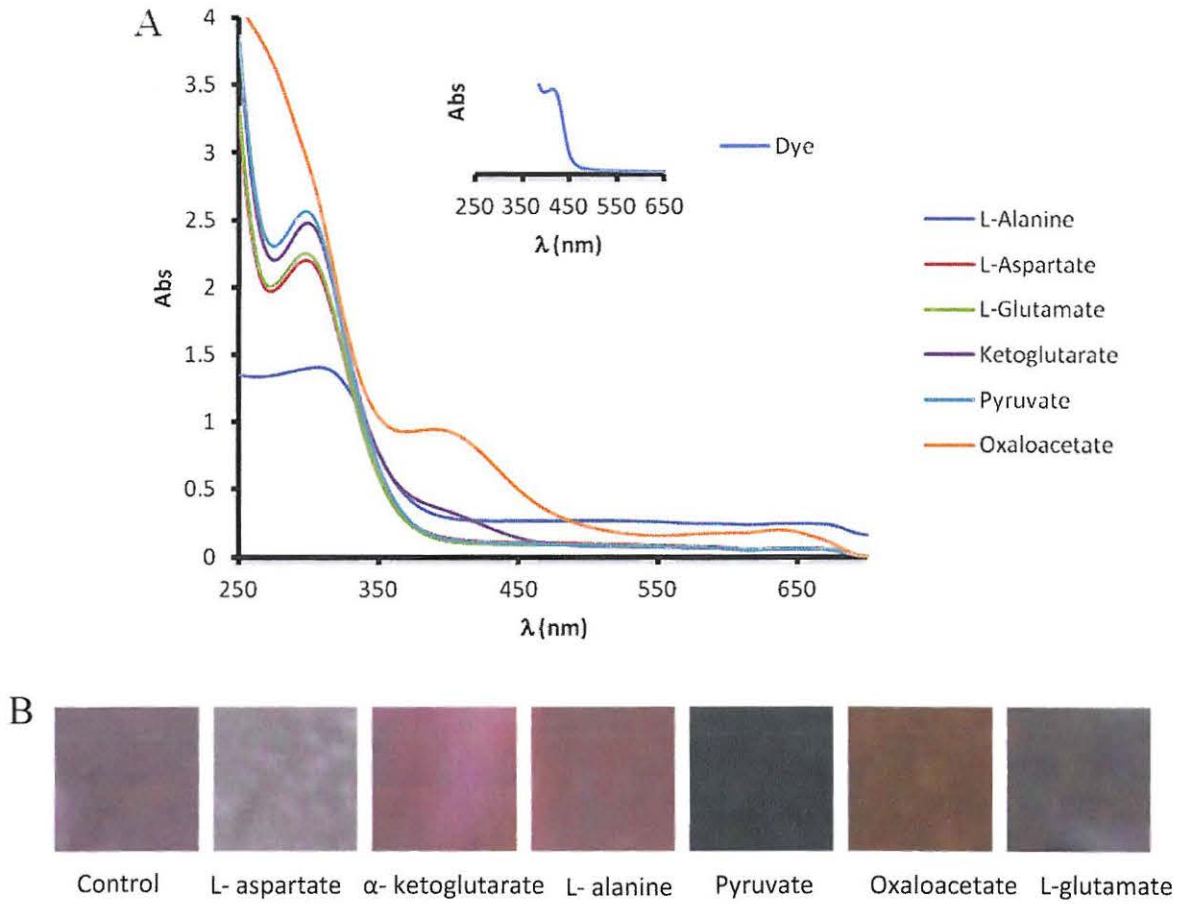

Figure 5.30: A) UV-Vis response of the diazonium dye (inset) and that of the dye upon interaction with 10 mM standard solutions of aspartate, ketoglutarate, alanine, pryruvate, oxaloacetate and glutamate. B) Photographs showing the interaction of colorimetric probe strips upon exposure to the same standards for 5 min @ pH 7.4 and ambient temperature

To demonstrate selectivity of the colorimetric probe, the electrospun test strips elicited different colour changes when exposed to a variety of dicarboxylic acids, including glutamic, malaic and succinic, known to compete as well as interact identically with amino, aldehyde and keto acid substrates. The distinct colours for each acid (see Fig.5.31) while upon interacting with a mixture of glutamic, malaic, succinic and relatively smaller concentration of oxaloacetic acid the probe, based on visual detection, favored oxaloacetic acid (Fig. 5.32) as it turned brown.

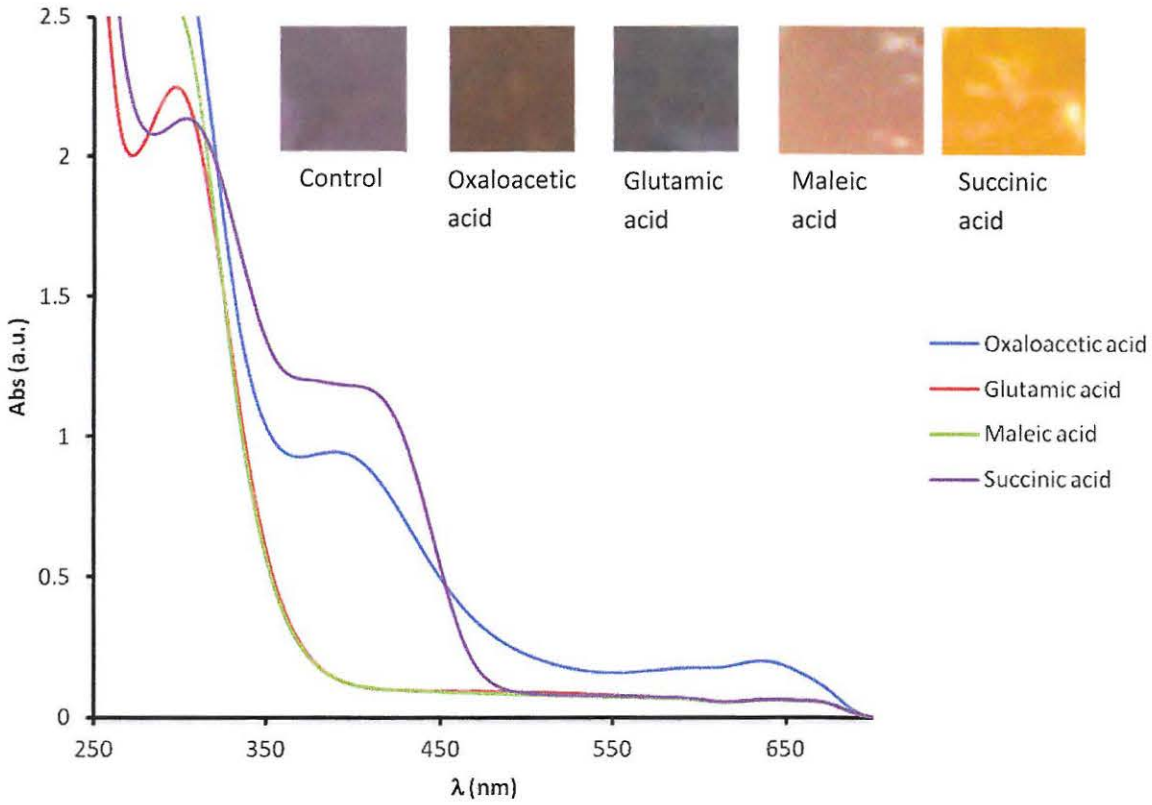

Figure 5.31: UV-Vis response and photographs depicting colorimetric interaction of the probe stripes with dicarboxylic acids, glutamic, malaic, succinic, which are known to inhibit the aspartate aminotransferase activity

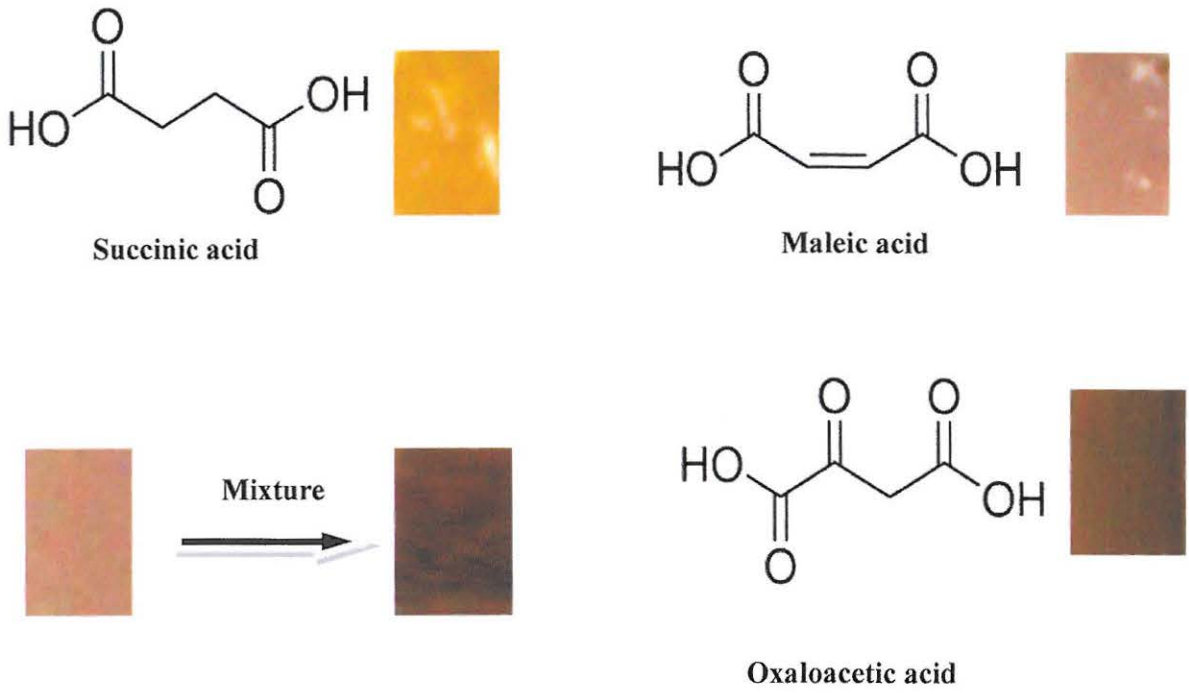

Figure 5.32: Colorimetric interaction of the probe stripes with dicarboxylic acids that are known to inhibit the AST activity

The electrospun colorimetric probe strips rapidly changed to distinct colours observed almost immediately upon addition of the test samples. The colour fully developed in approximately 60–300 s by visual inspection and the colour formed was stable for as long as the probe strips remained sufficiently wet. On the basis that the colorimetric probe strips provided distinct and unambiguous colour indication upon exposure to standard solutions of different analytes the probe was applied to plasma samples. According to one review (Kersaudy-Kerhoas and Sollier, 2013) plasma is rich with indicators of various diseases, which renders separating plasma from blood of clinical importance especially for diagnostics.

5.8.2 Application in biological matrix

The conditions with the spiked plasma samples were such that aspartate concentrations varied over 0.8 – 100.8 mM concentration range while α-ketoglutarate was kept constant at 10.8 mM and that levels of oxaloacetate produced represented the AST levels in the sample. In addition, the activity of AST (U/L), as determined by Eqn. 4.1(Chp. 4), was equivalent to oxaloacetate concentration in μg/ml. While monitoring AST activity at 530 nm a linear relationship was obtained at oxaloacetate concentration range 0.4 – 7.4 μg/ml (Fig. 5.33). The procedure was reproducible after evaluating five replicate measurements for each test and since the probe is a disposable type a new test strip was used with every measurement.

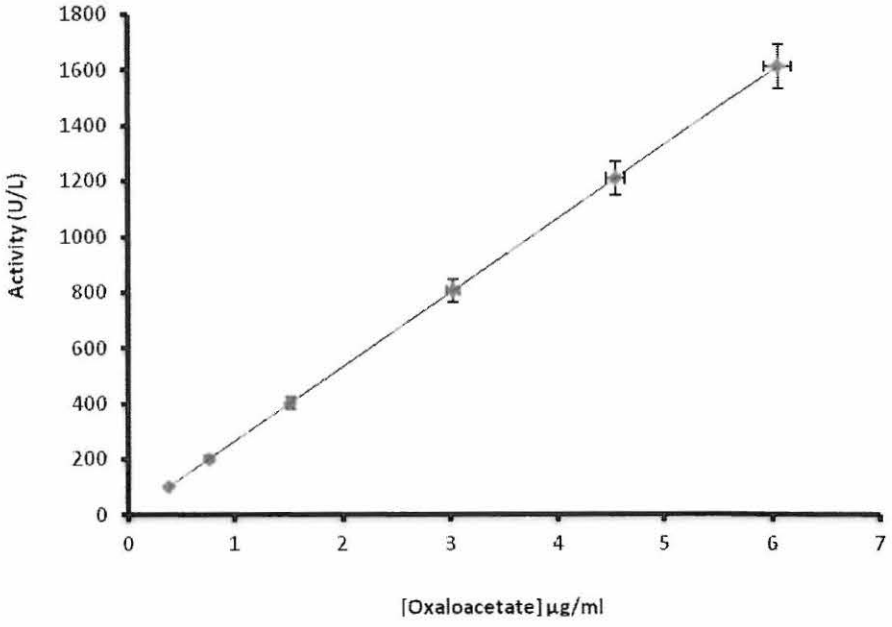

Figure 5.33: Standard curve of oxaloacetate concentration against aspartate aminotransferase activity. The reactions were carried out at pH 7.4 at ambient temperature

Figure 5.34 shows representative photographs of the colorimetric probe strips upon interaction with increasing concentration of oxaloacetate.

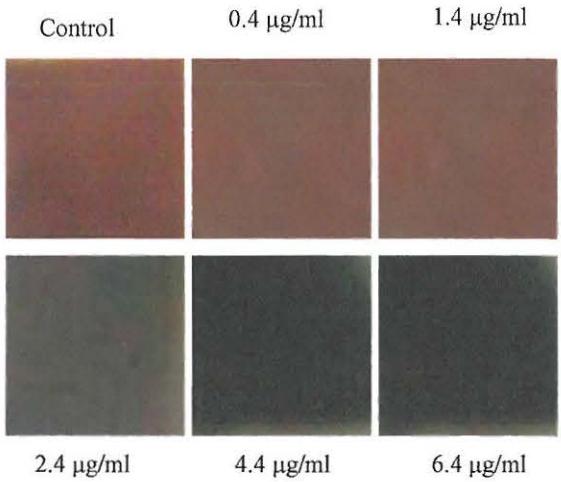

Figure 5.34: Photographs of the colorimetric response of the diazonium dye incorporate nylon 6 probe strips upon exposure to increasing oxaloacetate concentration. The reactions were carried out at pH 7.4 at ambient temperature

The colour intensified with increasing concentration of oxaloacetate and from our experimental calculations 2.4 µg/ml was equivalent to 10 times the normal AST activity. At aspartate aminotransferase levels below 10 times the highest normal AST activity in plasma there was no visually detectable quantity of enzyme-catalyzed substrate reaction product formed. The incorporated diazonium dye only changed colour to a shade of brown indicative of a positive test. The test was eye decipherable rather than requiring either colorimetric or reflectometric devices. Furthermore, the colorimetric probe can be used by relatively untrained persons as the probe provided an objective indication of the presence/absence of liver toxicity.

Conclusions

An electrospun simple colorimetric probe based on polystyrene-Au NPs was developed. Taking advantage of several fascinating features of the PS-Au NPs combination, the probe showed an excellent response towards 17β-estradiol and possessed high sensitivity with the lowest naked-eye detection limit of 100 ng/mℓ. This colorimetric system does not employ any sophisticated instrumentation therefore it guarantees a user-friendly, rapid and on-site detection of 17β-estradiol. Furthermore, relative to other nanoparticle-based colorimetric assays, this probe does not entail the use of complex nanoparticles modification (e.g. biological material). The probe warrants further investigation as it has shown potential to profile for estrogenic compounds in aqueous environments. As a way forward, a thiol functionalized polystyrene maybe used to enhance stability of the probe over harsh environmental conditions that include a wide range of temperature, concentration and pH.

Another simple, rapid, accurate and cost effective diagnostic method was developed for AST. The protocol entailed colorimetric detection for AST, based on reacting oxaloacetate with a diazonium salt. An approach that is attractive especially when employed with a dye incorporated electrospun fibre to achieve qualitative as well as semiquantitative eyeball detection of enzyme-markers for liver toxicity. The lowest naked eye detection limit of 2.4 μg/ml oxalaoacetate equivalence of 10 times the normal AST activity was attained. Taking advantage of several fascinating features of the nano structured fiber (e.g. extremely large specific surface area and high porosity) the probe offers easy handling, as well as sensitive and selective colour change for oxaloacetate. However, the probe needs a more rigorous exposure to real samples. In addition, assuming the absence of matrix effects that can suppress the chromic transition, the only two parameters that would affect the limit of analyte detection are the relationship between colour intensity and dye as well as the sharpness of the eye sight of the observer. Finally, the colorimetric probe offers a promising solid-state platform for diagnosis of AST in other biological fluids such as blood or urine.

References

AGARWAL, S., GREINER, A. & WENDORFF, J. H. 2013. Functional materials by electrospinning of polymers. *Progress in Polymer Science,* 38, 963-991.

AGARWAL, S. K., SINGH, S. S., VERMA, S. & KUMAR, S. 2000. Antifungal activity of anthraquinone derivatives from Rheum emodi. *Journal of Ethnopharmacology,* 72, 43-46.

AGHDAM, R. M., NAJARIAN, S., SHAKHESI, S., KHANLARI, S., SHAABANI, K. & SHARIFI, S. 2012. Investigating the effect of PGA on physical and mechanical properties of electrospun PCL/PGA blend nanofibers. *Journal of Applied Polymer Science,* 124, 123-131.

AMACHER, D. E. 2010. The discovery and development of proteomic safety biomarkers for the detection of drug-induced liver toxicity. *Toxicology and Applied Pharmacology,* 245, 134-142.

ARNOLD, K. E., BOXALL, A. B. A., BROWN, A. R., CUTHBERT, R. J., GAW, S., HUTCHINSON, T. H., JOBLING, S., MADDEN, J. C., METCALFE, C. D., NAIDOO, V., SHORE, R. F., SMITS, J. E., TAGGART, M. A. & THOMPSON, H. M. 2013. Assessing the exposure risk and impacts of pharmaceuticals in the environment on individuals and ecosystems. *Biology Letters,* 9.

ARNOLD, P. M. & PARSLOW, G. R. 1995. Designing a coupled assay system for aspartate aminotransferase. *Biochemical Education,* 23, 40-41.

ASHAYER, R., MANNAN, S. H. & SAJJADI, S. 2008. Synthesis and characterization of gold nanoshells using poly(diallyldimethyl ammonium chloride). *Colloids and Surfaces A: Physicochemical and Engineering Aspects,* 329, 134-141.

ATKINSON, A. J., , JR., COLBURN, W. A., DEGRUTTOLA, V. G., DEMETS, D. L., DOWNING, G. J., HOTH, D. F., OATES, J. A., PECK, C. C., SCHOOLEY, R. T., SPILKER, B. A., WOODCOCK, J. & ZEGER, S. L. 2001. Biomarkers and surrogate endpoints: Preferred definitions and conceptual framework. *Clinical Pharmacology and Therapeutics,* 69, 89-95.

BABSON, A. L., SHAPIRO, P. O., WILLIAMS, P. A. R. & PHILLIPS, G. E. 1962. The use of a diazonium salt for the determination of glutamic-oxalacetic transaminase in serum. *Clinica Chimica Acta,* 7, 199-205.

BARAKAT, N. A. M., ABADIR, M. F., SHEIKH, F. A., KANJWAL, M. A., PARK, S. J. & KIM, H. Y. 2010. Polymeric nanofibers containing solid nanoparticles prepared by electrospinning and their applications. *Chemical Engineering Journal,* 156, 487-495.

BAUMAN, D., PŁÓCIENNIK, A. & INGLOT, K. 2009. Molecular Interactions in Monolayers of Azo Dye/Liquid Crystal Mixtures at Interfaces. *Acta Physica Polonica A,* 116, 203-210.

BEIJA, M., CHARREYRE, M.-T. & MARTINHO, J. M. G. 2011. Dye-labelled polymer chains at specific sites: Synthesis by living/controlled polymerization. *Progress in Polymer Science,* 36, 568-602.

BHARDWAJ, N. & KUNDU, S. C. 2010. Electrospinning: A fascinating fiber fabrication technique. *Biotechnology Advances,* 28, 325-347.

BINDU, R. L., NAIR, C. P. R. & NINAN, K. N. 2000. Phenolic resins bearing maleimide groups: Synthesis and characterization. *Journal of Polymer Science Part A: Polymer Chemistry,* 38, 641-652.

BOCHAROVA, V., ZAVALOV, O., MACVITTIE, K., ARUGULA, M. A., GUZ, N. V., DOKUKIN, M. E., HALAMEK, J., SOKOLOV, I., PRIVMAN, V. & KATZ, E. 2012. A biochemical logic approach to biomarker-activated drug release. *Journal of Materials Chemistry,* 22, 19709-19717.

BURTON, S. J., STEAD, C. V. & LOWE, C. R. 1988. Design and applications of biomimetic anthraquinone dyes. II. The interaction of C.I. reactive blue 2 analogues bearing terminal ring modifications with horse liver alcohol dehydrogenase. *Journal of Chromatography,* 455, 201-216.

CELEBIOGLU, A. & UYAR, T. 2013. Electrospinning of nanofibers from non-polymeric systems: Electrospun nanofibers from native cyclodextrins. *Journal of Colloid and Interface Science,* 404, 1-7.

CHANDRA, P., SINGH, J., SINGH, A., SRIVASTAVA, A., GOYAL, R. N. & SHIM, Y. B. 2013. Gold Nanoparticles and Nanocomposites in Clinical Diagnostics Using Electrochemical Methods. *Journal of Nanoparticles,* 2013, 12.

CHARERNSRIWILAIWAT, N., OPANASOPIT, P., ROJANARATA, T., NGAWHIRUNPAT, T. & SUPAPHOL, P. 2010. Preparation and characterization of chitosan-hydroxybenzotriazole/polyvinyl alcohol blend nanofibers by the electrospinning technique. *Carbohydrate Polymers,* 81, 675-680.

CHEN, H., HE, M., PEI, J. & LIU, B. 2002. End-group analysis of blue light-emitting polymers using matrix-assisted laser desorption/ionization time-of-flight mass spectrometry. *Analytical Chemistry,* 74, 6252-6258.

CHEN, W., DENG, H.-H., HONG, L., WU, Z.-Q., WANG, S., LIU, A.-L., LIN, X.-H. & XIA, X.-H. 2012. Bare gold nanoparticles as facile and sensitive colorimetric probe for melamine detection. *Analyst,* 137, 5382-5386.

CHEN, W. Y., HUANG, J. T., CHENG, Y. C., CHIEN, C. C. & TSAO, C. W. 2011. Fabrication of nanostructured silicon by metal-assisted etching and its effects on matrix-free laser desorption/ionization mass spectrometry. *Analytica Chimica Acta,* 687, 97-104.

CHIGOME, S. & TORTO, N. 2011. A review of opportunities for electrospun nanofibers in analytical chemistry. *Analytica Chimica Acta,* 706, 25-36.

CHIU, T.-C., CHANG, L.-C., CHIANG, C.-K. & CHANG, H.-T. 2008. Determining Estrogens Using Surface-Assisted Laser Desorption/Ionization Mass Spectrometry with Silver Nanoparticles as the Matrix. *Journal of the American Society for Mass Spectrometry,* 19, 1343-1346.

CHRISSAFIS, K. & BIKIARIS, D. 2011. Can nanoparticles really enhance thermal stability of polymers? Part I: An overview on thermal decomposition of addition polymers. *Thermochimica Acta,* 523, 1-24.

CIARDELLI, F., RUGGERI, G. & PUCCI, A. 2013. Dye-containing polymers: methods for preparation of mechanochromic materials. *Chemical Society Reviews,* 42, 857-870.

CLONIS, Y. D., LABROU, N. E., KOTSIRA, V. P., MAZITSOS, C., MELISSIS, S. & GOGOLAS, G. 2000. Biomimetic dyes as affinity chromatography tools in enzyme purification. *Journal of Chromatography A,* 891, 33-44.

COLBORN, T., VOM SAAL, F. S. & SOTO, A. M. 1993. Developmental effects of endocrine-disrupting chemicals in wildlife and humans. *Environmental Health Perspectives,* 101, 378-384.

COLVIN, V. L. 2003. The potential environmental impact of engineered nanomaterials. *Nat Biotech,* 21, 1166-1170.

CONNOLLY, P. 1995. Clinical diagnostics opportunities for biosensors and bioelectronics. *Biosensors and Bioelectronics,* 10, 1-6.

CORBIERRE, M. K., CAMERON, N. S., SUTTON, M., MOCHRIE, S. G., LURIO, L. B., RÜHM, A. & LENNOX, R. B. 2001. Polymer-stabilized gold nanoparticles and their incorporation into polymer matrices. *J Am Chem Soc,* 123, 10411-10412.

CORONADO, E. A., ENCINA, E. R. & STEFANI, F. D. 2011. Optical properties of metallic nanoparticles: manipulating light, heat and forces at the nanoscale. *Nanoscale,* 3, 4042-4059.

COTE, L. J., KIM, F. & HUANG, J. 2008. Langmuir−Blodgett Assembly of Graphite Oxide Single Layers. *Journal of the American Chemical Society,* 131, 1043-1049.

CUNNINGHAM, V. & LAMELA, H. 2010. Optical and optoacoustic measurements of the absorption properties of spherical gold nanoparticles within a highly scattering medium. *Optics & Laser Technology,* 42, 769-774.

D'ORAZIO, P. 2003. Biosensors in clinical chemistry. *Clinica Chimica Acta,* 334, 41-69.

DAI, Y., NIU, J., LIU, J., YIN, L. & XU, J. 2010. In situ encapsulation of laccase in microfibers by emulsion electrospinning: Preparation, characterization, and application. *Bioresource Technology,* 101, 8942-8947.

DE LA TORRE, F., MOYA-GARCIA, A. A., SUAREZ, M. F., RODRIGUEZ-CASO, C., CANAS, R. A., SANCHEZ-JIMENEZ, F. & CANOVAS, F. M. 2009. Molecular Modeling and Site-Directed Mutagenesis Reveal Essential Residues for Catalysis in a Prokaryote-Type Aspartate Aminotransferase. *Plant Physiology,* 149, 1648-1660.

DIAMANTI-KANDARAKIS, E., BOURGUIGNON, J.-P., GIUDICE, L. C., HAUSER, R., PRINS, G. S., SOTO, A. M., ZOELLER, R. T. & GORE, A. C. 2009. Endocrine-Disrupting Chemicals: An Endocrine Society Scientific Statement. *Endocrine Reviews,* 30, 293-342.

DING, Y.-M., YUAN, X.-Y., ZHAO, J., GUO, W.-C. & WANG, X.-K. 2007. Formation of Ultrafine Apatite Fibers by Sol-gel/Electrospinning. *Chemical Research in Chinese Universities,* 23, 366-369.

DINI, F., MARTINELLI, E., PAOLESSE, R., FILIPPINI, D., D'AMICO, A., LUNDSTRÖM, I. & DI NATALE, C. 2011. Polymer matrices effects on the sensitivity and the selectivity of optical chemical sensors. *Sensors and Actuators B: Chemical,* 154, 220-225.

DIPLAS, S., WATTS, J. F., MORTON, S. A., BEAMSON, G., TSAKIROPOULOS, P., CLARK, D. T. & CASTLE, J. E. 2001. Electron spectroscopy with Cr Kβ photons: high energy XPS and X-AES. *Journal of Electron Spectroscopy and Related Phenomena,* 113, 153-166.

DOLIN, M. I. 1968. Kinetics of Malic-Lactic Transhydrogenase: EFFECT OF THE KETO-ENOL TAUTOMERISM OF OXALACETATE ON THE KINETICS OF OXALACETATE FORMATION AND UTILIZATION. *Journal of Biological Chemistry,* 243, 3916-3923.

DOSHI, J. & RENEKER, D. H. 1995. Electrospinning process and applications of electrospun fibers. *Journal of Electrostatics,* 35, 151-160.

DYKMAN, L. & KHLEBTSOV, N. 2012. Gold nanoparticles in biomedical applications: recent advances and perspectives. *Chemical Society Reviews,* 41, 2256-2282.
ERKURT, E. A., ÜNYAYAR, A. & KUMBUR, H. 2007. Decolorization of synthetic dyes by white rot fungi, involving laccase enzyme in the process. *Process Biochemistry,* 42, 1429-1435.
FANG, J., NIU, H., LIN, T. & WANG, X. 2008. Applications of electrospun nanofibers. *Chinese Science Bulletin,* 53, 2265-2286.
FANG, J., NIU, H., WANG, H., WANG, X. & LIN, T. 2013. Enhanced mechanical energy harvesting using needleless electrospun poly(vinylidene fluoride) nanofibre webs. *Energy & Environmental Science,* 6, 2196-2202.
FENNESSEY, S. F. & FARRIS, R. J. 2004. Fabrication of aligned and molecularly oriented electrospun polyacrylonitrile nanofibers and the mechanical behavior of their twisted yarns. *Polymer,* 45, 4217-4225.
FORWARD, K. M. & RUTLEDGE, G. C. 2012. Free surface electrospinning from a wire electrode. *Chemical Engineering Journal,* 183, 492-503.
FU, G. D., LEI, J. Y., YAO, C., LI, X. S., YAO, F., NIE, S. Z., KANG, E. T. & NEOH, K. G. 2008. Core–Sheath Nanofibers from Combined Atom Transfer Radical Polymerization and Electrospinning. *Macromolecules,* 41, 6854-6858.
GADD, J. B., TREMBLAY, L. A. & NORTHCOTT, G. L. 2010. Steroid estrogens, conjugated estrogens and estrogenic activity in farm dairy shed effluents. *Environmental Pollution,* 158, 730-736.
GAO, J., HUANG, X., LIU, H., ZAN, F. & REN, J. 2012. Colloidal Stability of Gold Nanoparticles Modified with Thiol Compounds: Bioconjugation and Application in Cancer Cell Imaging. *Langmuir,* 28, 4464-4471.
GARDENIERS, J. G. E. & VAN DEN BERG, A. 2004. Lab-on-a-chip systems for biomedical and environmental monitoring. *Analytical and Bioanalytical Chemistry,* 378, 1700-1703.
GILL, I. & BALLESTEROS, A. 2003. Immunoglobulin–Polydiacetylene Sol–Gel Nanocomposites as Solid-State Chromatic Biosensors. *Angewandte Chemie,* 115, 3386-3389.
GONZÁLEZ DE REQUENA, D., NÚÑEZ, M., JIMÉNEZ-NÁCHER, I. & SORIANO, V. 2002. Liver toxicity caused by nevirapine. *AIDS,* 16, 290-291.
GONZALEZ, E., LIEMPD, S., CONDE-VANCELLS, J., GUTIERREZ-DE JUAN, V., PEREZ-CORMENZANA, M., MAYO, R., BERISA, A., ALONSO, C., MARQUEZ, C., BARR, J., LU, S., MATO, J. & FALCON-PEREZ, J. 2012. Serum UPLC-MS/MS metabolic profiling in an experimental model for acute-liver injury reveals potential biomarkers for hepatotoxicity. *Metabolomics,* 8, 997-1011.
GRAEWERT, M. A. & SVERGUN, D. I. 2013. Impact and progress in small and wide angle X-ray scattering (SAXS and WAXS). *Current Opinion in Structural Biology,* 23, 748-754.
GUILLETTE, L. J., CRAIN, D. A., GUNDERSON, M. P., KOOLS, S. A. E., MILNES, M. R., ORLANDO, E. F., ROONEY, A. A. & WOODWARD, A. R. 2000. Alligators and Endocrine Disrupting Contaminants: A Current Perspective. *American Zoologist,* 40, 438-452.
GÜLTEKIN, I. & INCE, N. H. 2007. Synthetic endocrine disruptors in the environment and water remediation by advanced oxidation processes. *Journal of Environmental Management,* 85, 816-832.

GUO, L., ZHONG, J., WU, J., FU, F., CHEN, G., ZHENG, X. & LIN, S. 2010. Visual detection of melamine in milk products by label-free gold nanoparticles. *Talanta,* 82, 1654-1658.
GUPTA, T. 2011. Exposure Science: Monitoring Environmental Contaminants. *In:* EDITOR-IN-CHIEF: JEROME, O. N. (ed.) *Encyclopedia of Environmental Health.* Burlington: Elsevier.
HANSELMAN, T. A., GRAETZ, D. A. & WILKIE, A. C. 2003. Manure-Borne Estrogens as Potential Environmental Contaminants: A Review. *Environmental Science and Technology,* 37, 5471-5478.
HANSELMAN, T. A., GRAETZ, D. A., WILKIE, A. C., SZABO, N. J. & DIAZ, C. S. 2006. Determination of Steroidal Estrogens in Flushed Dairy Manure Wastewater by Gas Chromatography-Mass Spectrometry. *J. Environ. Qual.,* 35, 695-700.
HE, P., SHEN, L., LIU, R., LUO, Z. & LI, Z. 2011. Direct Detection of β-Agonists by Use of Gold Nanoparticle-Based Colorimetric Assays. *Analytical Chemistry,* 83, 6988-6995.
HE, P. & URBAN, M. W. 2005. Phospholipid-Stabilized Au−Nanoparticles. *Biomacromolecules,* 6, 1224-1225.
HERSAM, M. & WEISS, P. 2011. Applications: High-Performance Materials and Emerging Areas. *Nanotechnology Research Directions for Societal Needs in 2020.* Springer Netherlands.
HOLČAPEK, M., VOLNÁ, K. & VANĚRKOVÁ, D. 2007. Effects of functional groups on the fragmentation of dyes in electrospray and atmospheric pressure chemical ionization mass spectra. *Dyes and Pigments,* 75, 156-165.
HOLLERITH, C., WERNICKE, D., BÜHLER, M., FEILITZSCH, F. V., HUBER, M., HÖHNE, J., HERTRICH, T., JOCHUM, J., PHELAN, K., STARK, M., SIMMNACHER, B., WEILAND, W. & WESTPHAL, W. 2004. Energy dispersive X-ray spectroscopy with microcalorimeters. *Nuclear Instruments and Methods in Physics Research Section A: Accelerators, Spectrometers, Detectors and Associated Equipment,* 520, 606-609.
HOPKINS, W. A., DURANT, S. E., STAUB, B. P., ROWE, C. L. & JACKSON, B. P. 2006. Reproduction, embryonic development, and maternal transfer of contaminants in the amphibian Gastrophryne carolinensis. *Environmental Health Perspectives,* 114, 661-666.
HOWIE, A. F., SPENCER, E. & BECKETT, G. J. 1992. Aspartate aminotransferase, alanine aminotransferase, and glutathione transferase in plasma during and after sedation by low-dose isoflurane or midazolam. *Clinical Chemistry,* 38, 476-479.
HUANG, L.-M., LIAO, W.-H., LING, H.-C. & WEN, T.-C. 2009. Simultaneous synthesis of polyaniline nanofibers and metal (Ag and Pt) nanoparticles. *Materials Chemistry and Physics,* 116, 474-478.
HUANG, X.-J., CHOI, Y.-K., IM, H.-S., YARIMAGA, O., YOON, E. & KIM, H.-S. 2006. Aspartate Aminotransferase (AST/GOT) and Alanine Aminotransferase (ALT/GPT) Detection Techniques. *Sensors,* 6, 756-782.
HUANG, X. & EL-SAYED, M. A. 2010. Gold nanoparticles: Optical properties and implementations in cancer diagnosis and photothermal therapy. *Journal of Advanced Research,* 1, 13-28.
HUANG, Z.-M., ZHANG, Y. Z., KOTAKI, M. & RAMAKRISHNA, S. 2003. A review on polymer nanofibers by electrospinning and their applications in nanocomposites. *Composites Science and Technology,* 63, 2223-2253.
IGNATOVA, M., MANOLOVA, N., TOSHKOVA, R., RASHKOV, I., GARDEVA, E., YOSSIFOVA, L. & ALEXANDROV, M. 2012. Quaternized chitosan-coated

nanofibrous materials containing gossypol: Preparation by electrospinning, characterization and antiproliferative activity towards HeLa cells. *International Journal of Pharmaceutics,* 436, 10-24.
INGLOT, K., KALETA, A., MARTYŃSKI, T. & BAUMAN, D. 2008. Molecular aggregation in Langmuir–Blodgett films of azo dye/liquid crystal mixtures. *Dyes and Pigments,* 77, 303-314.
INGLOT, K., MARTYŃSKI, T. & BAUMAN, D. 2009. Molecular organization and aggregation in Langmuir and Langmuir-Blodgett films of azo dye/liquid crystal mixtures. *Opto-Electronics Review,* 17, 120-128.
ISLAM, M. S. & KARIM, M. R. 2010. Fabrication and characterization of poly(vinyl alcohol)/alginate blend nanofibers by electrospinning method. *Colloids and Surfaces A: Physicochemical and Engineering Aspects,* 366, 135-140.
JAIN, P. K., LEE, K. S., EL-SAYED, I. H. & EL-SAYED, M. A. 2006. Calculated Absorption and Scattering Properties of Gold Nanoparticles of Different Size, Shape, and Composition: Applications in Biological Imaging and Biomedicine. *Journal of Physical Chemistry B,* 110, 7238-7248.
JIALI, N., TAO, Z. & ZHONGFAN, L. 2007. One-step seed-mediated growth of 30–150 nm quasispherical gold nanoparticles with 2-mercaptosuccinic acid as a new reducing agent. *Nanotechnology,* 18, 325607.
JIANG, G., WANG, L. & CHEN, W. 2007. Studies on the preparation and characterization of gold nanoparticles protected by dendrons. *Materials Letters,* 61, 278-283.
JIANG, G., ZHANG, S. & QIN, X. 2013. High throughput of quality nanofibers via one stepped pyramid-shaped spinneret. *Materials Letters,* 106, 56-58.
KALISHWARALAL, K., DEEPAK, V., RAM KUMAR PANDIAN, S. & GURUNATHAN, S. 2009. Biological synthesis of gold nanocubes from Bacillus licheniformis. *Bioresource Technology,* 100, 5356-5358.
KAREN, A., MAN, N., SHIBAMORI, T. & TAKAHASHI, K. 2003. TOF-SIMS characterization of industrial materials: from silicon wafer to polymer. *Applied Surface Science,* 203–204, 541-546.
KAVANAGH, A., BYRNE, R., DIAMOND, D. & FRASER, K. J. 2012. Stimuli Responsive Ionogels for Sensing Applications—An Overview. *Membranes,* 2, 16-39.
KAYACI, F., OZGIT-AKGUN, C., DONMEZ, I., BIYIKLI, N. & UYAR, T. 2012. Polymer–Inorganic Core–Shell Nanofibers by Electrospinning and Atomic Layer Deposition: Flexible Nylon–ZnO Core–Shell Nanofiber Mats and Their Photocatalytic Activity. *ACS Applied Materials & Interfaces,* 4, 6185-6194.
KERSAUDY-KERHOAS, M. & SOLLIER, E. 2013. Micro-scale blood plasma separation: from acoustophoresis to egg-beaters. *Lab on a Chip.*
KHANNA, P. K., GOKHALE, R., SUBBARAO, V. V. V. S., VISHWANATH, A. K., DAS, B. K. & SATYANARAYANA, C. V. V. 2005. PVA stabilized gold nanoparticles by use of unexplored albeit conventional reducing agent. *Materials Chemistry and Physics,* 92, 229-233.
KIEFER, J., RASUL, N. H., GHOSH, P. K. & VON LIERES, E. 2014. Surface and bulk porosity mapping of polymer membranes using infrared spectroscopy. *Journal of Membrane Science,* 452, 152-156.
KIM, C., CHO, Y. J., YUN, W. Y., NGOC, B. T. N., YANG, K. S., CHANG, D. R., LEE, J. W., KOJIMA, M., KIM, Y. A. & ENDO, M. 2007. Fabrications and structural

characterization of ultra-fine carbon fibres by electrospinning of polymer blends. *Solid State Communications,* 142, 20-23.
KIM, D., HEO, J., KIM, M., LEE, Y. W. & HAN, S. W. 2009. Size-controlled synthesis of monodisperse gold nanooctahedrons and their surface-enhanced Raman scattering properties. *Chemical Physics Letters,* 468, 245-248.
KIM, G., CHO, Y.-S. & KIM, W. D. 2006. Stability analysis for multi-jets electrospinning process modified with a cylindrical electrode. *European Polymer Journal,* 42, 2031-2038.
KIM, S., EOM, M. S., SEO, S. H. & HAN, M. S. 2013. Highly sensitive gold nanoparticle-based colorimetric probe for phytate detection with high selectivity over various phosphate derivatives. *Tetrahedron Letters,* 54, 5284-5287.
KIM, Y., YOU, Y.-J. & AHN, B.-Z. 2001. Naphthazarin derivatives (VIII): Synthesis, inhibitory effect on DNA topoisomerase-I, and antiproliferative activity of 6-(1-acyloxyalkyl)-5,8-dimethoxy-1,4-naphthoquinones. *Archiv der Pharmazie,* 334, 318-322.
KIM, Y. H. & SUN, G. 2000. Dye molecules as bridges for functional modifications of nylon: Antimicrobial functions. *Textile Research Journal,* 70, 728-733.
KLEIN, S., PETERSEN, S., TAYLOR, U., BARCIKOWSKI, S. & RATH, D. 2010. Quantitative visualization of colloidal and intracellular gold nanoparticles by confocal microscopy. *Journal of Biomedical Optics,* 15, 036015-036015-11.
KOCHKODAN, V., JOHNSON, D. J. & HILAL, N. 2013. Polymeric membranes: Surface modification for minimizing (bio)colloidal fouling. *Advances in Colloid and Interface Science.*
KOOIJ, E. S., AHMED, W., HELLENTHAL, C., ZANDVLIET, H. J. W. & POELSEMA, B. 2012. From nanorods to nanostars: Tuning the optical properties of gold nanoparticles. *Colloids and Surfaces A: Physicochemical and Engineering Aspects,* 413, 231-238.
KUNDU, S. & LIANG, H. 2008. Polyelectrolyte-mediated non-micellar synthesis of monodispersed 'aggregates' of gold nanoparticles using a microwave approach. *Colloids and Surfaces A: Physicochemical and Engineering Aspects,* 330, 143-150.
LABROU, N. E. & CLONIS, Y. D. 1995. Oxaloacetate Decarboxylase: On the Mode of Interaction with Substrate-Mimetic Affinity Ligands. *Archives of Biochemistry and Biophysics,* 321, 61-70.
LEE, T. H., KIM, W. R. & POTERUCHA, J. J. 2012. Evaluation of Elevated Liver Enzymes. *Clinics in Liver Disease,* 16, 183-198.
LI, C., LI, D., WAN, G., XU, J. & HOU, W. 2011. Facile synthesis of concentrated gold nanoparticles with low size-distribution in water: temperature and pH controls. *Nanoscale Research Letters,* 6, 1-10.
LI, D. & XIA, Y. 2004. Electrospinning of nanofibers: Reinventing the wheel? *Advanced Materials,* 16, 1151-1170.
LI, F., ZHAO, Y. & SONG, Y. 2010. *Core-Shell Nanofibers: Nano Channel and Capsule by Coaxial Electrospinning.*
LI, P., ZHANG, L., AI, K., LI, D., LIU, X. & WANG, E. 2008. Coating didodecyldimethylammonium bromide onto Au nanoparticles increases the stability of its complex with DNA. *Journal of Controlled Release,* 129, 128-134.
LI, Y., SI, Y., WANG, X., DING, B., SUN, G., ZHENG, G., LUO, W. & YU, J. 2013. Colorimetric Sensor Strips for Lead (II) Assay Utilizing Nanogold Probes Immobilized Polyamide-6/Nitrocellulose Nano-fibers/nets. *Biosensors and Bioelectronics.*

LIU, G., HONG, X. & TSANG, S. C. E. 2013. In situ formation of gold nanoparticles in alkylamine-polyol assemblies. *New Journal of Chemistry,* 37, 2969-2972.
LIU, J. & LU, Y. 2007. Colorimetric Cu2+ detection with a ligation DNAzyme and nanoparticles. *Chemical Communications*, 4872-4874.
LIU, Y., DING, Y., ZHANG, Y. & LEI, Y. 2012. Pt–Au nanocorals, Pt nanofibers and Au microparticles prepared by electrospinning and calcination for nonenzymatic glucose sensing in neutral and alkaline environment. *Sensors and Actuators B: Chemical,* 171–172, 954-961.
LU, F., DOANE, T. L., ZHU, J.-J. & BURDA, C. 2012. Gold nanoparticles for diagnostic sensing and therapy. *Inorganica Chimica Acta,* 393, 142-153.
LUTY-BLOCHO, M., PACŁAWSKI, K., JAWORSKI, W., STRESZEWSKI, B. & FITZNER, K. 2011. Kinetic Studies of Gold Nanoparticles Formation in the Batch and in the Flow Microreactor System. *In:* STAROV, V. & PROCHÁZKA, K. (eds.) *Trends in Colloid and Interface Science XXIV.* Springer Berlin Heidelberg.
MACHA, S. F. & LIMBACH, P. A. 2002. Matrix-assisted laser desorption/ionization (MALDI) mass spectrometry of polymers. *Current Opinion in Solid State and Materials Science,* 6, 213-220.
MAIKALA, R. V. 2010. Modified Beer's Law – historical perspectives and relevance in near-infrared monitoring of optical properties of human tissue. *International Journal of Industrial Ergonomics,* 40, 125-134.
MARAZUELA, M. & MORENO-BONDI, M. 2002. Fiber-optic biosensors – an overview. *Analytical and Bioanalytical Chemistry,* 372, 664-682.
MAZITSOS, C. F., RIGDEN, D. J., TSOUNGAS, P. G. & CLONIS, Y. D. 2002. Galactosyl-biomimetic dye-ligands for the purification of Dactylium dendroides galactose oxidase. *Journal of Chromatography A,* 954, 137-150.
MEDINA-RAMÍREZ, I., GONZÁLEZ-GARCÍA, M. & LIU, J. 2009. Nanostructure characterization of polymer-stabilized gold nanoparticles and nanofilms derived from green synthesis. *Journal of Materials Science,* 44, 6325-6332.
MERCADO-PAGÁN, Á. E., KANG, Y., KER, D. F. E., PARK, S., YAO, J., BISHOP, J. & YANG, Y. P. 2013. Synthesis and characterization of novel elastomeric poly(D,L-lactide urethane) maleate composites for bone tissue engineering. *European Polymer Journal,* 49, 3337-3349.
MERICAN, Z., SCHILLER, T. L., HAWKER, C. J., FREDERICKS, P. M. & BLAKEY, I. 2007. Self-Assembly and Encoding of Polymer-Stabilized Gold Nanoparticles with Surface-Enhanced Raman Reporter Molecules. *Langmuir,* 23, 10539-10545.
MERRETT, K., CORNELIUS, R. M., MCCLUNG, W. G., UNSWORTH, L. D. & SHEARDOWN, H. 2002. Surface analysis methods for characterizing polymeric biomaterials. *Journal of Biomaterials Science, Polymer Edition,* 13, 593-621.
MILDVAN, D., LANDAY, A., DE GRUTTOLA, V., MACHADO, S. G. & KAGAN, J. 1997. An approach to the validation of markers for use in AIDS clinical trials. *Clinical Infectious Diseases,* 24, 764-774.
MONTAUDO, G., SAMPERI, F. & MONTAUDO, M. S. 2006. Characterization of synthetic polymers by MALDI-MS. *Progress in Polymer Science,* 31, 277-357.
MOON, S., TANAKA, S.-I. & SEKINO, T. 2010. Crystal Growth of Thiol-Stabilized Gold Nanoparticles by Heat-Induced Coalescence. *Nanoscale Research Letters,* 5, 813 - 817.

MUKHERJEE, P., AHMAD, A., MANDAL, D., SENAPATI, S., SAINKAR, S. R., KHAN, M. I., RAMANI, R., PARISCHA, R., AJAYAKUMAR, P. V., ALAM, M., SASTRY, M. & KUMAR, R. 2001. Bioreduction of AuCl4− Ions by the Fungus, Verticillium sp. and Surface Trapping of the Gold Nanoparticles Formed. *Angewandte Chemie International Edition,* 40, 3585-3588.

NARAGHI, M., CHASIOTIS, I., KAHN, H., WEN, Y. & DZENIS, Y. 2007. Novel method for mechanical characterization of polymeric nanofibers. *Review of Scientific Instruments,* 78, 1 - 7.

NITANAN, T., OPANASOPIT, P., AKKARAMONGKOLPORN, P., ROJANARATA, T., NGAWHIRUNPAT, T. & SUPAPHOL, P. 2012. Effects of processing parameters on morphology of electrospun polystyrene nanofibers. *Korean Journal of Chemical Engineering,* 29, 173-181.

NIU, H.-T., JIANG, X., HE, J. & CHENG, J.-P. 2009. Cyanine dye-based chromofluorescent probe for highly sensitive and selective detection of cyanide in water. *Tetrahedron Letters,* 50, 6668-6671.

NYBLOM, H., BERGGREN, U., BALLDIN, J. & OLSSON, R. 2004. HIGH AST/ALT RATIO MAY INDICATE ADVANCED ALCOHOLIC LIVER DISEASE RATHER THAN HEAVY DRINKING. *Alcohol and Alcoholism,* 39, 336-339.

OISHI, K. & MORIUCHI, A. 2010. Removal of dissolved estrogen in sewage effluents by β-cyclodextrin polymer. *Science of The Total Environment,* 409, 112-115.

OKAFOR, O. Y., ERUKAINURE, O. L., AJIBOYE, J. A., ADEJOBI, R. O., OWOLABI, F. O. & KOSOKO, S. B. 2011. Modulatory effect of pineapple peel extract on lipid peroxidation, catalase activity and hepatic biomarker levels in blood plasma of alcohol–induced oxidative stressed rats. *Asian Pacific Journal of Tropical Biomedicine,* 1, 12-14.

OLENIN, A. Y. & LISICHKIN, G. V. 2011. Metal nanoparticles in condensed media: preparation and the bulk and surface structural dynamics. *Russian Chemical Reviews,* 80, 605-630.

OLOWU, R. A., AROTIBA, O., MAILU, S. N., WARYO, T. T., BAKER, P. & IWUOHA, E. 2010. Electrochemical Aptasensor for Endocrine Disrupting 17β-Estradiol Based on a Poly(3,4-ethylenedioxylthiopene)-Gold Nanocomposite Platform. *Sensors,* 10, 9872-9890.

OUARI, O., PHAN, T., ZIARELLI, F., CASANO, G., AUSSENAC, F., THUREAU, P., GIGMES, D., TORDO, P. & VIEL, S. 2013. Improved Structural Elucidation of Synthetic Polymers by Dynamic Nuclear Polarization Solid-State NMR Spectroscopy. *ACS Macro Letters,* 2, 715-719.

OZCANLI, T., ERDOGAN, A., OZDEMIR, S., ONEN, B., OZMEN, M., DOKSAT, K. & SONSUZ, A. 2006. Severe liver enzyme elevations after three years of olanzapine treatment: A case report and review of olanzapine associated hepatotoxicity. *Progress in Neuro-Psychopharmacology and Biological Psychiatry,* 30, 1163-1166.

OZER, J., RATNER, M., SHAW, M., BAILEY, W. & SCHOMAKER, S. 2008. The current state of serum biomarkers of hepatotoxicity. *Toxicology,* 245, 194-205.

PARI, L. & SURESH, A. 2008. Effect of grape (Vitis vinifera L.) leaf extract on alcohol induced oxidative stress in rats. *Food and Chemical Toxicology,* 46, 1627-1634.

PASTORIZA-SANTOS, I. & LIZ-MARZÁN, L. 2000. Reduction of silver nanoparticles in DMF. Formation of monolayers and stable colloids. *Pure and Applied Chemistry,* 72, 83-90.

PATEL, S. U., MANZO, G. M., PATEL, S. U., KULKARNI, P. S. & CHASE, G. G. 2012. Permeability of Electrospun Superhydrophobic Nanofiber Mats. *Journal of Nanotechnology,* 2012.

PATUNGWASA, W. & HODAK, J. H. 2008. pH tunable morphology of the gold nanoparticles produced by citrate reduction. *Materials Chemistry and Physics,* 108, 45-54.

PETTY, J. D., HUCKINS, J. N., ALVAREZ, D. A., BRUMBAUGH, W. G., CRANOR, W. L., GALE, R. W., RASTALL, A. C., JONES-LEPP, T. L., LEIKER, T. J., ROSTAD, C. E. & FURLONG, E. T. 2004. A holistic passive integrative sampling approach for assessing the presence and potential impacts of waterborne environmental contaminants. *Chemosphere,* 54, 695-705.

POLLOCK, N. R., ROLLAND, J. P., KUMAR, S., BEATTIE, P. D., JAIN, S., NOUBARY, F., WONG, V. L., POHLMANN, R. A., RYAN, U. S. & WHITESIDES, G. M. 2012. A Paper-Based Multiplexed Transaminase Test for Low-Cost, Point-of-Care Liver Function Testing. *Science Translational Medicine,* 4, 129-152.

PRASANTH, R., ARAVINDAN, V. & SRINIVASAN, M. 2012. Novel polymer electrolyte based on cob-web electrospun multi component polymer blend of polyacrylonitrile/poly(methyl methacrylate)/polystyrene for lithium ion batteries—Preparation and electrochemical characterization. *Journal of Power Sources,* 202, 299-307.

PUCCI, A., BIZZARRI, R. & RUGGERI, G. 2011. Polymer composites with smart optical properties. *Soft Matter,* 7, 3689-3700.

RAMAIAH, S. K. 2007. A toxicologist guide to the diagnostic interpretation of hepatic biochemical parameters. *Food and Chemical Toxicology,* 45, 1551-1557.

RAMAKRISHNA, S., FUJIHARA, K., TEO, W. E., YONG, T., MA, Z. & RAMASESHAN, R. 2006. Electrospun nanofibers: Solving global issues. *Materials Today,* 9, 40-50.

RAPOSO, M. M. M., FERREIRA, A. M. F. P., AMARO, M., BELSLEY, M. & MOURA, J. C. V. P. 2009. The synthesis and characterization of heterocyclic azo dyes derived from 5-N,N-dialkylamino-2,2′-bithiophene couplers. *Dyes and Pigments,* 83, 59-65.

RAUF, M. A., MEETANI, M. A., KHALEEL, A. & AHMED, A. 2010. Photocatalytic degradation of Methylene Blue using a mixed catalyst and product analysis by LC/MS. *Chemical Engineering Journal,* 157, 373-378.

REYES-GASGA, J., GÓMEZ-RODRÍGUEZ, A., GAO, X. & JOSÉ-YACAMÁN, M. 2008. On the interpretation of the forbidden spots observed in the electron diffraction patterns of flat Au triangular nanoparticles. *Ultramicroscopy,* 108, 929-936.

RIEMENSCHNEIDER, M., BUCH, K., SCHMOLKE, M., KURZ, A. & GUDER, W. G. 1997. Diagnosis of Alzheimer's disease with cerebrospinal fluid tau protein and aspartate aminotransferase. *The Lancet,* 350, 784.

RÍOS, A., ESCARPA, A., GONZÁLEZ, M. C. & CREVILLÉN, A. G. 2006. Challenges of analytical microsystems. *TrAC Trends in Analytical Chemistry,* 25, 467-479.

RUTLEDGE, G. C. & FRIDRIKH, S. V. 2007. Formation of fibers by electrospinning. *Advanced Drug Delivery Reviews,* 59, 1384-1391.

SAÇMACI, M., ÇAVUŞ, H. K., ARI, H., ŞAHINGÖZ, R. & ÖZPOZAN, T. 2012. Novel acid mono azo dye compound: Synthesis, characterization, vibrational, optical and theoretical investigations of 2-[(E)-(8-hydroxyquinolin-5-yl)-diazenyl]-4,5-dimethoxybenzoic acid. *Spectrochimica Acta Part A: Molecular and Biomolecular Spectroscopy,* 97, 88-99.

SAID, S. S., ALOUFY, A. K., EL-HALFAWY, O. M., BORAEI, N. A. & EL-KHORDAGUI, L. K. 2011. Antimicrobial PLGA ultrafine fibers: Interaction with wound bacteria. *European Journal of Pharmaceutics and Biopharmaceutics,* 79, 108-118.

SCAMPICCHIO, M., ARECCHI, A., LAWRENCE, N. S. & MANNINO, S. 2010. Nylon nanofibrous membrane for mediated glucose biosensing. *Sensors and Actuators B: Chemical,* 145, 394-397.

SCAMPICCHIO, M., ARECCHI, A. & MANNINO, S. 2009. Optical nanoprobes based on gold nanoparticles for sugar sensing. *Nanotechnology,* 20.

SEETHAPATHY, S., GÓRECKI, T. & LI, X. 2008. Passive sampling in environmental analysis. *Journal of Chromatography A,* 1184, 234-253.

SELVAKANNAN, P. R., MANDAL, S., PHADTARE, S., GOLE, A., PASRICHA, R., ADYANTHAYA, S. D. & SASTRY, M. 2004. Water-dispersible tryptophan-protected gold nanoparticles prepared by the spontaneous reduction of aqueous chloroaurate ions by the amino acid. *Journal of Colloid and Interface Science,* 269, 97-102.

SEO, J.-S., SON, D.-M., LEE, H., KIM, J. & KIM, Y. 2009. The Characterization of Borohydride-Stabilized Nanosilvers in Laponite Sol Using 1H NMR: Its Ligand Exchange Reactions with MUA and TOP. *Bull. Korean Chem. Soc,* 30, 2651.

SHARMA, S., MOON, C. S., KHOGALI, A., HAIDOUS, A., CHABENNE, A., OJO, C., JELEBINKOV, M., KURDI, Y. & EBADI, M. 2013. Biomarkers in Parkinson's disease (recent update). *Neurochemistry International,* 63, 201-229.

SHIN, Y. M., HOHMAN, M. M., BRENNER, M. P. & RUTLEDGE, G. C. 2001. Electrospinning: A whipping fluid jet generates submicron polymer fibers. *Applied Physics Letters,* 78, 1149-1151.

SHIRAZI, M. M. A., KARGARI, A., BAZGIR, S., TABATABAEI, M., SHIRAZI, M. J. A., ABDULLAH, M. S., MATSUURA, T. & ISMAIL, A. F. 2013. Characterization of electrospun polystyrene membrane for treatment of biodiesel's water-washing effluent using atomic force microscopy. *Desalination,* 329, 1-8.

SHUKLA, R., BANSAL, V., CHAUDHARY, M., BASU, A., BHONDE, R. R. & SASTRY, M. 2005. Biocompatibility of Gold Nanoparticles and Their Endocytotic Fate Inside the Cellular Compartment: A Microscopic Overview. *Langmuir,* 21, 10644-10654.

SI, Y., REN, T., LI, Y., DING, B. & YU, J. 2012. Fabrication of magnetic polybenzoxazine-based carbon nanofibers with Fe3O4 inclusions with a hierarchical porous structure for water treatment. *Carbon,* 50, 5176-5185.

SINGHA, D., BARMAN, N. & SAHU, K. 2014. A facile synthesis of high optical quality silver nanoparticles by ascorbic acid reduction in reverse micelles at room temperature. *Journal of Colloid and Interface Science,* 413, 37-42.

SLARK, A. T. & HADGETT, P. M. 1999. The effect of polymer structure on specific interactions between dye solutes and polymers. *Polymer,* 40, 1325-1332.

SLOMKOWSKI, S. & BASINSKA, T. 2010. Polymer Nano- and Microparticle Based Systems for Medical Diagnostics. *Macromolecular Symposia,* 295, 13-22.

SMITHA, S. L. & GOPCHANDRAN, K. G. 2013. Surface enhanced Raman scattering, antibacterial and antifungal active triangular gold nanoparticles. *Spectrochimica Acta Part A: Molecular and Biomolecular Spectroscopy,* 102, 114-119.

SORIANO, V., BARREIRO, P. & NUÑEZ, M. 2006. Management of chronic hepatitis B and C in HIV-coinfected patients. *Journal of Antimicrobial Chemotherapy,* 57, 815-818.

SOROURADDIN, M. H., SAADATI, M. & SAMADI, A. 2010. A Simple and Cheap Device for Colorimetric Determination of Serum Iron. *Journal of the Chinese Chemical Society,* 57, 56-61.

SOUSA, V. S. & TEIXEIRA, M. R. 2013. Aggregation kinetics and surface charge of CuO nanoparticles: the influence of pH, ionic strength and humic acids. *Environmental Chemistry,* 10, 313-322.

STEJSKAL, J. 1994. Aspartate aminotransferase isozymes in plants: Comparison of two staining methods in polyacrylamide gels. *Biologia Plantarum,* 36, 359-364.

SULLIVAN, P., MOATE, J., STONE, B., ATKINSON, J. D., HASHISHO, Z. & ROOD, M. J. 2012. Physical and chemical properties of PAN-derived electrospun activated carbon nanofibers and their potential for use as an adsorbent for toxic industrial chemicals. *Adsorption,* 18, 265-274.

SUN, C. G., LIN, Q. & FU, N. Y. 2012. A novel squaraine dye with squaramide as a scaffold and the colorimetric detection of amine. *Chinese Chemical Letters,* 23, 217-220.

SUNG, Y. K., AHN, B. W. & KANG, T. J. 2012. Magnetic nanofibers with core (Fe3O4 nanoparticle suspension)/sheath (poly ethylene terephthalate) structure fabricated by coaxial electrospinning. *Journal of Magnetism and Magnetic Materials,* 324, 916-922.

TAKAHASHI, Y., YUKITA, W., CHATTERJEE, M. & SUZUKI, T. M. 2008. Preparation of highly dispersed gold nanoparticles inside the porous support assisted by amphiphilic vinyl maleate copolymer. *Reactive and Functional Polymers,* 68, 1476-1482.

TAN, S., HUANG, X. & WU, B. 2007. Some fascinating phenomena in electrospinning processes and applications of electrospun nanofibers. *Polymer International,* 56, 1330-1339.

TAN, Y. N., SU, X., LIU, E. T. & THOMSEN, J. S. 2010. Gold-nanoparticle-based assay for instantaneous detection of nuclear hormone receptor-response elements interactions. *Analytical Chemistry,* 82, 2759-2765.

TCHAIKOVSKI, S. N. & ROSING, J. 2010. Mechanisms of Estrogen-Induced Venous Thromboembolism. *Thrombosis Research,* 126, 5-11.

THERON, S. A., YARIN, A. L., ZUSSMAN, E. & KROLL, E. 2005. Multiple jets in electrospinning: experiment and modeling. *Polymer,* 46, 2889-2899.

THÉVENOT, D. R., TOTH, K., DURST, R. A. & WILSON, G. S. 2001. Electrochemical biosensors: Recommended definitions and classification. *Biosensors and Bioelectronics,* 16, 121-131.

THOPPEY, N. M., BOCHINSKI, J. R., CLARKE, L. I. & GORGA, R. E. 2010. Unconfined fluid electrospun into high quality nanofibers from a plate edge. *Polymer,* 51, 4928-4936.

TIJING, L. D., CHOI, W., JIANG, Z., AMARJARGAL, A., PARK, C.-H., PANT, H. R., IM, I.-T. & KIM, C. S. 2013. Two-nozzle electrospinning of (MWNT/PU)/PU nanofibrous composite mat with improved mechanical and thermal properties. *Current Applied Physics,* 13, 1247-1255.

TSUNOYAMA, H., ICHIKUNI, N., SAKURAI, H. & TSUKUDA, T. 2009. Effect of Electronic Structures of Au Clusters Stabilized by Poly(N-vinyl-2-pyrrolidone) on Aerobic Oxidation Catalysis. *Journal of the American Chemical Society,* 131, 7086-7093.

TU, Q., WANG, J.-C., LIU, R., HE, J., ZHANG, Y., SHEN, S., XU, J., LIU, J., YUAN, M.-S. & WANG, J. 2013. Antifouling properties of poly(dimethylsiloxane) surfaces modified with quaternized poly(dimethylaminoethyl methacrylate). *Colloids and Surfaces B: Biointerfaces,* 102, 361-370.

UEHARA, N. 2010. *Polymer-functionalized gold nanoparticles as versatile sensing materials.*
US, E. 2001. Removal of endocrine disruptor chemicals using drinking water treatment processes. Technology Transfer and Support Division National Risk Management Research Laboratory Office of Research and Development U.S. Environmental Protection Agency: Cincinnati, Ohio.
UTSUNOMIYA, S. & EWING, R. C. 2003. Application of High-Angle Annular Dark Field Scanning Transmission Electron Microscopy, Scanning Transmission Electron Microscopy-Energy Dispersive X-ray Spectrometry, and Energy-Filtered Transmission Electron Microscopy to the Characterization of Nanoparticles in the Environment. *ENVIRONMENTAL SCIENCE & TECHNOLOGY,* 37, 786-791.
VAN DER SCHUEREN, L., MOLLET, T., CEYLAN, Ö. & DE CLERCK, K. 2010. The development of polyamide 6.6 nanofibres with a pH-sensitive function by electrospinning. *European Polymer Journal,* 46, 2229-2239.
VAN ERP, T. S. & MARTENS, J. A. 2011. A standardization for BET fitting of adsorption isotherms. *Microporous and Mesoporous Materials,* 145, 188-193.
VARESANO, A., CARLETTO, R. A. & MAZZUCHETTI, G. 2009. Experimental investigations on the multi-jet electrospinning process. *Journal of Materials Processing Technology,* 209, 5178-5185.
VELLA, S., BEATTIE, P., CADEMARTIRI, R., LAROMAINE, A., MARTINEZ, A., PHILLIPS, S., MIRICA, K. & WHITESIDES, G. 2012. Measuring markers of liver function using a micropatterned paper device designed for blood from a fingerstick. *Anal Chem,* 84, 2883-2891.
VILELA, D., GONZÁLEZ, M. C. & ESCARPA, A. 2012. Sensing colorimetric approaches based on gold and silver nanoparticles aggregation: Chemical creativity behind the assay. A review. *Analytica Chimica Acta,* 751, 24-43.
VRANA, B., ALLAN, I. J., GREENWOOD, R., MILLS, G. A., DOMINIAK, E., SVENSSON, K., KNUTSSON, J. & MORRISON, G. 2005. Passive sampling techniques for monitoring pollutants in water. *TrAC Trends in Analytical Chemistry,* 24, 845-868.
WANG, C., XU, C., CHEN, F. & TANG, X. 2011a. Simultaneous determination of three naturally occurring estrogens in environmental waters by high-performance liquid chromatography. *Journal of Separation Science,* 34, 2371-2375.
WANG, H. S., FU, G. D. & LI, X. S. 2009. Functional polymeric nanofibers from electrospinning. *Recent Patents on Nanotechnology,* 3, 21-31.
WANG, L., MA, W., XU, L., CHEN, W., ZHU, Y., XU, C. & KOTOV, N. A. 2010. Nanoparticle-based environmental sensors. *Materials Science and Engineering: R: Reports,* 70, 265-274.
WANG, S., LI, Y., WU, X., DING, M., YUAN, L., WANG, R., WEN, T., ZHANG, J., CHEN, L., ZHOU, X. & LI, F. 2011b. Construction of uniformly sized pseudo template imprinted polymers coupled with HPLC–UV for the selective extraction and determination of trace estrogens in chicken tissue samples. *Journal of Hazardous Materials,* 186, 1513-1519.
WANG, X., DING, B., SUN, G., WANG, M. & YU, J. 2013. Electro-spinning/netting: A strategy for the fabrication of three-dimensional polymer nano-fiber/nets. *Progress in Materials Science,* 58, 1173-1243.

WANG, X., SI, Y., WANG, J., DING, B., YU, J. & AL-DEYAB, S. S. 2012. A facile and highly sensitive colorimetric sensor for the detection of formaldehyde based on electro-spinning/netting nano-fiber/nets. *Sensors and Actuators B: Chemical,* 163, 186-193.
WATSON, C. S., JENG, Y.-J. & GUPTARAK, J. 2011. Endocrine disruption via estrogen receptors that participate in nongenomic signaling pathways. *The Journal of Steroid Biochemistry and Molecular Biology,* 127, 44-50.
WEI, L., LIAO, P., WU, H., LI, X., PEI, F., LI, W. & WU, Y. 2008. Toxicological effects of cinnabar in rats by NMR-based metabolic profiling of urine and serum. *Toxicology and Applied Pharmacology,* 227, 417-429.
WISE, A., O'BRIEN, K. & WOODRUFF, T. 2010. Are Oral Contraceptives a Significant Contributor to the Estrogenicity of Drinking Water?†. *ENVIRONMENTAL SCIENCE & TECHNOLOGY,* 45, 51-60.
YAGI, T., YAMAMOTO, S. & NOZAKI, M. 1985. Simple colorimetric assay for aspartate aminotransferase. *Agric. Biol. Chem.,* 48, 2819-2821.
YAMASHITA, Y., KO, F., MIYAKE, H. & HIGASHIYAMA, A. 2008. Establishment of Nanofiber Preparation Technique by Electrospinning. *Sen'i Gakkaishi,* 64, 24-28.
YANG, P., ZHAN, S., HUANG, Z., ZHAI, J., WANG, D., XIN, Y., ZHANG, L., SUN, M. & SHAO, C. 2011. The fabrication of PPV/C60 composite nanofibers with highly optoelectric response by optimization solvents and electrospinning technology. *Materials Letters,* 65, 537-539.
YANG, R., HE, J., XU, L. & YU, J. 2009. Bubble-electrospinning for fabricating nanofibers. *Polymer,* 50, 5846-5850.
YANG, Y., LI, X., QI, M., ZHOU, S. & WENG, J. 2008. Release pattern and structural integrity of lysozyme encapsulated in core–sheath structured poly(dl-lactide) ultrafine fibers prepared by emulsion electrospinning. *European Journal of Pharmaceutics and Biopharmaceutics,* 69, 106-116.
YAZID, H., ADNAN, R., HAMID, S. A. & FARRUKH, M. A. 2010. Synthesis and characterization of gold nanoparticles supported on zinc oxide via the deposition-precipitation method. *Turkish Journal of Chemistry,* 34, 639-650.
YETISEN, A. K., AKRAM, M. S. & LOWE, C. R. 2013. Paper-based microfluidic point-of-care diagnostic devices. *Lab on a Chip,* 13, 2210-2251.
YING, G.-G., KOOKANA, R. S., KUMAR, A. & MORTIMER, M. 2009. Occurrence and implications of estrogens and xenoestrogens in sewage effluents and receiving waters from South East Queensland. *Science of The Total Environment,* 407, 5147-5155.
ZAMANLOO, M. R., SHAMKHALI, A. N., ALIZADEH, M., MANSOORI, Y. & IMANZADEH, G. 2012. A novel barbituric acid-based azo dye and its derived polyamides: Synthesis, spectroscopic investigation and computational calculations. *Dyes and Pigments,* 95, 587-599.
ZARGAR, B. & HATAMIE, A. 2013. A simple and fast colorimetric method for detection of hydrazine in water samples based on formation of gold nanoparticles as a colorimetric probe. *Sensors and Actuators B: Chemical,* 182, 706-710.
ZHANG, A., SUN, H., WANG, P., HAN, Y. & WANG, X. 2012. Recent and potential developments of biofluid analyses in metabolomics. *Journal of Proteomics,* 75, 1079-1088.
ZHANG, C., LI, Y., WANG, W., ZHAN, N., XIAO, N., WANG, S., LI, Y. & YANG, Q. 2011a. A novel two-nozzle electrospinning process for preparing microfiber reinforced pH-

sensitive nano-membrane with enhanced mechanical property. *European Polymer Journal,* 47, 2228-2233.
ZHANG, D., ZHANG, M., LIU, Z., YU, M., LI, F., YI, T. & HUANG, C. 2006. Highly selective colorimetric sensor for cysteine and homocysteine based on azo derivatives. *Tetrahedron Letters,* 47, 7093-7096.
ZHANG, G., LI, Y., XU, J., ZHANG, C., SHUANG, S., DONG, C. & CHOI, M. M. F. 2013. Glutathione-protected fluorescent gold nanoclusters for sensitive and selective detection of Cu2+. *Sensors and Actuators B: Chemical,* 183, 583-588.
ZHANG, M., LIU, Y.-Q. & YE, B.-C. 2011b. Colorimetric assay for sulfate using positively-charged gold nanoparticles and its application for real-time monitoring of redox process. *Analyst,* 136, 4558-4562.
ZHANG, Y., LI, B. & XU, C. 2010. Visual detection of ascorbic acid via alkyne-azide click reaction using gold nanoparticles as a colorimetric probe. *Analyst,* 135, 1579-1584.
ZHAO, W., BROOK, M. A. & LI, Y. 2008. Design of Gold Nanoparticle-Based Colorimetric Biosensing Assays. *ChemBioChem,* 9, 2363-2371.
ZHAO, Y., ZHOU, Y., WU, X., WANG, L., XU, L. & WEI, S. 2012. A facile method for electrospinning of Ag nanoparticles/poly (vinyl alcohol)/carboxymethyl-chitosan nanofibers. *Applied Surface Science,* 258, 8867-8873.
ZHENG, W., YATES, S. R. & BRADFORD, S. A. 2008. Analysis of Steroid Hormones in a Typical Dairy Waste Disposal System. *ENVIRONMENTAL SCIENCE & TECHNOLOGY,* 42, 530-535.
ZHOU, J., RALSTON, J., SEDEV, R. & BEATTIE, D. A. 2009. Functionalized gold nanoparticles: Synthesis, structure and colloid stability. *Journal of Colloid and Interface Science,* 331, 251-262.

http://www.matsceng.ohio-state.edu/ims/LR_Stericstablization

http://materialrulz.weebly.com/uploads/7/9/5/1/795167/

http://File:Electro-Steric_Stabilization.jpg

http://faculty.ksu.edu.sa

http://science.jrank.org/pages/2538/Enzyme-Environment.html

http://www.nature.com/nnano/journal/v7/n12/full/nnano.2012.186.html